ION OPTICS OF MASS SPECTROMETERS WITH VIRTUALLY ENLARGED RADIUS.

H A TASMAN

ION OPTICS OF MASS SPECTROMETERS WITH VIRTUALLY ENLARGED RADIUS.

PROEFSCHRIFT
TER VERKRIJGING VAN DE GRAAD VAN
DOCTOR IN DE WIS- EN NATUURKUNDE
AAN DE RIJKSUNIVERSITEIT TE LEIDEN,
OP GEZAG VAN DE RECTOR MAGNIFICUS
DR G. SEVENSTER, HOOGLERAAR IN DE
FACULTEIT DER GODGELEERDHEID,
TEGEN DE BEDENKINGEN VAN DE
FAGULTEIT DER WIS- EN NATUURKUNDE,
TE VERDEDIGEN OP WOENSDAG 18 OCTOBER 1961
TE 15 UUR,

DOOR

HERMAN ABEL TASMAN,
GEBOREN TE UTRECHT IN 1930

DRUK: V.R.B. KLEINE DER A 3 - 4 - GRONINGEN

PROMOTOR: PROF. DR J. KISTEMAKER.

Aan mijn ouders
Aan Roelie

This work is part of the program of research of the *"Stichting voor Fundamenteel Onderzoek der Materie" (F.O.M.)*, which is financially supported by the *"Nederlandse Organisatie voor Zuiver Wetenschappelijk Onderzoek" (Z.W.O.)*.

Na aan het Chr. Lyceum te Zeist in 1948 eindexamen Gymnasium B te hebben afgelegd, liet ik mij inschrijven aan de Rijks Universiteit te Groningen, waar ik in 1951 het Candidaatsexamen F aflegde. Aan het Anorganisch Chemisch Laboratorium aldaar verrichtte ik onder leiding van Prof. Dr E. H. Wiebenga en Dr K. H. Boswijk o. a. een röntgen-analytische herbepaling van de kristalstructuur van caesiumtrijodide.
In 1956 legde ik aldaar het Doctoraalexamen af in de Scheikunde met bijvak Natuurkunde.

Sinds 1956 ben ik werkzaam op het Laboratorium voor Massaspectrografie (thans: Laboratorium voor Massascheiding) te Amsterdam, onder leiding van Prof. Dr J. Kistemaker.
Ik hield mij voornamelijk bezig met vacuumtechniek en met de ontwikkeling van een nieuwe massaspectrometer met hoog oplossend vermogen. In nauwe samenwerking met Dr Ir A. J. H. Boerboom werden de tweede orde afbeeldingseigenschappen van inhomogene magneetvelden systematisch doorgerekend, en werd een instrument ontwikkeld gebaseerd op deze grondslagen.

In 1960 was ik gedurende een half jaar werkzaam op het Argonne National Laboratory, Physics Division, bij Chicago, Ill., U.S.A. In samenwerking met Dr W. A. Chupka en Dr J. Berkowitz deed ik daar o. a. onderzoekingen aan de massaspectra van monomeer en dimeer in de damp van alkalihalogeniden, en aan de verhouding van de ionisatie-botsingsdoorsneden van monomeer en dimeer in deze damp voor 80 eV electronen.

CONTENTS

CHAPTER 1

INTRODUCTION

1a: *Purpose and design of single and double focusing mass spectrometers.*

A mass spectrometer is an instrument which should transform a sample into a beam of charged particles, and resolve this beam into a spectrum according to the mass-to-charge ratio. Basically, such an instrument consists of an ion source (which converts the sample into ions and forms a beam); an analysing system (which resolves the beam into a mass spectrum); and a detecting system (for the detection of the resolved beam).

In this study we will not discuss the design of the ion source. We will only assume that it produces a beam of ions of nearly the same energy and small angular divergence, emerging from a narrow object slit. Between the ionising region and the defining (object) slit, the ions are accelerated by a high voltage (of the order of 1-10 kV); the energy spread in the beam is supposed to be small as compared with the accelerating voltage.

Neither will the detecting system itself be discussed here. We will confine ourselves to the study of the analysing field comprised between the defining slits of the source (object slit) and of the collector (image slit), and investigate the conditions for obtaining a high resolving power and a high transmission. However, these conditions depend on the type of the detecting system inasmuch as whether the different masses are to be collected simultaneously or subsequently.

There are several types of analysing systems. The most common type consists of a magnetic field, either alone or combined with an electrostatic deflecting field. The radius of deflection in the magnetic field is proportional to the momentum-to-charge ratio of the ions. The field or combination of fields also exhibits a lens action, and should focus the beam on the detecting system.

The aim of this study will be the discussion of the ion optical properties of this class of analysing systems, consisting either of a magnetic field alone (single focusing mass spectrometers), or of an electrostatic field plus a magnetic field, with the restriction that these should not overlap each other (tandem arrangement for double focusing mass spectrometers). In the latter case, for practical reasons the ion beam is supposed to pass first through the electrostatic field and subsequently through the magnetic field; this restriction is not essential from the ion-optical point of view.

For the simultaneous collection of the whole spectrum or of part of it, it may be focused on a photographic plate. The positions of the lines serve as a measure of the mass of the ions whereas the blackening gives some indication of their relative abundance. This method is employed in mass spectrographs. It requires good focusing of a considerable part of the spectrum on an image plane as flat as possible. The photographic plate integrates over the exposure time, and fluctuations in the beam intensity affect all lines identically. However, the stability of the electrostatic and magnetic fields should be high over the whole exposure time.

For subsequent detection, the ion current is measured which passes through a narrow collector slit, placed at a fixed position in the image plane. At given field strengths, only ions of one m/e (in single focusing instruments: mv/e) value can pass through the collector slit. By varying either the magnetic field strength, or the accelerating voltage and electrostatic field strength, the mass spectrum can be scanned, and the different ions measured subsequently. This method is employed in mass spectrometers. It requires good focusing and resolution only at one point in the image plane. Stabilisation of the ion beam intensity produced by the ion source is now essential for accurate abundance ratio measurements; however, the accuracy achievable in current measurements is much better than with photographic detection, whereas the application of secondary electron emission multipliers increases the sensitivity so far as to make the counting and measurement of individual ions possible.

For obtaining the highest possible accuracy in abundance ratio measurements, a variation of the second method lessens the need for ion current stabilisation. It consists of the simultaneous electrical measurement of the two masses to be compared, each being measured after a separate collector slit. Unless one of the slits is made wide, this method is only applicable to ions of a specified mass ratio.

This study concerns the ion optics of mass spectrometers for subsequent detection, where only that part of the image plane in the immediate environment of the collector slit is of interest. No attempt will be made to obtain a flat image plane.

A single focusing mass spectrometer resolves the ion beam according to the momentum-to-charge ratio instead of the desired mass-to-charge ratio. Energy spread in the ion beam thus results in broadening of the image and loss of resolving power. The relative energy spread should be much smaller than the required mass resolving power. Although the relative energy spread can be reduced by careful ion source design (Dubrovin et al.[1]) and by increasing the accelerating voltage of the ions,

the energy spread may be the limiting factor in the resolving power of single focusing instruments, particularly for ions from the dissociation of a two-atomic molecule, which are formed with considerable kinetic energy (Morrison and Stanton[2]). Fortunately, however, this effect can be compensated by the addition of an electrostatic deflecting field. An electrostatic field resolves an ion beam according to the energy of the ions, and by a suitable choice of the parameters the total energy dispersion of the combination can be made zero (at least in first order) whilst the m/e dispersion remains. This is achieved in double focusing mass spectrometers and mass spectrographs.

1b: *Theoretical limit on the resolving power. Aim of the virtual enlargement of the radius by inhomogeneous magnetic and toroidally curved electrostatic fields.*

Let us suppose that the analysing field produces a perfectly sharp image of the object slit on the image plane, and exhibits no optical aberrations. Let D_m denote the mass dispersion in radial direction at the image per unit $\delta m/m_o$, and M_{lat} the radial lateral magnification of the optical system. Two adjacent peaks in the mass spectrum corresponding to masses m_o and $m_o + \delta m$ are said to be resolved, if at no instant ions of both masses can reach the collector simultaneously when the mass spectrum is swept over the collector slit. It is evident that the "free space" in radial direction between the two adjacent peaks should exceed the collector slit width for complete resolution. If the mass resolving power R is defined as the reciprocal of the relative mass difference at which two adjacent peaks are just resolved, and if the object and image slit widths are denoted by s' and s'' respectively, we arrive at the inequality:

$$R \leqslant |D_m| / (|M_{lat}| s' + s''). \qquad (1,1)$$

For accurate abundance ratio measurements, s'' should exceed $|M_{lat}|\, s'$, such as to obtain flat-topped peaks, the height of which corresponds to the total ion current at a given mass. Consequently:

$$R < \tfrac{1}{2} |D_m / M_{lat}\, s'|. \qquad (1,2)$$

In the conventional symmetrical arrangement (object distance = image distance) with a homogeneous magnetic field with normal incidence and exit, we have:

$$M_{lat} = -1; \qquad (2,109)$$

whereas it follows from (2, 116) that:

$$D_m = r_m; \qquad (1,3)$$

and thus:

$$R < r_m/2s'. \qquad (1,4)$$

r_m is the radius of deflection of the main path in the magnetic field.

Evidently, two ways for increasing the resolving power are the reduction of s', or increasing r_m. The former cannot be extended far as it reduces the transmission and sensitivity of the apparatus, and increases the relative effect of inevitable aberrations. The latter was done in a number of very large and costly instruments with radii ranging from 1000 mm to 2740 mm [3-6].

Only little can be gained by increasing the object distance and decreasing the image distance. Then both D_m and M_{lat} decrease, but D_m/M_{lat} increases. However, the decrease of the dispersion and the large object distance are inconvenient.

The mass dispersion may be increased by using oblique incidence and exit. Denoting the object and image distances by l'_m and l''_m respectively, the sector angle by ϕ_m, and the angle of obliqueness between the normal at the field boundary and the main path by ϵ, (see Fig. 3 in the following chapter), we have in the symmetrical arrangement ($l'_m = l''_m$) still (2, 109); writing $T = \tan(\phi_m/2)$ and $t = \tan\epsilon$, we have:

$$D_m = r_m/(1 - t/T); \qquad (2,116)$$

$$l'_m = l''_m = r_m/(T - t). \qquad (2,115)$$

The object and image distances are increased by the same factor as the mass dispersion.

Another way for increasing the resolving power is the use of an inhomogeneous magnetic field. (Alekseevski et al.[7]). In a symmetrical arrangement, where the magnetic field strength in the median plane varies with the radius according to:

$$-\left(\frac{r_m}{B_z}\right)\left(\frac{\partial B_z}{\partial r}\right)_{r=r_m} = n, \quad (0 \leqslant n < 1), \qquad (2,33)$$

the mass dispersion equals:

$$D_m = r_m/(1 - n), \qquad (2,113)$$

and the object and image distances:

$$l'_m = l''_m = r_m\,(1-n)^{-\frac{1}{2}}\,\cot\left(\tfrac{1}{2}(1-n)^{\frac{1}{2}}\phi_m\right). \qquad (2,112)$$

Again, an increase in mass dispersion is accompanied by an increase in the object and image distances. However, by using

large angles of deflection and values of n close to unity, it is possible to build rather compact instruments with a high resolving power.

In the conventional design of a double focusing mass spectrometer, the electrostatic deflecting field consists of a cylindrical condensor. The radial field strength between coaxial cylindrical electrodes is proportional with $1/r$. This field exhibits a lens action on charged particles, together with energy dispersion (or velocity dispersion). (Herzog[8]). For comparison referring again to the symmetrical case where object distance l'_e and image distance l''_e are equal, we have:

$$l'_e = l''_e = \tfrac{1}{2}\sqrt{2}\, r_e \cot\left(\tfrac{1}{2}\sqrt{2}\,\phi_e\right); \qquad (3,55)$$

whereas the velocity dispersion D_v in radial direction at the image per unit of the relative velocity difference $\delta v/v_o$ equals:

$$D_v = 2 r_e . \qquad (3,56)$$

The velocity dispersion is twice the energy dispersion. r_e is the radius of deflection of the main path, ϕ_e is the sector angle, or angle of deflection. Due to the symmetry we have still $M_{lat} = -1$.

The velocity dispersion can be increased (with a simultaneous increase in l'_e and l''_e) by giving the equipotential surfaces and the electrodes of the deflecting field an extra curvature, such as to make them parts of toroids [9-13]. Denoting this second radius of curvature of the equipotential surface comprising the main path, by R_e, (positive if convex towards increasing r), and defining:

$$c = r_e/R_e, \quad (0 \leqslant c < 2) \qquad (3,7)$$

we now have:

$$l'_e = l''_e = r_e \frac{\cot\left(\tfrac{1}{2}\sqrt{2-c}\,\phi_e\right)}{\sqrt{2-c}} \qquad (3,53)$$

$$D_v = 4 r_e/(2-c). \qquad (3,54)$$

Evidently, the velocity dispersion has been increased by a factor $2/(2-c)$.

The ion optics of inhomogeneous magnetic and of toroidally curved electrostatic sector fields will be studied in detail in chapters 2 and 3. To realise such fields, appropriately shaped pole shoes and electrodes should be applied, which are discussed in chapter 4. Instruments, designed for obtaining a very high resolving power, require accurate realisation of the prescribed instrument parameters; in some cases the final adjustment is

best achieved by correcting devices, a number of which are presented in chapter 5. In chapter 6 and 7, a theoretical and numerical discussion will be given of the double focusing properties of tandem arrangements consisting of electrostatic and magnetic fields of the general type indicated above, with "virtually enlarged radius".

1c: *Two-directional focusing.*

In the conventional deflecting fields, i.e. the homogeneous magnetic field and the cylindrical electrostatic field, focusing occurs only in radial direction. No force affects the component of the ion trajectories normal to the median plane. Consequently, the maximum transmitted axial aperture angle is determined solely by the total path length and the image slit height, assuming the vacuum envelope dimensions to the sufficiently large.

Some axial focusing is caused by the fringing fields of the magnetic field if the boundaries are oblique, (see 2,57), but the practical importance of this effect is rather limited.

On the other hand, both inhomogeneous magnetic and toroidally curved electrostatic fields exhibit axial focusing action. At $n=\frac{1}{2}$, and at $c=1$ (spherical condensor), the axial and radial images coincide. At $\frac{1}{2}<n<1$, and $1<c<2$, the axial converging action of these fields exceeds the radial.

Two-directional focusing may also be achieved by the addition of some extra element which adds mutually differing extra convergences in axial and radial direction. Quadrupole lenses are suitable for this purpose. (Enge[14]). These lenses converge in one direction and diverge in the other.

In most cases, the transmission and sensitivity of the instrument are increased by (approximate) stigmatic focusing, where the radial and axial images coincide. Thereto the axial lateral magnification should be of the order of unity in absolute value. The axial focusing needs only be approximate, as deviations result only in some loss in intensity, but do not affect the mass dispersion and resolution. With $\frac{1}{2}<n<1$ and $1<c<2$, stigmatic focusing may be achieved by admitting an (extra) intermediate axial image between object and image slit.

The balancing of the radial and axial focusing of general electromagnetic fields has been studied by several authors [15-18]. The field with $n=\frac{1}{2}$ has been used for β-spectrometers [19], in a mass spectrometer [20], and in electromagnetic isotope separators [21-22]. The combination of a toroidally curved electrostatic field with $1<c<2$, with a homogeneous magnetic field also makes stigmatic focusing possible [23-26, 38]. A case of a combination of an electrostatic field with $1<c<2$ and a magnetic field with $\frac{1}{2}<n<1$ is presented in the literature [27]. Further examples will be given in Chapter 7.

CHAPTER 2

ION-OPTICAL PROPERTIES OF THE INHOMOGENEOUS MAGNETIC SECTOR FIELD

2a: *Assumptions; coordinate system.*

This chapter deals with the ion optics of a *sector field.* In first instance, the field strength is supposed to be independent of the path coordinate ψ, outside the deflecting field region it is supposed to be zero, dropping to zero abruptly at the field boundaries. In second instance, the first order focusing action due to the fringing fields with oblique incidence and/or exit is accounted for; otherwise their influences are neglected. A discussion of the influence of the fringing fields will be given in chapter 5.

In general, both the object and the image lie outside the deflecting field region. We will first calculate the trajectories in the field region, and then suppose the rectilinear paths in the field free object and image space to coincide with the path tangents at the field boundaries.

In the object and image space, the ion trajectories are expressed in the cartesian coordinates x_1, y_1, z_1, and x_2, y_2, z_2, respectively, the origins being located at the points of entrance and exit of the main path. In the deflecting field region the main path is assumed to be circular with radius r_m, and the ion trajectories are expressed in the dimensionless coordinates: normal coordinate $u = (r - r_m)/r_m$; binormal coordinate

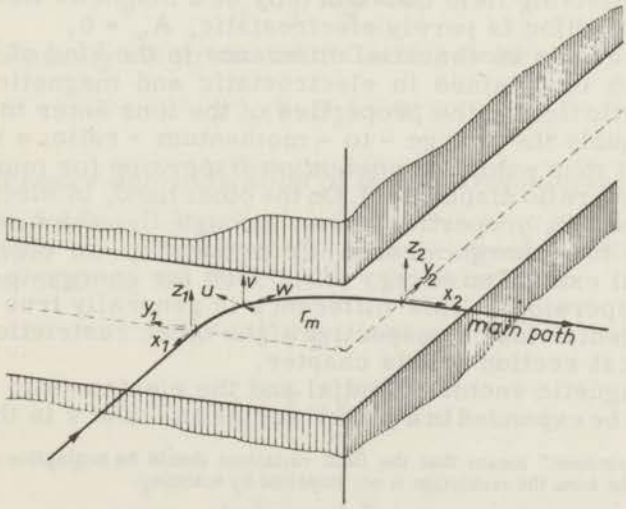

Fig. 1. Coordinate system

$v = z/r_m$; path coordinate $w = \psi$. (See Fig. 1). The median plane is supposed to be a plane of symmetry for the magnetic vector potential.

2b: *The Euler - Lagrange equations.*

The ion trajectories are defined by the Euler - Lagrange equations (Glaser [28,29]):

$$\frac{d}{dw}\left(\frac{\partial F}{\partial u'}\right) - \frac{\partial F}{\partial u} = 0, \qquad (2,1)$$

$$\frac{d}{dw}\left(\frac{\partial F}{\partial v'}\right) - \frac{\partial F}{\partial v} = 0. \qquad (2,2)$$

Here $u' = du/dw$; $v' = dv/dw$; and F is the "ion-optical index of refraction", which equals in the general case of a w-independent electromagnetic deflecting field which is constant or nearly constant *) in time:

$$F(u,v,u',v') = \sqrt{\frac{\varphi}{U}\left\{(1+u)^2 + (u'^2+v'^2)\right\}} - \eta(1+u)A_w. \qquad (2,3)$$

φ is the electrostatic potential, U is the potential through which the ions have been accelerated before entering into the deflecting field; both φ and U are zero for ions with zero kinetic energy. A_w is the w-component of the magnetic vector potential $\vec{A}$, which is chosen in such a way that A_w is the only component differing from zero.
η equals:

$$\eta = (e/2mU)^{\frac{1}{2}}. \qquad (2,4)$$

If the deflecting field consists only of a magnetic field, $\varphi = U$; if the deflection is purely electrostatic, $A_w = 0$.

(2,3) reveals an essential difference in the kind of dispersion which is obtained in electrostatic and magnetic fields. In magnetic fields, the properties of the ions enter through η, which equals the charge - to - momentum - ratio; a magnetic field will thus exhibit a *momentum dispersion* (or momentum-to-charge-ratio dispersion). On the other hand, in electrostatic fields the ion properties enter through U, which equals the energy - to - charge - ratio. Consequently, an electrostatic field will exhibit an *energy dispersion* (or energy-to-charge-ratio dispersion). This difference is generally true for time independent fields, irrespective of the other restrictions made in the first section of this chapter.

The magnetic vector potential and the electrostatic potential may now be expanded in a power series in u and v in the neigh-

*) "Nearly constant" means that the field variations should be neglegible in the transit time of the ions; the restriction is not impaired by scanning.

bourhood of the main path (u=v=0), and F may be written as a power series in u, v, u', and v'. This expansion of F contains no odd powers of u' or v', and symmetry of A_w and φ with respect to the median plane v = 0 causes terms with odd powers of v to vanish. Thus (2, 3) may be written, including terms up to the third order:

$$F(u, v, u', v') = F_{00} + F_{10}u + F_{20}u^2 + F_{02}v^2 + \tfrac{1}{2}(u'^2+v'^2) + \\ + F_{30}u^3 + F_{12}uv^2 - gu(u'^2+v'^2) + \ldots \quad (2,5)$$

In a purely magnetic field, $g = \frac{1}{2}$, and the coefficients F_{ij} depend on η and on the strength and shape of the magnetic field as expressed by A_w.

Successive approximations of the ion trajectories are defined by substituting (2, 5) into (2, 1)-(2, 2), retaining terms in (2, 5) up to one order higher than that of the approximation wanted. If u_o, α, v_o, α_z, are the values of u, u', v, v', respectively at w=0 (boundary conditions), (these quantities are supposed to be small of first order), then the order of approximation is defined as the highest degree in u_o, α, v_o, α_z, up to which *all* terms are included in the expansion for the ion trajectories.

The central path should be a possible trajectory for ions with $\eta = \eta_o$; $U = U_o$. This corresponds to the zeroth order approximation, which sets the condition for a purely magnetic deflecting field:

$$F_{10}(\eta_o, A_w) = 0; \quad (2,6)$$

and for a purely electrostatic deflecting field:

$$F_{10}(\varphi, U_o) = 0. \quad (2,7)$$

2c: *First order approximation of the ion trajectories.*

Retaining terms up to the second order in (2, 5), we find on substitution into (2, 1)-(2, 2) the two simultaneous differential equations defining the first order approximation:

$$u'' = 2F_{20}u + F_{10}; \quad (2,8)$$

$$v'' = 2F_{02}v. \quad (2,9)$$

Writing:

$$k_1^2 = -2F_{20}; \quad (2,10)$$

$$k_2^2 = -2F_{02}; \qquad (2,11)$$

and assuming:

$$k_1^2 \geqslant 0; \qquad k_2^2 \geqslant 0; \qquad (2,12)$$

the general solutions of (2, 8) and (2, 9) may written as:

$$u = a_1 \sin k_1 w + a_2 \cos k_1 w + F_{10}/k_1^2; \qquad (2,13)$$

$$v = b_1 \sin k_2 w + b_2 \cos k_2 w. \qquad (2,14)$$

Choosing as boundary conditions the parameters defining the ion trajectory at w = 0:

$$u(0) = u_o;\ u'(0) = \alpha;\ v(0) = v_o;\ v'(0) = \alpha_z, \qquad (2,15)$$

the particular solutions satisfying (2, 8) and (2, 9) read:

$$u = {}^{(1)}u(w) = u_o \cos k_1 w + \frac{\alpha}{k_1}\sin k_1 w + \frac{F_{10}}{k_1^2}(1-\cos k_1 w); \qquad (2,16)$$

$$v = {}^{(1)}v(w) = v_o \cos k_2 w + \frac{\alpha_z}{k_2}\sin k_2 w. \qquad (2,17)$$

If either of the conditions (2, 12) is not fulfilled, the field exerts a diverging action in radial or axial direction; we will not discuss these cases.

2d: *Second order approximation of the ion trajectories.*

Retaining the third order terms in (2, 5), substitution into (2, 1)-(2, 2) yields the simultaneous differential equations defining the second order approximation of the ion trajectories:

$$u'' - 2F_{20}u - F_{10} = 2guu'' + g(u'^2 - v'^2) + 2F_{30}u^2 + F_{12}v^2; \qquad (2,18)$$

$$v'' - 2F_{02}v = 2gu'v' + 2guv'' + 2F_{12}uv. \qquad (2,19)$$

(2, 19) gives the second order approximation related to focusing in axial direction (z- or v-direction). Small aberrations in

axial focusing are relatively unimportant, as they affect only the extension of the image in the direction of the image slit. Therefore, we will omit a discussion of (2, 19).

(2, 18) can be solved by the general method known as that of "variation of parameters", if the right hand member can be written as a function of w, say F(w):

$$u'' - 2F_{20}u - F_{10} = F(w). \qquad (2,20)$$

This can be accomplished by substituting the first order approximations (2, 16) and (2, 17) and their derivatives into the right hand member of (2, 18):

$$\begin{aligned} F(w) &= 2g\,{}^{(1)}u\,{}^{(1)}u'' + g\,{}^{(1)}u'^2 - {}^{(1)}v'^2 + \\ &\quad + 3F_{30}\,{}^{(1)}u^2 + F_{12}\,{}^{(1)}v^2 = \\ &= C_1\cos^2 k_1 w + C_2 \sin k_1 w \cos k_1 w + C_3 \sin^2 k_1 w + \\ &\quad + C_4 \cos k_1 w + C_5 \sin k_1 w + C_6 + \\ &\quad + C_7 \cos^2 k_2 w + C_8 \sin k_2 w \cos k_2 w + C_9 \sin^2 k_2 w, \end{aligned} \qquad (2,21)$$

where:

$$\begin{aligned} C_1 &= (3F_{30} - 2gk_1^2)u_o^2 + g\alpha^2 - 2F_{10}k_1^{-2}(3F_{30} - 2gk_1^2)u_o + \\ &\quad + F_{10}^2 k_1^{-4}(3F_{30} - 2gk_1^2); \\ C_2 &= 6(k_1^{-1}F_{30} - gk_1)u_o\alpha - 6k_1^{-3}(F_{30} - gk_1^2)\alpha; \\ C_3 &= gk_1^2 u_o^2 + (3k_1^{-2}F_{30} - 2g)\alpha^2 - 2gF_{10}u_o + gk_1^{-2}F_{10}^2; \\ C_4 &= 2k_1^{-2}F_{10}(3F_{30} - gk_1^2)u_o - 2k_1^{-4}F_{10}^2(3F_{30} - gk_1^2); \\ C_5 &= 2k_1^{-3}F_{10}(3F_{30} - gk_1^2)\alpha; \\ C_6 &= 3k_1^{-4}F_{10}^2 F_{30}; \\ C_7 &= F_{12}v_o^2 - g\alpha_z^2; \\ C_8 &= 2(k_2^{-1}F_{12} + 2gk_2)v_o\alpha_z; \\ C_9 &= k_2^{-2}F_{12}\alpha_z^2 - gk_2^2 v_o^2. \end{aligned} \qquad (2,22)$$

The particular solution of (2, 18) satisfying the boundary conditions (2, 15) is now given by:

$$\begin{aligned} u = {}^{(2)}u(w) = {}^{(1)}u(w) &+ \frac{\sin k_1 w}{k_1}\int_o^w \cos k_1 w \,.\, F(w)\,.\,dw + \\ &- \frac{\cos k_1 w}{k_1}\int_o^w \sin k_1 w.\ F(w).\,dw. \end{aligned} \qquad (2,23)$$

Straightforward integration leads to the second order approximation of the ion trajectories:

$$u = {}^{(2)}u(w) =$$
$$= H_1 u_o + H_2 \alpha + H_3 + H_{11} u_o^2 + H_{12} u_o \alpha + H_{22} \alpha^2 +$$
$$+ H_{44} v_o^2 + H_{45} v_o \alpha_z + H_{55} \alpha_z^2, \qquad (2,24)$$

where:

$$H_1 = \cos k_1 w - \tfrac{2}{3} k_1^{-4} F_{10} (3F_{30} - 2gk_1^2)(\sin^2 k_1 w - \cos k_1 w + 1) +$$
$$- \tfrac{2}{3} k_1^{-2} g F_{10} (1 - \cos k_1 w)^2 + k_1^{-4} F_{10} (3F_{30} - gk_1^2) k_1 w \sin k_1 w;$$

$$H_2 = k_1^{-1} \sin k_1 w + 2k_1^{-5} F_{10} (gk_1^2 - F_{30}) \sin k_1 w (1 - \cos k_1 w) +$$
$$+ k_1^{-5} F_{10} (3F_{30} - gk_1^2)(\sin k_1 w - k_1 w \cos k_1 w);$$

$$H_3 = k_1^{-2} F_{10} (1 - \cos k_1 w) + \tfrac{1}{3} k_1^{-6} F_{10}^2 (3F_{30} - 2gk_1^2)(\sin^2 k_1 w - \cos k_1 w + 1) +$$
$$+ \tfrac{1}{3} g k_1^{-4} F_{10}^2 (1 - \cos k_1 w)^2 - k_1^{-6} F_{10}^2 (3F_{30} - gk_1^2) k_1 w \sin k_1 w +$$
$$+ 3k_1^{-6} F_{10}^2 F_{30} (1 - \cos k_1 w);$$

$$H_{11} = \tfrac{1}{3} k_1^{-2} (3F_{30} - 2gk_1^2)(\sin^2 k_1 w - \cos k_1 w + 1) + \tfrac{1}{3} g (1 - \cos k_1 w)^2;$$

$$H_{12} = 2k_1^{-3} (F_{30} - gk_1^2) \sin k_1 w (1 - \cos k_1 w);$$

$$H_{22} = \tfrac{1}{3} g k_1^{-2} (\sin^2 k_1 w - \cos k_1 w + 1) + \tfrac{1}{3} k_1^{-4} (3F_{30} - 2gk_1^2)(1 - \cos k_1 w)^2;$$

$$H_{44} = k_1^{-2} (k_1^2 - 4k_2^2)^{-1} \{ F_{12} [k_1^2 \cos^2 k_2 w - (k_1^2 - 2k_2^2) \cos k_1 w - 2k_2^2] +$$
$$- gk_2^2 [-k_1^2 \cos^2 k_2 w + 2k_2^2 \cos k_1 w + k_1^2 - 2k_2^2] \};$$

$$H_{45} = 2k_2^{-1} (k_1^2 - 4k_2^2)^{-1} (F_{12} + gk_2^2)(\sin k_2 w \cos k_2 w - (k_2/k_1) \sin k_1 w);$$

$$H_{55} = k_1^{-2} k_2^{-2} (k_1^2 - 4k_2^2)^{-1} \{ F_{12} [-k_1^2 \cos^2 k_2 w + 2k_2^2 \cos k_1 w + k_1^2 - 2k_2^2] \} +$$
$$- gk_2^2 [k_1^2 \cos^2 k_2 w - (k_1^2 - 2k_2^2) \cos k_1 w - 2k_2^2] \}. \qquad (2,25)$$

2e: *Correlation with the magnetic field shape.*

The coefficients F_{00}, F_{10}, F_{20}, F_{02}, F_{30}, F_{12}, and g, should now be expressed in the magnetic field parameters and η of the ions. This may be accomplished by expanding A_w in a power series in u and v:

$$A_w = \sum_{i,k=0}^{\infty} a_{ik}^{*} u^i v^{2k}, \qquad (2,26)$$

(where the symmetry of A_w with respect to the median plane excludes terms with odd powers of v), and using the relation:

$$\operatorname{div} \vec{A} = 0. \qquad (2,27)$$

$\vec{A}$ is chosen in such a way that A_w is the only component of $\vec{A}$ differing from zero, and thus the relation

$$\nabla^2 A_w = 0 \qquad (2,27a)$$

is equivalent to (2,27). The components of the magnetic field strength are related to A_w through: (Grümm [18])

$$B_u = -\partial A_w/\partial v; \qquad (2,28)$$

$$B_v = \frac{1}{1+u}\frac{\partial}{\partial u}\left\{(1+u)A_w\right\}. \qquad (2,29)$$

Instead of the coefficients a^*_{ik} in (2,26), suitably chosen coefficients B, B_1, B_2, etc. may be written, which express the relations between the a^*_{ik} derived from (2,27) or (2,27a): (Grümm [18])

$$A_w = \tfrac{1}{2}B + \tfrac{1}{2}Bu + \tfrac{1}{2}B_1(u^2-v^2) - \tfrac{1}{3}(B_1+B_2)u^3 + (\tfrac{1}{2}B_1+B_2)uv^2 + \ldots \qquad (2,30)$$

$$B_u = B_1 v - (B_1+2B_2)uv + \ldots \qquad (2,31)$$

$$B_v = B + B_1 u - (\tfrac{1}{2}B_1+B_2)u^2 + B_2 v^2 + \ldots \qquad (2,32)$$

The condition

$$-\left[\left(\frac{r_m}{B_z}\right)\left(\frac{\partial B_z}{\partial r}\right)\right]_{r=r_m,\, z=0} = n, \qquad (2,33)$$

mentioned in the preceding chapter, corresponds to:

$$B_1/B = -n. \qquad (2,34)$$

The coefficient B_2 is so far undetermined. It may be written in the convenient form:

$$B_2/B = \tfrac{1}{2}\{X(1-n)-n\}. \qquad (2,35)$$

For $X \to n$ the field shape as defined by (2,30)-(2,35) reduces to that of a field which varies in the median plane proportional to r^{-n}, as may be seen by comparing (2,32) with the Taylor expansion of $B_v(u,0) = B(1+u)^{-n}$. For the more interesting case of the magnetic field between conical pole faces, it will be shown in chapter 4 that

$$X \equiv 2n. \qquad (4,10)$$

(2,30), (2,34), and (2,35) may now be substituted into (2,3), together with the condition for a purely magnetic deflecting field $\varphi = U$, yielding:

$$\begin{aligned} g &= \tfrac{1}{2}\,; \\ F_{00} &= 1 - \tfrac{1}{2}\eta B; \\ F_{10} &= 1 - \eta B; \\ F_{20} &= -\tfrac{1}{2}(1-n)\eta B; \\ F_{02} &= -\tfrac{1}{2}n\eta B; \\ F_{30} &= \tfrac{1}{6}X(1-n)\eta B; \\ F_{12} &= \tfrac{1}{2}\{n-X(1-n)\}\eta B. \end{aligned} \qquad (2,36)$$

If the ions have a velocity spread according to:

$$v = v_o(1+\beta) \qquad (2,37)$$

and if all ions have the same mass m_o and charge e, (2,37) is equivalent to:

$$\eta = \eta_o/(1+\beta) \qquad (2,38)$$

The product ηB may be expressed in β if we remind that the zeroth order approximation (2,6) sets the condition:

$$\eta_o B = 1. \qquad (2,39)$$

β is supposed to be a small quantity, small of the same order as α, u_o, α_z, v_o. We substitute (2,36), (2,38), (2,39), into (2,24)-(2,25), and expand (2,24) in a Taylor series in β. Retaining terms up to the second order in u_o, α, v_o, α_z, and β, we find the following expression for the second order approximation of the ion trajectories: (Tasman and Boerboom [30]; Wachsmuth, Boerboom and Tasman [31])

$$\begin{aligned} u = {}^{(2)}u(w) = \qquad\qquad (2,40) \\ = D_1 u_o + D_2\alpha + D_3\beta + D_{11}u_o^2 + D_{12}u_o\alpha + D_{22}\alpha^2 + \\ + D_{13}u_o\beta + D_{23}\alpha\beta + D_{33}\beta^2 + D_{44}v_o^2 + D_{45}v_o\alpha_z + D_{55}\alpha_z^2 . \end{aligned}$$

where, with:

$$\begin{aligned} w^* &= (1-n)^{\frac{1}{2}}\, w; \\ w^\dagger &= n^{\frac{1}{2}}\, w; \end{aligned} \qquad (2,41)$$

$$D_1 = \cos w^*$$

$$D_2 = (1-n)^{-\frac{1}{2}} \sin w^*$$

$$D_3 = (1-n)^{-1}(1-\cos w^*)$$

$$D_{11} = \tfrac{1}{6}\{(X-3)\sin^2 w^* + X(1-\cos w^*)\};$$

$$D_{12} = \tfrac{1}{3}(1-n)^{-\frac{1}{2}}(X-3)\sin w^*(1-\cos w^*);$$

$$D_{22} = \tfrac{1}{6}(1-n)^{-1}\{(X-3)\cos^2 w^* - (2X-3)\cos w^* + X\};$$

$$D_{13} = \tfrac{1}{6}(1-n)^{-1}\{-2(X-3)\sin^2 w^* - 2X(1-\cos w^*) + 3(X-n)w^*\sin w^*\};$$

$$D_{23} = \tfrac{1}{6}(1-n)^{-3/2}\{2(X-3)\sin w^*\cos w^* + (X-3n+6)\sin w^* - 3(X-n)w^*\cos w^*\};$$

$$D_{33} = \tfrac{1}{6}(1-n)^{-2}\{(X-3)\sin^2 w^* + 4X(1-\cos w^*) - 3(X-n)w^*\sin w^*\};$$

$$D_{44} = \tfrac{1}{4}(1-5n)^{-1}\{\langle 2n-X(1-n)\rangle\cos 2w\dagger - 2(n-X+3nX)\cos w^* - X(1-5n)\};$$

$$D_{45} = \tfrac{1}{2}(1-5n)^{-1}\langle 2n-X(1-n)\rangle\{n^{-\frac{1}{2}}\sin 2w\dagger - 2(1-n)^{-\frac{1}{2}}\sin w^*\};$$

$$D_{55} = -\tfrac{1}{4}n^{-1}(1-5n)^{-1}\{\langle 2n-X(1-n)\rangle\cos 2w\dagger - 2n(1-2X)\cos w^* + X(1-5n)\}.$$

(2, 42)

2f: *Imaging properties of the inhomogeneous magnetic sector field.*

If the boundaries are plane and normal to the main path at the points where it enters and leaves the field, the boundary conditions (2, 15) are easily related to the parameters in the object space. From Fig. 2 we read the relations:

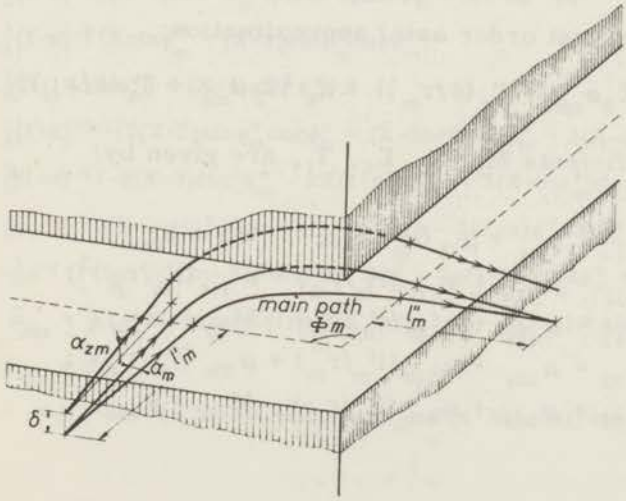

Fig. 2.

$$u_o = (l'_m/r_m)\alpha_m; \quad \alpha = (1+u_o)\alpha_m = \alpha_m + (l'_m/r_m)\alpha_m^2;$$
$$v_o = (l'_m/r_m)\alpha_{zm} + \delta/r_m; \quad \alpha_z = \alpha_{zm} + (l'_m/r_m)\alpha_m\alpha_{zm} \qquad (2,43)$$

The rectilinear path in the image space may be defined by the relations:

$$y_2 = y_2(x_2) = y_2(0) + (dy_2/dx_2)x_2; \qquad (2,44)$$
$$z_2 = z_2(x_2) = z_2(0) + (dz_2/dx_2)x_2. \qquad (2,45)$$

If the sector angle equals ϕ_m, we may write analogous to (2, 43):

$$y_2(0) = r_m u(\phi_m); \qquad z_2(0) = r_m v(\phi_m);$$
$$dy_2/dx_2 = u'(\phi_m)/(1+u(\phi_m)) \equiv u'(\phi_m).(1-u(\phi_m)); \qquad (2,46)$$
$$dz_2/dx_2 = v'(\phi_m)/(1+u(\phi_m)) \equiv v'(\phi_m).(1-u(\phi_m)).$$

From (2, 17), (2, 40)-(2, 42), (2, 43)-(2,46) we find the following expression for the second order radial approximation of the ion trajectory in the image space:

$$y_2 = r_m\{M_1\alpha_m + M_2\beta + M_{11}\alpha_m^2 + M_{12}\alpha_m\beta + M_{22}\beta^2 + M_{33}\alpha_{zm}^2 + M_{34}\alpha_{zm}(\delta/r_m) + M_{44}(\delta/r_m)^2\} + x_2\{N_1\alpha_m + N_2\beta + N_{11}\alpha_m^2 + N_{12}\alpha_m\beta + N_{22}\beta^2 + N_{33}\alpha_{zm}^2 + N_{34}\alpha_{zm}(\delta/r_m) + N_{44}(\delta/r_m)^2\}; \qquad (2,47)$$

and for the first order axial approximation:

$$z_2 = r_m\{\Sigma_3\alpha_{zm} + \Sigma_4(\delta/r_m)\} + x_2\{T_3\alpha_{zm} + T_4(\delta/r_m)\}. \qquad (2,48)$$

The coefficients M_i, N_i, Σ_i, T_i, are given by:

$$M_1 = \mu_{1a} + \mu_{1b}(l'_m/r_m); \quad M_2 = \mu_{2a};$$
$$M_{11} = \mu_{11a} + \mu_{11b}(l'_m/r_m) + \mu_{11c}(l'_m/r_m)^2;$$
$$M_{12} = \mu_{12a} + \mu_{12b}(l'_m/r_m); \quad M_{22} = \mu_{22a}; \qquad (2,49)$$
$$M_{33} = \mu_{33a} + \mu_{33b}(l'_m/r_m) + \mu_{33c}(l'_m/r_m)^2;$$
$$M_{34} = \mu_{34a} + \mu_{34b}(l'_m/r_m); \quad M_{44c} = \mu_{44a}.$$

$$
\begin{aligned}
N_1 &= \nu_{1a} + \nu_{1b}\,(l'_m/r_m); \quad N_2 = \nu_{2a}; \\
N_{11} &= \nu_{11a} + \nu_{11b}\,(l'_m/r_m) + \nu_{11c}(l'_m/r_m)^2; \\
N_{12} &= \nu_{12a} + \nu_{12b}\,(l'_m/r_m); \quad N_{22} = \nu_{22a}; \\
N_{33} &= \nu_{33a} + \nu_{33b}\,(l'_m/r_m) + \nu_{33c}\,(l'_m/r_m)^2; \\
N_{34} &= \nu_{34a} + \nu_{34b}\,(l'_m/r_m); \quad N_{44} = \nu_{44a}.
\end{aligned} \tag{2,50}
$$

$$
\Sigma_3 = \sigma_{3a} + \sigma_{3b}\,(l'_m/r_m); \qquad \Sigma_4 = \sigma_{4a}. \tag{2,51}
$$

$$
T_3 = \tau_{3a} + \tau_{3b}\,(l'_m/r_m); \qquad T_4 = \tau_{4a}. \tag{2,52}
$$

As will appear from further generalisations, the expressions (2,47)-(2,52) are valid for *any* sector field in the degree of approximation used here. For the special case of normal entry and exit at plane boundaries, the coefficients μ_i, ν_i, σ_i, τ_i, are equal to $\bar{\mu}_i$, $\bar{\nu}_i$, $\bar{\sigma}_i$, $\bar{\tau}_i$, respectively, which read with the abbreviations:

$$
\phi^*_m = (1-n)^{\frac{1}{2}}\,\phi_m; \quad \phi^\dagger_m = n^{\frac{1}{2}}\phi_m; \tag{2,53}
$$

$$
\begin{aligned}
\bar{\mu}_{1a} &= (1-n)^{-\frac{1}{2}}\sin\phi^*_m; \qquad \bar{\mu}_{1b} = \cos\phi^*_m; \\
\bar{\mu}_{2a} &= (1-n)^{-1}(1-\cos\phi^*_m); \\
\bar{\mu}_{11a} &= \tfrac{1}{6}(1-n)^{-1}\{(X-3)\cos^2\phi^*_m - (2X-3)\cos\phi^*_m + X\}; \\
\bar{\mu}_{11b} &= \tfrac{1}{3}(1-n)^{-\frac{1}{2}}\{X\sin\phi^*_m - (X-3)\sin\phi^*_m\cos\phi^*_m\}; \\
\bar{\mu}_{11c} &= \tfrac{1}{6}\{X(1-\cos\phi^*_m) + (X-3)\sin^2\phi^*_m\}; \\
\bar{\mu}_{12a} &= \tfrac{1}{6}(1-n)^{-3/2}\{2(X-3)\sin\phi^*_m\cos\phi^*_m + (X-3n+6)\sin\phi^*_m - 3(X-n)\phi^*_m\cos\phi^*_m\}; \\
\bar{\mu}_{12b} &= \tfrac{1}{6}(1-n)^{-1}\{-2(X-3)\sin^2\phi^*_m - 2X(1-\cos\phi^*_m) + 3(X-n)\phi^*_m\sin\phi^*_m\}; \\
\bar{\mu}_{22a} &= \tfrac{1}{6}(1-n)^{-2}\{(X-3)\sin^2\phi^*_m + 4X(1-\cos\phi^*_m) - 3(X-n)\phi^*_m\sin\phi^*_m\}; \\
\bar{\mu}_{33a} &= -\tfrac{1}{4}n^{-1}(1-5n)^{-1}\{\langle 2n-X(1-n)\rangle\cos 2\phi^\dagger_m - 2n(1-2X)\cos\phi^*_m + X(1-5n)\}; \\
\bar{\mu}_{33b} &= \bar{\mu}_{34a} = \tfrac{1}{2}(1-5n)^{-1}\langle 2n-X(1-n)\rangle\{n^{-\frac{1}{2}}\sin 2\phi^\dagger_m - 2(1-n)^{-\frac{1}{2}}\sin\phi^*_m\}; \\
\bar{\mu}_{33c} &= \bar{\mu}_{44a} = \tfrac{1}{2}\bar{\mu}_{34b} = \\
&= \tfrac{1}{4}(1-5n)^{-1}\{\langle 2n-X(1-n)\rangle\cos 2\phi^\dagger_m - 2\langle n-X(1-3n)\rangle\cos\phi^*_m - X(1-5n)\}.
\end{aligned} \tag{2,54}
$$

$$\bar{\nu}_{1a} = \cos\phi_m^*; \qquad \bar{\nu}_{1b} = -(1-n)^{\frac{1}{2}}\sin\phi_m^*;$$

$$\bar{\nu}_{2a} = (1-n)^{-\frac{1}{2}}\sin\phi_m^*;$$

$$\bar{\nu}_{11a} = \tfrac{1}{6}(1-n)^{-\frac{1}{2}}\{-2X\sin\phi_m^*\cos\phi_m^* + (2X-3)\sin\phi_m^*\};$$

$$\bar{\nu}_{11b} = \tfrac{1}{3}X\{2\sin^2\phi_m^* + \cos\phi_m^* - 1\};$$

$$\bar{\nu}_{11c} = \tfrac{1}{6}(1-n)^{\frac{1}{2}}X\sin\phi_m^*(2\cos\phi_m^* + 1);$$

$$\bar{\nu}_{12a} = \tfrac{1}{6}(1-n)^{-1}\{-4X\sin^2\phi_m^* + 2X(1-\cos\phi_m^*) + 3(X-n)\phi_m^*\sin\phi_m^*\};$$

$$\bar{\nu}_{12b} = \tfrac{1}{6}(1-n)^{-\frac{1}{2}}\{-4X\sin\phi_m^*\cos\phi_m^* + (X-3n+6)\sin\phi_m^* + 3(X-n)\phi_m^*\cos\phi_m^*\};$$

$$\bar{\nu}_{22a} = \tfrac{1}{6}(1-n)^{-3/2}\{2X\sin\phi_m^*\cos\phi_m^* + (X+3n-6)\sin\phi_m^* - 3(X-n)\phi_m^*\cos\phi_m^*\};$$

$$\bar{\nu}_{33a} = \tfrac{1}{2}(1-5n)^{-1}\{n^{-\frac{1}{2}}(2n-X(1-n))\sin 2\phi_m^\dagger + (1-n)^{\frac{1}{2}}(2X-1)\sin\phi_m^*\};$$

$$\bar{\nu}_{33b} = \bar{\nu}_{34a} = (1-5)^{-1}(2n-X(1-n))(\cos 2\phi_m^\dagger - \cos\phi_m^*);$$

$$\bar{\nu}_{33c} = \bar{\nu}_{44a} = \tfrac{1}{2}\bar{\nu}_{34b} =$$

$$= \tfrac{1}{2}(1-5n)^{-1}\{-(2n-X(1-n))n^{\frac{1}{2}}\sin 2\phi_m^\dagger + (n-X(1-n))(1-n)^{\frac{1}{2}}\sin\phi_m^*\}. \qquad (2,55)$$

$$\bar{\sigma}_{3a} = n^{-\frac{1}{2}}\sin\phi_m^\dagger; \quad \bar{\sigma}_{3b} = \bar{\sigma}_{4a} = \bar{\tau}_{3a} = \cos\phi_m^\dagger; \quad \bar{\tau}_{3b} = \bar{\tau}_{4a} = -n^{\frac{1}{2}}\sin\phi_m^\dagger. \qquad (2,56)$$

If the field boundaries are plane, but the incidence and/or exit of the main path is oblique, the situation becomes more complex. The general expressions (2,47)-(2,52) are still equally applicable, but instead of (2,54)-(2,56) more general expressions should be used.

In case of oblique incidence and/or exit, the axial focusing action due to the stray fields has to be taken into account. (Herzog [8.32]). They act as thin lenses on the entrance and exit side, which have focal lengths for axial focusing f'_{str} and f''_{str} respectively, given by:

$$r_m/f'_{str} = \tan\epsilon'; \qquad r_m/f''_{str} = \tan\epsilon''. \qquad (2,57)$$

The meaning of ϵ' and ϵ'' may be seen from Figs. 3-5; they are taken to be positive as indicated in these figures.

The radial effect of oblique incidence may be deduced from Fig. 4, which represents a projection on the median plane. The object is projected at O; OAE is the main path; OA = l'_m; MA = ME = r_m. If the trajectories in the field region are measured

in the coordinates u, v, w, (Fig. 1), the origin of w may still be chosen. With normal incidence we chose w=0 at the point of entrance of the main path. Now in Fig. 4, two such coordinate systems are indicated, differing only in origin. The first

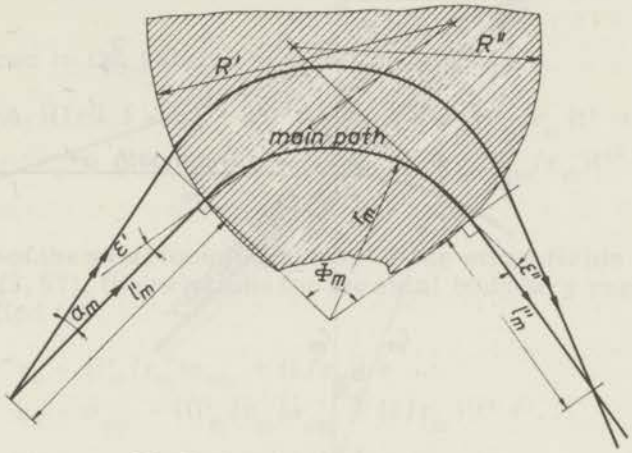

Fig. 3. Curved oblique boundaries.

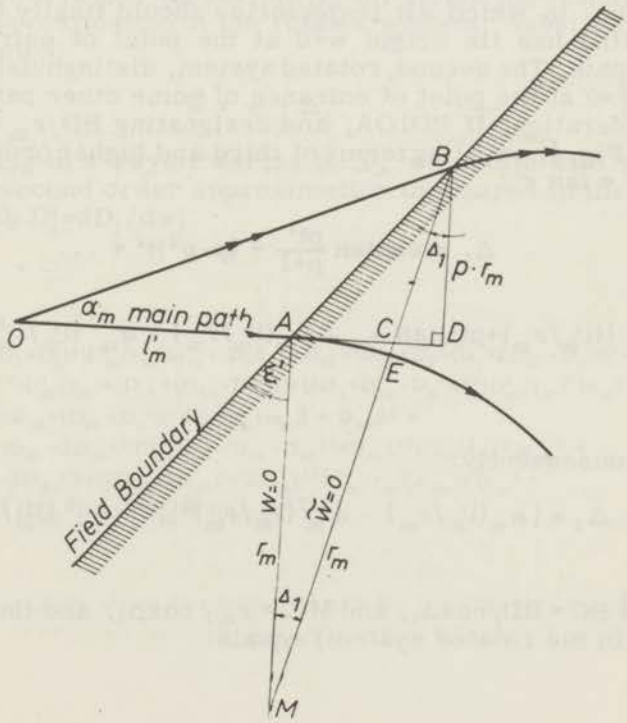

Fig. 4. Oblique entrance.

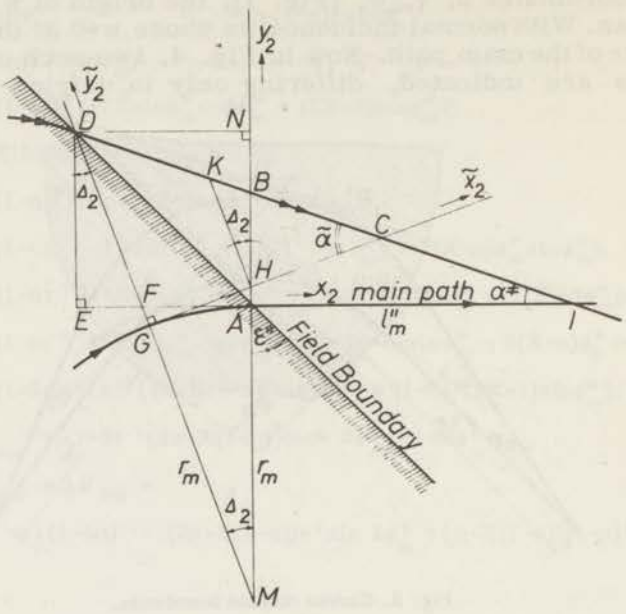

Fig. 5. Oblique exit.

system, in which all trajectories should finally be expressed, still has its origin w=0 at the point of entrance of the main path. The second, rotated system, distinghuished by a $''$, has $\tilde{w}=0$ at the point of entrance of some other path OB under consideration. If BD⊥OA, and designating $BD/r_m = p$, we read from Fig. 4, omitting terms of third and higher order and writing $t' = \tan \epsilon'$:

$$\Delta_1 = \arctan \frac{pt'}{p+1} = (p-p^2)t' + \ldots \qquad (2,58)$$

$$p = \{(l'_m/r_m)+pt'\}\tan \alpha_m = \alpha_m(l'_m/r_m) + \alpha_m{}^2(l'_m/r_m)t' + \ldots \qquad (2,59)$$

and consequently:

$$\Delta_1 = \{\alpha_m(l'_m/r_m) - \alpha_m{}^2(l'_m/r_m)^2\}t' + \alpha_m{}^2(l'_m/r_m)t'^2 + \ldots \qquad (2,60)$$

Now $BC = BD/\cos\Delta_1$, and $MC = r_m/\cos\Delta_1$, and thus $\tilde{u}_o$(measured in the rotated system) equals:

$$\tilde{u}_o = \frac{BE}{r_m} = \frac{p+1}{\cos\Delta_1} - 1 =$$
$$= \alpha_m(l'_m/r_m) + \alpha_m{}^2(l'_m/r_m)t' + \tfrac{1}{2}\alpha_m{}^2(l'_m/r_m)^2 t'^2 + \ldots \qquad (2,61)$$

$\tilde{\alpha}$ (measured in the rotated system) equals:

$$\tilde{\alpha} = (\alpha_m+\Delta_1)(1+\tilde{u}_o) = \alpha_m + \alpha_m{}^2(l'_m/r_m) + \alpha_m(l'_m/r_m)t' + \alpha_m{}^2(l'_m/r_m)t'^2 + \ldots \qquad (2,62)$$

Because of the axial focusing action of the stray fields represented by (2, 57), the relations for the axial boundary conditions are modified to:

$$v_o = (l'_m/r_m)\alpha_{zm} + (\delta/r_m) + \ldots \qquad (2,63)$$
$$\alpha_z = \alpha_{zm} - \{(l'_m/r_m)\alpha_{zm} + (\delta/r_m)\}t' + \ldots \qquad (2,64)$$

(2, 63)-(2, 64) are valid for the rotated as well as for the fixed coordinate system.

Substitution of (2, 61)-(2, 64) into (2, 40) yields the radial second order approximation in the rotated system. Substituting in this expression:

$$\tilde{w} = w - \Delta_1, \qquad (2,65)$$

and expanding in a Taylor series in Δ_1, we obtain with (2, 60) the radial second order approximation measured in the fixed system (with $D'_j = dD_j/dw$):

$$\begin{aligned}
u = u(w) = \\
= [D_2+\{D_1+D_2t'\}(l'_m/r_m)]\alpha_m + D_3\beta + [D_{22}+\{D_{12}+D_2+(D_1+2D_{22}-D_2')t' + \\
+D_2t'^2\}(l'_m/r_m)+\{D_{11}+(D_{12}-D_1')t'+(\tfrac{1}{2}D_1+D_{22}-D_2')t'^2\}(l'_m/r_m)^2]\alpha_m{}^2 + \\
+[D_{23}+\{D_{13}+(D_{23}-D_3')t'\}(l'_m/r_m)]\alpha_m\beta + D_{33}\beta^2 + \\
+[D_{55}+\{D_{45}-2D_{55}t'\}(l'_m/r_m)+\{D_{44}-D_{45}t'+D_{55}t'^2\}(l'_m/r_m)^2]\alpha_{zm}{}^2 + \\
+[\{D_{45}-2D_{55}t'\}+\{2D_{44}-2D_{45}t'+2D_{55}t'^2\}(l'_m/r_m)]\alpha_{zm}(\delta/r_m) + \\
+[D_{44}-D_{45}t'+D_{55}t'^2](\delta/r_m)^2.
\end{aligned} \qquad (2,66)$$

To find the relations for oblique exit, the projection on the median plane is represented in Fig. 5. Besides the fixed coordinate system x_2, y_2, (with its origin at the point of exit A of the main path GAI, and with the x_2-axis coinciding with the main path in the image space), a second, rotated coordinate system is indicated, distinguished by a "~". The plane $\tilde{x}_2=0$ of this second system includes the point of exit of some other path DBCI under consideration. $GM = AM = r_m$. Writing $\tilde{U} = DG/r_m$, the path DBCI is represented relative to the rotated system by:

$$\tilde{y}_2 = r_m\tilde{U} - \tilde{x}_2\tan\tilde{\alpha} . \qquad (2,67)$$

Writing $U^{\ddagger} = AB/r_m$, the corresponding expression relative to the fixed coordinate system is:

$$y_2 = r_m U^{\ddagger} - x_2\tan\alpha^{\ddagger} . \qquad (2,68)$$

We designate by U, U', U'', the values of u, du/dw, d^2u/dw^2, respectively at $w = \phi_m$, irrespective of the termination of the deflecting field by the field boundary. We have:

$$\tilde{U} = U - U'\Delta_2 + \tfrac{1}{2}U''\Delta_2^2 - \ldots \qquad (2,69)$$

Now $MF = r_m/\cos\Delta_2$; $DE = DF\cos\Delta_2$; $DN = EA = DE\tan\epsilon''$, and consequently, writing $t'' = \tan\epsilon''$:

$$\Delta_2 = \arcsin(DN/DM) = Ut'' - U^2t''^2 - UU't''^2 - \tfrac{1}{2}U^2t''^3 + \ldots \qquad (2,70)$$

$$\tilde{U} = U - UU't'' + \ldots \qquad (2,71)$$

We have:

$$\tilde{\alpha} = -\tilde{U}' + \tilde{U}\tilde{U}' + \ldots = -U' + UU' + UU''t'' + \ldots \qquad (2,72)$$

Now $\Delta DCG \backsim \Delta KCH$, and thus: $KH = r_m(\tilde{U} - \tan\tilde{\alpha}\tan\Delta_2)$. As $\Delta KBH \backsim \Delta DBM$, it follows that:

$$U^{\ddagger} = AB/r_m = U + \tfrac{1}{2}U^2t''^2 + \ldots \qquad (2,73)$$

From Fig. 5, we read:

$$\alpha^{\ddagger} = \tilde{\alpha} - \Delta_2 = -U'+UU'+(-U+UU''+U^2)t''+UU't''^2+\tfrac{1}{2}U^2t''^3 + \ldots \qquad (2,74)$$

Substitution of (2,73)-(2,74) into (2,68), using (2,66), and evaluating the expressions D_j and their derivatives for $w = \phi_m$,

leads to the second order radial approximation of the ion trajectory in the image space with oblique incidence and exit. Before evaluating the results, however, we will include the effect of curved boundaries.

A discussion of the effect of curved boundaries for homogeneous magnetic sector fields was presented by König and Hintenberger [33]. The curvature changes only some of the second order coefficients of the μ_i, ν_i. The effect of boundary curvature being of second order, the reasoning of König and Hintenberger applies equally to inhomogeneous magnetic sector fields. The radii of curvature of the entrance and exit boundaries R' and R'' are to be taken positive as indicated in Fig. 3.

On evaluation of the above arguments, it is found that the coefficients μ_i, ν_i, for the general case of oblique curved boundaries, appearing in (2,47), (2,49)-(2,50), may be expressed in the coefficients $\bar{\mu}_i$, $\bar{\nu}_i$, for the corresponding case of normal entry and exit at plane boundaries with the same field shape and sector angle. Using the abbreviations:

$$t' = \tan \epsilon'; \qquad \rho' = \frac{r_m}{2R'\cos^3\epsilon'};$$
$$t'' = \tan \epsilon''; \qquad \rho'' = \frac{r_m}{2R''\cos^3\epsilon''}; \tag{2,75}$$

these relations read: (Tasman, Boerboom, and Wachsmuth [34])

$$\begin{aligned}
&\mu_{1a} = \bar{\mu}_{1a}; \qquad \mu_{1b} = \bar{\mu}_{1b} + \bar{\mu}_{1a} t';\\
&\mu_{2a} = \bar{\mu}_{2a}; \qquad \mu_{11a} = \bar{\mu}_{11a} + \tfrac{1}{2}\bar{\mu}_{1a}{}^2 t''^2;\\
&\mu_{11b} = \bar{\mu}_{11b} + 2\bar{\mu}_{11a} t' + \bar{\mu}_{1a} t'^2 + \bar{\mu}_{1b}\bar{\mu}_{1a} t''^2 + \bar{\mu}_{1a}{}^2 t't''^2;\\
&\mu_{11c} = \bar{\mu}_{11c} + (\bar{\mu}_{11b} - n\bar{\mu}_{1a})t' + (\bar{\mu}_{11a} - \tfrac{1}{2}\bar{\mu}_{1b})t'^2 + \tfrac{1}{2}\bar{\mu}_{1b}{}^2 t''^2 +\\
&\qquad + \bar{\mu}_{1a}\bar{\mu}_{1b} t't''^2 + \tfrac{1}{2}\bar{\mu}_{1a}{}^2 t'^2 t''^2 + \rho'\bar{\mu}_{1a};\\
&\mu_{12a} = \bar{\mu}_{12a} + \bar{\mu}_{1a}\bar{\mu}_{2a} t''^2;\\
&\mu_{12b} = \bar{\mu}_{12b} + (\bar{\mu}_{12a} - \bar{\mu}_{1a})t' + \bar{\mu}_{1b}\bar{\mu}_{2a} t''^2 + \bar{\mu}_{1a}\bar{\mu}_{2a} t't''^2;\\
&\mu_{22a} = \bar{\mu}_{22a} + \tfrac{1}{2}\bar{\mu}_{2a} t''^2; \qquad \mu_{33a} = \bar{\mu}_{33a};\\
&\mu_{33b} = \mu_{34a} = \bar{\mu}_{33b} - 2\bar{\mu}_{33a} t';\\
&\mu_{33c} = \mu_{44a} = \tfrac{1}{2}\mu_{34b} = \bar{\mu}_{33c} - \bar{\mu}_{33b} t' + \bar{\mu}_{33a} t'^2.
\end{aligned} \tag{2,76}$$

$$
\begin{aligned}
\nu_{1a} &= \bar{\nu}_{1a} + \bar{\mu}_{1a} t'';\\
\nu_{1b} &= \bar{\nu}_{1b} + \bar{\nu}_{1a} t' + \bar{\mu}_{1b} t'' + \bar{\mu}_{1a} t' t'';\\
\nu_{2a} &= \bar{\nu}_{2a} + \bar{\mu}_{2a} t'';\\
\nu_{11a} &= \bar{\nu}_{11a} + (\bar{\mu}_{11a} - n\bar{\mu}_{1a}^{\,2}) t'' - \bar{\mu}_{1a}\bar{\nu}_{1a} t''^2 - \tfrac{1}{2}\bar{\mu}_{1a}^{\,2} t''^3 + \rho''\bar{\mu}_{1a}^{\,2};\\
\nu_{11b} &= \bar{\nu}_{11b} + 2\bar{\nu}_{11a} t' + (\bar{\mu}_{11b} - 2n\bar{\mu}_{1a}\bar{\mu}_{1b}) t'' + \bar{\nu}_{1a} t'^2 +\\
&\quad + 2(\bar{\mu}_{11a} - n\bar{\mu}_{1a}^{\,2}) t' t'' - (\bar{\mu}_{1a}\bar{\nu}_{1b} + \bar{\mu}_{1b}\bar{\nu}_{1a}) t''^2 +\\
&\quad - \bar{\mu}_{1a}\bar{\mu}_{1b} t''^3 - 2\bar{\mu}_{1a}\bar{\nu}_{1a} t' t''^2 + \bar{\mu}_{1a} t'^2 t'' +\\
&\quad - \bar{\mu}_{1a}^{\,2} t' t''^3 + 2\rho''(\bar{\mu}_{1a}\bar{\mu}_{1b} + \bar{\mu}_{1a}^{\,2} t');\\
\nu_{11c} &= \bar{\nu}_{11c} + (\bar{\nu}_{11b} - n\bar{\nu}_{1a}) t' + (\bar{\mu}_{11c} - n\bar{\mu}_{1b}^{\,2}) t'' + (\bar{\nu}_{11a} - \tfrac{1}{2}\bar{\nu}_{1b}) t'^2 +\\
&\quad + (\bar{\mu}_{11a} - n\bar{\mu}_{1a}^{\,2} - \tfrac{1}{2}\bar{\mu}_{1b}) t'^2 t'' + (\bar{\mu}_{11b} - 2n\bar{\mu}_{1a}\bar{\mu}_{1b} - n\bar{\mu}_{1a}) t' t'' +\\
&\quad - \bar{\mu}_{1b}\bar{\nu}_{1b} t''^2 - (\bar{\mu}_{1a}\bar{\nu}_{1b} + \bar{\mu}_{1b}\bar{\nu}_{1a}) t' t''^2 - \tfrac{1}{2}\bar{\mu}_{1b}^{\,2} t''^3 +\\
&\quad - \bar{\mu}_{1a}\bar{\mu}_{1b} t' t''^3 - \bar{\mu}_{1a}\bar{\nu}_{1a} t'^2 t''^2 - \tfrac{1}{2}\bar{\mu}_{1a}^{\,2} t'^2 t''^3 +\\
&\quad + \rho''(\bar{\mu}_{1b}^{\,2} + 2\bar{\mu}_{1a}\bar{\mu}_{1b} t' + \bar{\mu}_{1a}^{\,2} t'^2) + \rho'(\bar{\nu}_{1a} + \bar{\mu}_{1a} t'');\\
\nu_{12a} &= \bar{\nu}_{12a} + (\bar{\mu}_{12a} - 2n\bar{\mu}_{1a}\bar{\mu}_{2a} - \bar{\mu}_{1a}) t'' - (\bar{\mu}_{1a}\bar{\nu}_{2a} + \bar{\mu}_{2a}\bar{\nu}_{1a}) t''^2 +\\
&\quad - \bar{\mu}_{1a}\bar{\mu}_{2a} t''^3 + 2\rho''\bar{\mu}_{1a}\bar{\mu}_{2a};\\
\nu_{12b} &= \bar{\nu}_{12b} + (\bar{\nu}_{12a} - \bar{\nu}_{1a}) t' + (\bar{\mu}_{12b} - 2n\bar{\mu}_{1b}\bar{\mu}_{2a} - \bar{\mu}_{1b}) t'' +\\
&\quad - (\bar{\mu}_{1b}\bar{\nu}_{2a} + \bar{\mu}_{2a}\bar{\nu}_{1b}) t''^2 + (\bar{\mu}_{12a} - 2n\bar{\mu}_{1a}\bar{\mu}_{2a} - 2\bar{\mu}_{1a}) t' t'' +\\
&\quad - \bar{\mu}_{1b}\bar{\mu}_{2a} t''^3 - (\bar{\mu}_{1a}\bar{\nu}_{2a} + \bar{\mu}_{2a}\bar{\nu}_{1a}) t' t''^2 - \bar{\mu}_{1a}\bar{\mu}_{2a} t' t''^3 +\\
&\quad + 2\rho''(\bar{\mu}_{1b}\bar{\mu}_{2a} + \bar{\mu}_{1a}\bar{\mu}_{2a} t');\\
\nu_{22a} &= \bar{\nu}_{22a} + (\bar{\mu}_{22a} - n\bar{\mu}_{2a}^{\,2} - \bar{\mu}_{2a}) t'' - \bar{\mu}_{2a}\bar{\nu}_{2a} t''^2 - \tfrac{1}{2}\bar{\mu}_{2a}^{\,2} t''^3 + \rho''\bar{\mu}_{2a}^{\,2};\\
\nu_{33a} &= \bar{\nu}_{33a} + \bar{\mu}_{33a} t'';\\
\nu_{33b} &= \nu_{34a} = \bar{\nu}_{33b} - 2\bar{\nu}_{33a} t' + \bar{\mu}_{33b} t'' - 2\bar{\mu}_{33a} t' t'';\\
\nu_{33c} &= \nu_{44a} = \tfrac{1}{2}\nu_{34b} = \bar{\nu}_{33c} - \bar{\nu}_{33b} t' + \bar{\mu}_{33c} t'' + \bar{\nu}_{33a} t'^2 +\\
&\quad - \bar{\mu}_{33b} t' t'' + \bar{\mu}_{33a} t'^2 t''.
\end{aligned}
\qquad (2,77)
$$

The axial focusing effect, due to the fringing fields, and represented by (2,57), should be taken into account in the coefficients σ_j, τ_j. If these are expressed in the corresponding coefficients $\bar{\sigma}_j$, $\bar{\tau}_j$, for normal incidence and exit, the relations read:

$$
\left.
\begin{aligned}
&\sigma_{3a} = \bar{\sigma}_{3a}; \qquad \sigma_{3b} = \sigma_{4a} = \bar{\sigma}_{3b} + \bar{\sigma}_{3a} t';\\
&\tau_{3a} = \bar{\tau}_{3a} + \bar{\sigma}_{3a} t'';\\
&\tau_{3a} = \tau_{4a} = \bar{\tau}_{3b} + \bar{\tau}_{3a}(t'+t'') + \bar{\sigma}_{3a} t' t''.
\end{aligned}
\right\} \qquad (2,78)
$$

For homogeneous magnetic sector fields ($n = X = 0$), the results become identical with those derived by Hintenberger and König [35] for this case.

2g: *Discussion.*

The contribution to y_2 of the term proportional to α_m vanishes for $x_2 = -r_m(M_1/N_1)$. For very small values of β, a beam of ions of equal mass and charge, emerging from an object slit at the object distance l'_m from the entrance boundary, is then focused in first order at the image distance:

$$l''_m = -r_m(M_1/N_1). \tag{2,79}$$

This first order focusing property may be put in the familiar form:

$$(l'_m - g')(l''_m - g'') = f^2, \tag{2,80}$$

where, using the abbreviations (2,53) and (2,75):

$$\frac{g'}{r_m} = \frac{(1-n)^{\frac{1}{2}}\cos\phi^*_m + \sin\phi^*_m t''}{(1-n)\sin\phi^*_m - (1-n)^{\frac{1}{2}}\cos\phi^*_m(t'+t'') - \sin\phi^*_m t't''}; \tag{2,81}$$

$$\frac{g''}{r_m} = \frac{(1-n)^{\frac{1}{2}}\cos\phi^*_m + \sin\phi^*_m t'}{(1-n)\sin\phi^*_m - (1-n)^{\frac{1}{2}}\cos\phi^*_m(t'+t'') - \sin\phi^*_m t't''}; \tag{2,82}$$

$$\frac{f}{r_m} = \frac{1}{(1-n)^{\frac{1}{2}}\sin\phi^*_m - \cos\phi^*_m(t'+t'') - (1-n)^{-\frac{1}{2}}\sin\phi^*_m t't''}. \tag{2,83}$$

Similarly, first order focusing in axial direction occurs at the axial image distance l''_{zm}:

$$l''_{zm} = -r_m(\Sigma_3/T_3), \tag{2,84}$$

which may again be put in the form:

$$(l'_{zm} - g'_z)(l''_{zm} - g''_z) = f_z^2, \tag{2,85}$$

where:

$$\frac{g'_z}{r_m} = \frac{n^{\frac{1}{2}}\cos\phi^\dagger_m + \sin\phi^\dagger_m t''}{n\sin\phi^\dagger_m - n^{\frac{1}{2}}\cos\phi^\dagger_m(t'+t'') - \sin\phi^\dagger_m t't''}; \tag{2,86}$$

$$\frac{g_z''}{r_m} = \frac{n^{\frac{1}{2}}\cos\phi_m^{\dagger} + \sin\phi_m^{\dagger} t'}{n\sin\phi_m^{\dagger} - n^{\frac{1}{2}}\cos\phi_m^{\dagger}(t'+t'') - \sin\phi_m^{\dagger} t't''}; \qquad (2,87)$$

$$\frac{f_z}{r_m} = \frac{1}{n^{\frac{1}{2}}\sin\phi_m^{\dagger} - \cos\phi_m^{\dagger}(t'+t'') - n^{-\frac{1}{2}}\sin\phi_m^{\dagger} t't''}. \qquad (2,88)$$

If all ions are of the same energy eU, but a small difference in mass is allowed according to:

$$m = m_o + \delta m, \qquad (2,89)$$

the corresponding difference in η equals, instead of (2,38),

$$\eta = \eta_o/(1+\frac{\delta m}{2m_o}). \qquad (2,90)$$

Consequently, the mass dispersion in the y_2-direction at the image distance l_m'', per unit $\delta m/m_o$ for a monoenergetic ion beam is given by:

$$D_m = \tfrac{1}{2} r_m(M_2 - (M_1/N_1)N_2). \qquad (2,91)$$

However, the focusing plane of the mass spectrum need not be perpendicular to the main path, as the image distance depends on the mass difference:

$$l_m'' = -r_m\frac{M_1 + \frac{1}{2}M_{12}(\delta m/m_o)}{N_1 + \frac{1}{2}N_{12}(\delta m/m_o)}. \qquad (2,92)$$

Elimination of $(\delta m/m_o)$ from (2,91) and (2,92) gives the inclination of the focusing plane.

Object and image are at the same electrostatic potential. Thus the lateral magnification M_{lat} is the reciprocal of the angular magnification M_{ang} (both in radial direction). Omitting terms of second order in y_2, we have:

$$M_{ang} = \partial(dy_2/dx_2)/\partial\alpha_m = N_1, \qquad (2,93)$$

and consequently:

$$M_{lat} = 1/N_1. \qquad (2,94)$$

The same result is found (as it should), if the axial magnification M_{ax} is derived from (2,80):

$$M_{ax} = \partial l''_m / \partial l'_m = -(l''-g'')/(l'_m-g'), \qquad (2,95)$$

and the relation:

$$M_{lat} = -M_{ang} \cdot M_{ax} \qquad (2,96)$$

is used.

Similarly, we have in axial direction the magnifications:

$$M^z_{ang} = T_3 ; \qquad (2,97)$$

$$M^z_{lat} = 1/T_3 . \qquad (2,98)$$

If all ions have the same momentum ($\eta = \eta_o$), the image of an infinitely narrow object slit is broadened, at the correct image distance l''_m, by the following second order aberrations: (Boerboom [36])

by the second order angular aberration by the amount:

$$A_{11}\alpha_m^2 = r_m(M_{11} - (M_1/N_1)N_{11})\alpha_m^2 ; \qquad (2,99)$$

by the sagittal second order angular aberration by the amount:

$$A_{33}\alpha_{zm}^2 = r_m(M_{33} - (M_1/N_1)N_{33})\alpha_{zm}^2 ; \qquad (2,100)$$

by the agammatism by the amount:

$$A_{34}\alpha_{zm}(\delta/r_m) = r_m(M_{34} - (M_1/N_1)N_{34})\alpha_{zm}(\delta/r_m); \qquad (2,101)$$

and by the image curvature by the amount:

$$A_{44}(\delta/r_m)^2 = r_m(M_{44} - (M_1/N_1)N_{44})(\delta/r_m)^2 . \qquad (2,102)$$

When all ions in the object space travel parallel to the median plane ($\alpha_{zm} = 0$), elimination of (δ/r_m) from (2,48) and (2,102) yields the radius of curvature R_{im} of the image:

$$R_{im} = r_m \frac{(\Sigma_4 - (M_1/N_1)T_4)^2}{2(M_{44} - (M_1/N_1)N_{44})} ; \qquad (2,103)$$

where a positive value of R_{im} means that the centre of curvature has a positive y_2 coordinate.

However, it has been demonstrated by Berry [37], that the fringing fields affect the aberrations outside the median plane. Berry showed, that the stray fields of a homogeneous magnetic sector field produce an image curvature, which is independent

of the shape of the fringing fields. The fringing fields also influence the sagittal second order angular aberration and the agammatism, but in the latter cases the effect can be reduced by reducing the extension of the stray fields by shims. Although the reasoning by Berry is strictly valid only for homogeneous sector fields, it should be approximately correct for inhomogeneous sector fields also. Then the fringing fields alone produce a curved image with radius of curvature R_{fr}, in our notation given by:

$$\frac{r_m}{R_{fr}} = \frac{1 - N_1}{N_1} = \mu_{1b} + \nu_{1b}(l''_m/r_m) - 1. \qquad (2,104)$$

The radius of the image, resulting from both effects, is then given by:

$$R_{total} = \frac{R_{im}R_{fr}}{R_{im} + R_{fr}}. \qquad (2,105)$$

In a mass spectrometer, comprising the inhomogeneous magnetic sector field as the analysing element, and with object and collector slit widths s' and s'' respectively, the mass resolving power (the reciprocal of the relative mass difference $\delta m/m_o$ which will just be resolved) equals:

$$R = D_m/(s' M_{lat} + s'' + \Sigma A_i), \qquad (2,106)$$

where ΣA_i stands for the total image broadening due to all aberrations. Among these are first order aberrations due to energy spread and to misalignment, and the second order aberrations mentioned above.

As follows from (2,4), a certain relative energy difference causes the same displacement in the image as a relative mass difference of the same magnitude, and thus energy spread in the ion beam may limit the resolving power attainable with a single focusing arrangement. The elimination of this chromatic aberration requires a combination of electrostatic and magnetic fields; it will be discussed in chapters 6 and 7. Unless such an elimination of the first order chromatic aberration is achieved, neither the second order chromatic aberration (proportional to β^2), nor the mixed second order aberration (proportional to $\alpha_m\beta$) have an appreciable influence on the sharpness of the image. The aberrations due to misalignment, incorrect positioning of the slits, etc. will be discussed in chapter 5.

The only radial aberration not mentioned above is the distor-

sion in radial direction. As the object slit width is always very small as compared with r_m, its influence results only in a slight shift of the image position in the focusing plane, together with an inclination in the top of an otherwise ideally "flat-topped" peak.

Aberrations in axial focusing result only in loss of intensity, and not in loss of resolving power, and are usually of secondary importance.

2h: *Symmetric arrangement.*

A special case of particular importance is the "symmetric arrangement", in which the object and image distances are equal, and in addition to the median plane the plane $w = \phi_m^*/2$ is also a plane of symmetry. This case is particularly interesting as most existing mass spectrometers satisfy these specifications. On the other hand many of the general expressions derived in this chapter simplify considerably if the extra symmetry is imposed.

Using the abbreviations (2,53) and (2,75), we introduce the extra abbreviations:

$$\begin{aligned} T &= \tan(\phi_m^*/2); \\ t &= t' = t''; \\ \rho &= \rho' = \rho''. \end{aligned} \qquad (2,107)$$

The object and image distances are now equal to:

$$l'_m = l''_m = l_m = r_m \frac{1}{(1-n)^{\frac{1}{2}}T - t}. \qquad (2,108)$$

In this case all magnifications in radial direction equal minus unity:

$$M_{ang} = M_{lat} = M_{ax} = -1. \qquad (2,109)$$

The mass dispersion per unit $\delta m/m_o$ reduces in this case to:

$$D_m = \frac{T}{T - (1-n)^{-\frac{1}{2}}t} \cdot \frac{1}{1-n} r_m. \qquad (2,110)$$

The coefficient A_{11} of the second order angular aberration now takes the form:

$$A_{11} = r_m \frac{-2t^3+3(1-n)^{\frac{1}{2}}Tt^2-2nt+\frac{1}{3}(1-n)^{\frac{1}{2}}(2T^3+3T)X+2\rho-(1-n)^{\frac{1}{2}}T^3}{\{(1-n)^{\frac{1}{2}}T-t\}^3} \qquad (2,111)$$

If moreover both entrance and exit are normal (t=0), further simplification results:

$$l_m = \frac{r_m}{(1-n)^{\frac{1}{2}}T}; \qquad (2,112)$$

$$D_m = \frac{r_m}{1-n}; \qquad (2,113)$$

$$A_{11} = \frac{r_m}{1-n}\left\{\frac{\cos\phi_m^*+5}{3(1-\cos\phi_m^*)}X + \frac{2\rho}{(1-n)^{\frac{1}{2}}T^3} - 1\right\}. \qquad (2,114)$$

For the homogeneous magnetic sector field (n=X=0; $T = \tan(\phi_m/2)$) we have in this symmetric arrangement:

$$l_m = \frac{r_m}{T-t}; \qquad (2,115)$$

$$D_m = \frac{r_m}{1-t/T}; \qquad (2,116)$$

$$A_{11} = r_m\left\{\frac{2\rho}{(T-t)^3} - \frac{T+2t}{T-t}\right\}. \qquad (2,117)$$

CHAPTER 3

ION-OPTICAL PROPERTIES OF THE TOROIDALLY CURVED ELECTROSTATIC SECTOR FIELD

3a: *Assumptions; coordinate system.*

The calculation of the ion trajectories is performed along the same lines as in the preceding chapter. The field strength within the field boundaries is supposed to be independent of the path coordinate ψ, outside the boundaries it is supposed to be zero, dropping to zero abruptly at the boundaries. The effect of fringing fields is neglected. In this case, there is no image curvature nor axial focusing action due to the fringing fields other than the effects treated in chapter 4. Again, the rectilinear paths in the field free object and image space will be supposed to coincide with the tangents at the boundaries to the trajectories in the field region.

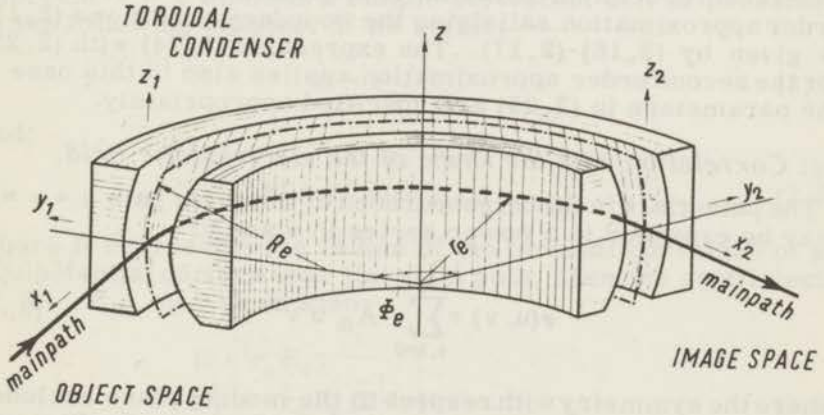

Fig. 6. Toroidally curved electrostatic sector field.

The arrangement is illustrated schematically in Fig. 6. The main path is supposed to be circular with radius r_e. The median plane is supposed to be a plane of symmetry for the electrostatic potential. The equipotential surface containing the main path is (in general) not cylindrical; it may be approximated by a part of a toroid. The radius of the "extra" toroidal curvature of this equipotential surface, normal to the median plane, is denoted by R_e. R_e is taken positive if the equipotential surface is convex with respect to the toroidal curvature to the side of increasing radius r. In Fig. 6, R_e is positive. To create such

a toroidally curved electrostatic field, a pair of toroidally curved deflecting electrodes is required, the shape of which will be indicated in the following chapter.

Within the deflecting field region, the ion trajectory will again be expressed in the dimensionless coordinates: normal coordinate $u = (r - r_e)/r_e$; binormal coordinate $v = z/r_e$; path coordinate $w = \psi$. In the object and image space, the trajectories are expressed in the cartesian coordinates x_1, y_1, z_1, and x_2, y_2, z_2, respectively, the origins being located at the points of entry and exit of the main path.

3b: *First and second order approximation of the ion trajectories.*

The reasoning is analogous to that in the preceding chapter. Again the trajectories are defined by the Euler - Lagrange equations (2, 1)-(2, 2). In the expression (2, 3) for F, however, we now have $A_w = 0$, and φ/U is a function of u and v. The coefficients F_{ij} in the expansion (2, 5) for F now depend on φ/U. The zeroth order approximation is presented by (2, 7); the first order approximation satisfying the boundary conditions (2, 15) is given by (2, 16)-(2, 17). The expression (2, 24) with (2, 25) for the second order approximation applies also to this case if the parameters in (2, 25) are specified appropriately.

3c: *Correlation with the shape of the electrostatic field.*

The potential φ in the neighbourhood of the main path $u = v = 0$ may be expanded in a power series in u and v:

$$\varphi(u, v) = \sum_{i,k=0}^{\infty} A_{ik}\, u^i v^{2k}, \qquad (3, 1)$$

where the symmetry with respect to the median plane excludes terms with odd powers of v. Relations between the coefficients A_{ik} follow from the condition that in the abscence of space charge (which is assumed here), φ should satisfy Laplace's equation:

$$\nabla^2 \varphi = 0, \qquad (3, 2)$$

which reads in the coordinate system (u, v, w):

$$\frac{\partial^2 \varphi}{\partial u^2} + \frac{\partial^2 \varphi}{\partial v^2} + \frac{1}{1+u}\frac{\partial \varphi}{\partial u} = 0. \qquad (3, 2a)$$

Writing instead of the coefficients A_{ik} suitably chosen coefficients E, E_1, E_2, ..., which express the relations between

them derivable from (3, 2) or (3, 2a), we may write for φ: (Grümm [18])

$$\varphi(u, v) = \tag{3, 3}$$
$$= U - Eu - \tfrac{1}{2}E_1u^2 + \tfrac{1}{2}(E + E_1)v^2 - \tfrac{1}{6}E_2u^3 - \tfrac{1}{2}(E-E_1-E_2)uv^2 + \ldots$$

The electrostatic field strength $\vec{E}$ is defined by:

$$\vec{E} = - \text{grad } \varphi, \tag{3, 4}$$

and thus its components E_u, E_v, are:

$$E_u(u, v) = E + E_1u + \tfrac{1}{2}E_2u^2 + \tfrac{1}{2}(E-E_1-E_2)v^2 + \ldots \tag{3, 5}$$

$$\vdots$$

$$E_v(u, v) = -(E+E_1)v + (E - E_1+E_2)uv + \ldots \tag{3, 6}$$

Calculations of the potential distribution in a toroidal condensor have been published by Hachenberg [11], Svartholm [16], and Albrecht [12,13], whereas a simple derivation will be presented in the following chapter. If we define:

$$c = r_e/R_e. \tag{3, 7}$$

and:

$$R_e' = (\partial R/\partial r)_{r=r_e,\, z=0} \tag{3, 8}$$

where R represents the radius of the toroidal curvature of an equipotential surface near the main path, then the coefficients E, E_1, E_2, may be written:

$$\begin{aligned} E &= r_e E_o; \\ E_1 &= -r_e E_o(1+c); \\ E_2 &= r_e E_o\{2(1+c)+c^2(1+R_e')\}. \end{aligned} \tag{3, 9}$$

From (3, 3), (3, 9), it follows that the coefficients in (2, 5) equal:

$$\begin{aligned} F_{00} &= 1; \\ F_{10} &= 1 - \frac{r_e E_o}{2U}; \\ F_{20} &= -\tfrac{1}{2}\frac{r_e E_o}{2U}\left\{1 - c + \frac{r_e E_o}{2U}\right\} \\ F_{02} &= \tfrac{1}{2}\frac{r_e E_o}{2U}(-c); \end{aligned} \tag{3, 10}$$

$$F_{30} = \tfrac{1}{6}\frac{r_e E_o}{2U}\left\{1 + c - c^2\,(1 + R'_e) + 3c\,\frac{r_e E_o}{2U} - 3\left(\frac{r_e E_o}{2U}\right)^2\right\};$$

$$F_{12} = \tfrac{1}{2}\frac{r_e E_o}{2U}\left\{c^2(1 + R'_e) - \frac{r_e E_o}{2U}c\right\} \qquad (3,10)$$

$$g = \tfrac{1}{2}\left(1 + \frac{r_e E_o}{2U}\right).$$

If all ions have the same mass m_o and charge e, and if a velocity spread is allowed according to:

$$v = v_o\,(1 + \beta), \qquad (3,37)$$

which is then equivalent to:

$$U = U_o(1 + \beta)^2, \qquad (3,11)$$

we see from (2,7), (3,10) and (3,11), that:

$$(r_e E_o / 2U) = (1 + \beta)^{-2}\,. \qquad (3,12)$$

and

$$\begin{aligned}
F_{20} &= (1 + \beta)^{-2}\,(\tfrac{1}{2}c - 1 + \beta - \tfrac{3}{2}\beta^2 + \ldots);\\
F_{02} &= \tfrac{1}{2}(1 + \beta)^{-2}\,(-c);\\
F_{30} &= \tfrac{1}{6}(1 + \beta)^2\left\{1 + c - c^2\,(1 + R'_e) + 3c\,(1 + \beta)^{-2} - 3\,(1 + \beta)^{-4}\right\};\\
F_{12} &= (1 + \beta)^{-2}\,.\,\tfrac{1}{2}\left\{-c + c^2\,(1 + R'_e) - 2c\beta + 3c\beta^2 - \ldots\right.;\\
g &= \tfrac{1}{2}\left\{1 + (1 + \beta)^{-2}\right\}.
\end{aligned} \qquad (3,13)$$

From (2,24)-(2,25) and (3,13) we find the radial second order approximation for the ion trajectories:

$$u = {}^{(2)}u(w) = D_1 u_o + D_2\alpha + D_3\beta + D_{11}\,u_o^2 + D_{12}\,u_o\alpha + D_{22}\,\alpha^2 + D_{13}\,u_o\beta + D_{23}\alpha\beta + D_{33}\,\beta^2 + D_{44}\,v_o^2 + D_{45}\,v_o\alpha_z + D_{55}\alpha_z^2, \qquad (3,14)$$

where, with the abbreviations:

$$\begin{aligned}
&\kappa = (2 - c)^{\frac{1}{2}}; \qquad w^* = \kappa w; \qquad w^\dagger = c^{\frac{1}{2}} w;\\
&\Gamma = 3c - 3 - \tfrac{1}{2}c^2\,(1 + R'_e); \qquad \Delta = c + c^2\,(1 + R'_e);
\end{aligned} \qquad (3,15)$$

$$D_1 = \cos w^*; \qquad D_2 = \kappa^{-1} \sin w^*;$$

$$D_3 = 2\kappa^{-2}(1-\cos w^*);$$

$$D_{11} = \tfrac{1}{3}\kappa^{-2}\{(2\Gamma-\kappa^2) - (\Gamma+\kappa^2)\cos w^* - (\Gamma-2\kappa^2)\cos^2 w^*\};$$

$$D_{12} = \tfrac{1}{3}\kappa^{-3}\{2(\Gamma-2\kappa^2)\sin w^*(1-\cos w^*)\};$$

$$D_{22} = \tfrac{1}{3}\kappa^{-4}\{(\Gamma+\kappa^2) - (2\Gamma-\kappa^2)\cos w^* + (\Gamma-2\kappa^2)\cos^2 w^*\};$$

$$D_{13} = \tfrac{1}{3}\kappa^{-4}\{-4(2\Gamma-\kappa^2) + 4(\Gamma+\kappa^2)\cos w^* + 4(\Gamma-2\kappa^2)\cos^2 w^* + (6\Gamma+3\kappa^2+3\kappa^4) w^* \sin w^*\};$$

$$D_{23} = \tfrac{1}{3}\kappa^{-5}\{(2\Gamma+11\kappa^2+3\kappa^4)\sin w^* + 4(\Gamma-2\kappa^2)\sin w^*\cos w^* - (6\Gamma+3\kappa^2+3\kappa^4) w^* \cos w^*\};$$

$$D_{33} = \tfrac{1}{3}\kappa^{-6}\{(20\Gamma+20\kappa^2+3\kappa^4)\sin w^* - (16\Gamma+28\kappa^2+3\kappa^4)\cos w^* - 4(\Gamma-2\kappa^2)\cos^2 w^* - (12\Gamma+6\kappa^2+6\kappa^4) w^* \sin w^*\};$$

$$D_{44} = \tfrac{1}{2}\kappa^{-2}(2-5c)^{-1}\Delta\{\kappa^2\cos^2 w\dagger - (2-3c)\cos w^* - 2c\} + c\kappa^{-2}(\cos w^* - 1);$$

$$D_{45} = (2-5c)^{-1}\Delta\{c^{-\frac{1}{2}}\sin w\dagger \cos w\dagger - \kappa^{-1}\sin w^*\};$$

$$D_{55} = \tfrac{1}{2}\kappa^{-2}c^{-1}(2-5c)^{-1}\Delta\{-\kappa^2\cos^2 w\dagger + 2c\cos w^* + (2-3c)\} + \kappa^{-2}(\cos w^* - 1).$$

(3, 16)

3d: *Imaging properties of the toroidally curved electrostatic sector field.*

For the case of plane boundaries and normal incidence and exit of the main path, the relations of the parameters in the object space and the boundary conditions read, similar to (2, 43): (See Fig. 7)

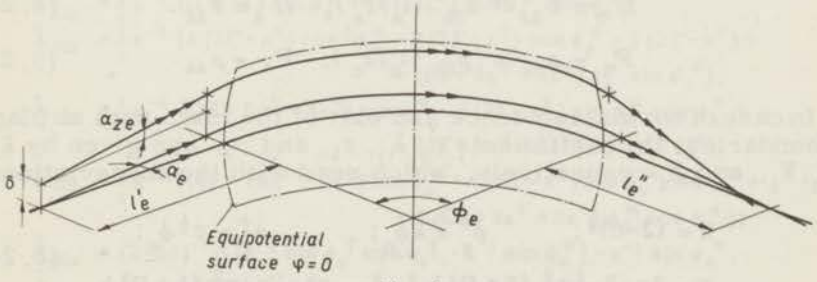

Fig. 7.

$$u_o = (l'_e/r_e)\alpha_e; \qquad \alpha = \alpha_e + (l'_e/r_e)\alpha_e^2; \qquad (3, 17)$$

$$v_o = (l'_e/r_e)\alpha_{ze} + \delta/r_e; \quad \alpha_z = \alpha_{ze} + (l'_e/r_e)\alpha_e\alpha_{ze}.$$

From relations similar to (2, 44)-(2, 46) we find the radial second order approximation of the ion trajectories in the image space:

$$y_2 = r_e \{K_1\alpha_e + K_2\beta + K_{11}\alpha_e^2 + K_{12}\alpha_e\beta + K_{22}\beta^2 + + K_{33}\alpha_{ze}^2 + K_{34}\alpha_{ze}(\delta/r_e) + K_{44}(\delta/r_e)^2\} + + x_2\{L_1\alpha_2 + L_2\beta + L_{11}\alpha_e^2 + L_{12}\alpha_e\beta + L_{22}\beta^2 + + L_{33}\alpha_{ze}^2 + L_{34}\alpha_{ze}(\delta/r_e) + L_{44}(\delta/r_e)^2\}; \tag{3,18}$$

and the first order axial approximation:

$$z_2 = r_e\{\Pi_3\alpha_{ze} + \Pi_4(\delta/r_e)\} + x_2\{P_3\alpha_{ze} + P_4(\delta/r_e)\}. \tag{3,19}$$

The coefficients K_i, L_i, Π_i, P_i, are given by:

$$\begin{aligned} K_1 &= \kappa_{1a} + \kappa_{1b}(l'_e/r_e); & K_2 &= \kappa_{2a}; \\ K_{11} &= \kappa_{11a} + \kappa_{11b}(l'_e/r_e) + \kappa_{11c}(l'_e/r_e)^2; & & \\ K_{12} &= \kappa_{12a} + \kappa_{12b}(l'_e/r_e); & K_{22} &= \kappa_{22a}; \\ K_{33} &= \kappa_{33a} + \kappa_{33b}(l'_e/r_e) + \kappa_{33c}(l'_e/r_e)^2; & & \\ K_{34} &= \kappa_{34a} + \kappa_{34b}(l'_e/r_e); & K_{44} &= \kappa_{44a}. \end{aligned} \tag{3,20}$$

$$\begin{aligned} L_1 &= \lambda_{1a} + \lambda_{1b}(l'_e/r_e); & L_2 &= \lambda_{2a}; \\ L_{11} &= \lambda_{11a} + \lambda_{11b}(l'_e/r_e) + \lambda_{11c}(l'_e/r_e)^2; & & \\ L_{12} &= \lambda_{12a} + \lambda_{12b}(l'_e/r_e); & L_{22} &= \lambda_{22a}; \\ L_{33} &= \lambda_{33a} + \lambda_{33b}(l'_e/r_e) + \lambda_{33c}(l'_e/r_e)^2; & & \\ L_{34} &= \lambda_{34a} + \lambda_{34b}(l'_e/r_e); & L_{44} &= \lambda_{44a}. \end{aligned} \tag{3,21}$$

$$\Pi_3 = \pi_{3a} + \pi_{3b}(l'_e/r_e); \quad \Pi_4 = \pi_{4a}. \tag{3,22}$$

$$P_3 = \rho_{3a} + \rho_{3b}(l'_e/r_e); \quad P_4 = \rho_{4a}. \tag{3,23}$$

In case of normal incidence and exit of the main path at plane boundaries, the coefficients κ_i, λ_i, π_i, and ρ_i, are given by $\bar{\kappa}_i$, $\bar{\lambda}_i$, $\bar{\pi}_i$, and $\bar{\rho}_i$ respectively, which read with the abbreviations:

$$\begin{aligned} &\kappa = (2-c)^{\frac{1}{2}}; \qquad \phi_e^* = \kappa\phi_e; \qquad \phi_e^\dagger = c^{\frac{1}{2}}\phi_e; \\ &\Gamma = 3c - 3 - \tfrac{1}{2}c^2(1+R'_e); \qquad \Delta = c + c^2(1+R'_e). \end{aligned} \tag{3,24}$$

$$\bar{\kappa}_{1a} = \kappa^{-1} \sin\phi_e^*; \qquad \bar{\kappa}_{1b} = \cos\phi_e^*;$$
$$\bar{\kappa}_{2a} = 2\kappa^{-2}(1 - \cos\phi_e^*);$$
$$\bar{\kappa}_{11a} = \tfrac{1}{3}\kappa^{-4}\{(\Gamma+\kappa^2) - (2\Gamma-\kappa^2)\cos\phi_e^* + (\Gamma-2\kappa^2)\cos^2\phi_e^*\};$$
$$\bar{\kappa}_{11b} = \tfrac{1}{3}\kappa^{-3}\{(2\Gamma-\kappa^2)\sin\phi_e^* - 2(\Gamma-2\kappa^2)\sin\phi_e^*\cos\phi_e^*\};$$
$$\bar{\kappa}_{11c} = \tfrac{1}{3}\kappa^{-2}\{(2\Gamma-\kappa^2) - (\Gamma+\kappa^2)\cos\phi_e^* - (\Gamma-2\kappa^2)\cos^2\phi_e^*\};$$
$$\bar{\kappa}_{12a} = \tfrac{1}{3}\kappa^{-5}\{(2\Gamma+11\kappa^2+3\kappa^4)\sin\phi_e^* + 4(\Gamma-2\kappa^2)\sin\phi_e^*\cos\phi_e^* + - (6\Gamma+3\kappa^2+3\kappa^4)\phi_e^*\cos\phi_e^*\};$$
$$\bar{\kappa}_{12b} = \tfrac{1}{3}\kappa^{-4}\{-4(2\Gamma-\kappa^2) + 4(\Gamma+\kappa^2)\cos\phi_e^* + 4(\Gamma-2\kappa^2)\cos^2\phi_e^* + + (6\Gamma+3\kappa^2+3\kappa^4)\phi_e^*\sin\phi_e^*\};$$
$$\bar{\kappa}_{22a} = \tfrac{1}{3}\kappa^{-6}\{(20\Gamma+20\kappa^2+3\kappa^4) - (16\Gamma+28\kappa^2+3\kappa^4)\cos\phi_e^* + -4(\Gamma-2\kappa^2)\cos^2\phi_e^* - 2(6\Gamma+3\kappa^2+3\kappa^4)\phi_e^*\sin\phi_e^*\};$$
$$\bar{\kappa}_{33a} = \tfrac{1}{2}\kappa^{-2}c^{-1}(2-5c)^{-1}\Delta\{-\kappa^2\cos^2\phi_e\dagger + (2c)\cos\phi_e^* + (2-3c)\} + + \kappa^{-2}(\cos\phi_e^* - 1);$$
$$\bar{\kappa}_{33b} = \bar{\kappa}_{34a} = (2-5c)^{-1}\Delta\{c^{-\frac{1}{2}}\sin\phi_e\dagger\cos\phi_e\dagger - \kappa^{-1}\sin\phi_e^*\};$$
$$\bar{\kappa}_{33c} = \bar{\kappa}_{44a} = \tfrac{1}{2}\bar{\kappa}_{34b} =$$
$$= \tfrac{1}{2}\kappa^{-2}(2-5c)^{-1}\Delta\{\kappa^2\cos^2\phi_e\dagger - (2-3c)\cos\phi_e^* - 2c\} + + c\kappa^{-2}(\cos\phi_e^* - 1). \qquad (3,25)$$

$$\bar{\lambda}_{1a} = \cos\phi_e^*; \qquad \bar{\lambda}_{1b} = -\kappa\sin\phi_e^*;$$
$$\bar{\lambda}_{2a} = 2\kappa^{-1}\sin\phi_e^*;$$
$$\bar{\lambda}_{11a} = \tfrac{1}{3}\kappa^{-3}\{(2\Gamma-\kappa^2)\sin\phi_e^* - (2\Gamma-\kappa^2)\sin\phi_e^*\cos\phi_e^*\};$$
$$\bar{\lambda}_{11b} = \tfrac{1}{3}\kappa^{-2}\{-2(2\Gamma-\kappa^2)\cos^2\phi_e^* + (2\Gamma-\kappa^2)\cos\phi_e^* + (2\Gamma-\kappa^2)\};$$
$$\bar{\lambda}_{11c} = \tfrac{1}{3}\kappa^{-1}\{(\Gamma+\kappa^2)\sin\phi_e^* + (2\Gamma-\kappa^2)\sin\phi_e^*\cos\phi_e^*\};$$
$$\bar{\lambda}_{12a} = \tfrac{1}{3}\kappa^{-4}\{4(2\Gamma-\kappa^2)\cos^2\phi_e^* - 2(2\Gamma-\kappa^2)\cos\phi_e^* - 2(2\Gamma-\kappa^2) + + (6\Gamma+3\kappa^2+3\kappa^4)\phi_e^*\sin\phi_e^*\};$$
$$\bar{\lambda}_{12b} = \tfrac{1}{3}\kappa^{-3}\{(2\Gamma+5\kappa^2+3\kappa^4)\sin\phi_e^* - 4(2\Gamma-\kappa^2)\sin\phi_e^*\cos\phi_e^* + + (6\Gamma+3\kappa^2+3\kappa^4)\phi_e^*\cos\phi_e^*\};$$
$$\bar{\lambda}_{22a} = \tfrac{1}{3}\kappa^{-5}\{(4\Gamma+10\kappa^2-3\kappa^4)\sin\phi_e^* + 4(2\Gamma-\kappa^2)\sin\phi_e^*\cos\phi_e^* + - 2(6\Gamma+3\kappa^2+3\kappa^4)\phi_e^*\cos\phi_e^*\};$$
$$\bar{\lambda}_{33a} = (2-5c)^{-1}\Delta\{c^{-\frac{1}{2}}\sin\phi_e\dagger\cos\phi_e\dagger - \kappa^{-1}\sin\phi_e^*\} - \kappa^{-1}\sin\phi_e^*;$$
$$\bar{\lambda}_{33b} = \bar{\lambda}_{34a} = (2-5c)^{-1}\Delta\{2\cos^2\phi_e\dagger - \cos\phi_e^* - 1\};$$
$$\bar{\lambda}_{33c} = \bar{\lambda}_{44a} = \tfrac{1}{2}\bar{\lambda}_{34b} =$$
$$= (2-5c)^{-1}\Delta\{-c^{\frac{1}{2}}\sin\phi_e\dagger\cos\phi_e\dagger + \tfrac{1}{2}(2-3c)\kappa^{-1}\sin\phi_e^*\} + - 2c\kappa^{-1}\sin\phi_e^*.$$

(3,26)

$$\begin{aligned} \bar{\pi}_{3a} &= c^{-\frac{1}{2}} \sin \phi_e^{\dagger}; \\ \bar{\pi}_{3b} &= \bar{\pi}_{4a} = \bar{\rho}_{3a} = \cos \phi_e^{\dagger}; \\ \bar{\rho}_{3b} &= \bar{\rho}_{4a} = -c^{\frac{1}{2}} \sin \phi_e^{\dagger}. \end{aligned} \tag{3,27}$$

Retaining the symmetry with respect to the median plane, oblique incidence and/or exit could be realised by making the sector angle of the electrodes different from that of the main path. However, this would complicate the definition of the "boundary" considerably, as it would introduce a field component E_w parallel to the main path. In the previous calculations this component E_w was assumed to be zero.

A curved boundary with the axis of the curvature normal to the median plane, would also introduce considerable complications, and would be far from easy to realise in practice.

However, a curved boundary with the axis of curvature in the median plane may be realised readily by shaping the ends of the deflecting electrodes correspondingly.

Unlike with the magnetic sector field, the fringing fields here do not produce effects which are independent of their shape, as the first order axial focusing and image curving effects in the magnetic case. Therefore, their influences are fully within the scope of chapter 5, and need not be discussed here.

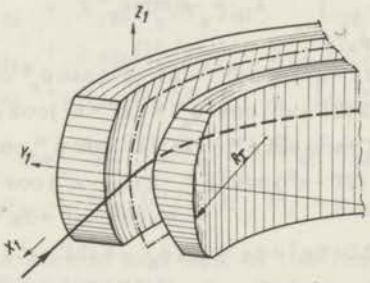

Fig. 8. Curved entrance boundary.

We will now discuss the effect of a curved entrance boundary as shown in Fig. 8. Its radius of curvature R_I is said to be positive if the boundary is convex towards field-free space, as it is in Fig. 8. From considerations analogous to those used in the preceding chapter (König and Hintenberger[33]), it may be seen that the ions are subjected to an extra angle of deflection δ_1:

$$\delta_1 = -\tfrac{1}{2} \frac{v_o^2 \, r_e}{R_I}. \tag{3,28}$$

As δ_1 is small of second order, its influence is accounted for if we replace α_e in (3,18) by α_e*:

$$\alpha_e^* = \alpha_e + \delta_1, \tag{3,29}$$

and l'_e in (3,20)-(3,21) by l'^*_e:

$$l'^*_e = l'_e \ \alpha_e / \alpha_e^*. \tag{3,30}$$

Similarly, a curved exit boundary with radius R_{II} produces an extra angle of deflection δ_2 at the exit side:

$$\delta_2 = -\tfrac{1}{2} \frac{v (\phi_e)^2 r_e}{R_{II}}, \tag{3,31}$$

which gives rise to an additional term $-x_2 \delta_2$ at the right hand side of (3,18). Combining these arguments, we see, that the coefficients $\kappa_i, \lambda_i, \pi_i, \rho_i$, for a toroidal condensor with curved boundaries may be expressed in the corresponding coefficients for plane boundaries:

$$\begin{aligned}
&\kappa_{1a} = \bar{\kappa}_{1a}; \quad \kappa_{1b} = \bar{\kappa}_{1b}; \quad \kappa_{2a} = \bar{\kappa}_{2a}; \quad \kappa_{11a} = \bar{\kappa}_{11a}; \\
&\kappa_{11b} = \bar{\kappa}_{11b}; \quad \kappa_{11c} = \bar{\kappa}_{11c}; \quad \kappa_{12a} = \bar{\kappa}_{12a}; \quad \kappa_{12a} = \bar{\kappa}_{12b}; \\
&\kappa_{22a} = \bar{\kappa}_{22a}; \quad \kappa_{33a} = \bar{\kappa}_{33a}; \quad \kappa_{33b} = \kappa_{34a} = \bar{\kappa}_{33b}; \\
&\kappa_{33c} = \kappa_{44a} = \tfrac{1}{2}\kappa_{34b} = \bar{\kappa}_{33c} + \bar{\kappa}_{1a} (r_e / R_I).
\end{aligned} \tag{3,32}$$

$$\begin{aligned}
&\bar{\lambda}_{1a} = \bar{\lambda}_{1a}; \quad \lambda_{1b} = \bar{\lambda}_{1b}; \quad \lambda_{2a} = \bar{\lambda}_{2a}; \quad \lambda_{11a} = \bar{\lambda}_{11a}; \\
&\lambda_{11b} = \bar{\lambda}_{11b}; \quad \lambda_{11c} = \bar{\lambda}_{11c}; \quad \lambda_{12a} = \bar{\lambda}_{12a}; \quad \lambda_{12b} = \bar{\lambda}_{12b}; \\
&\lambda_{22a} = \bar{\lambda}_{22a}; \quad \lambda_{33a} = \bar{\lambda}_{33a} + \tfrac{1}{2} \bar{\pi}_{3a}{}^2 (r_e / R_{II}); \\
&\lambda_{33b} = \lambda_{34a} = \bar{\lambda}_{33b} + \bar{\pi}_{3a} \bar{\pi}_{3b} (r_e / R_{II}); \\
&\lambda_{33c} = \lambda_{44a} = \tfrac{1}{2} \lambda_{34b} = \bar{\lambda}_{33c} + \tfrac{1}{2} \bar{\lambda}_{1a} (r_e / R_I) + \tfrac{1}{2} \bar{\pi}_{3b}{}^2 (r_e / R_{II}).
\end{aligned} \tag{3,33}$$

$$\pi_{3a} = \bar{\pi}_{3a}; \quad \pi_{3b} = \pi_{4a} = \rho_{3a} = \bar{\pi}_{3b}; \quad \rho_{3b} = \rho_{4a} = \bar{\rho}_{3b}. \tag{3,34}$$

The focusing properties of the toroidal condensor as expressed by (3,18)-(3,27) are equivalent to the expressions derived in a different manner by Ewald and Liebl [10]. Essentially the same method for the calculation of the effect of curved boundaries was used by Liebl and Ewald [38], who specified their result to the case $L_1=0$, which condition is met in most mass spectrographs for photographic detection.

3e: *Discussion.*

Analogous to section 2g in the preceding chapter, we see that first order radial direction focusing occurs at the radial image distance:

$$l''_e = -r_e (K_1/L_1), \tag{3,35}$$

which may be expressed in the conventional form:

$$(l'_e - g')(l''_e - g'') = f^2, \tag{3,36}$$

where: (Ewald en Liebl [9])

$$g' = g'' = r_e \frac{\cot \phi_e^*}{\kappa}; \tag{3,37}$$

$$f = \frac{r_e}{\kappa \sin \phi_e^*}. \tag{3,38}$$

In axial direction first order direction focusing occurs at the axial image distance l''_{ze}:

$$l''_{ze} = -r_e (\Pi_3/P_3), \tag{3,39}$$

which is equivalent to:

$$(l'_{ze} - g'_z)(l''_{ze} - g''_z) = f_z^2; \tag{3,40}$$

$$g'_z = g''_z = r_e \frac{\cot \phi_e^\dagger}{c^{\frac{1}{2}}}; \tag{3,41}$$

$$f_z = \frac{r_e}{c^{\frac{1}{2}} \sin \phi_e^\dagger}. \tag{3,42}$$

The velocity dispersion for a beam of ions of the same mass - to - charge ratio, per unit $\delta v/v_o = \beta$, equals:

$$D_v = r_e \{K_2 - (K_1/L_1)L_2\}. \tag{3,43}$$

Analogous to (2,93)-(2,94) and (2,97)-(2,98), we have:

$$M_{ang} = L_1; \tag{3,44}$$

$$M_{lat} = 1/L_1; \tag{3,45}$$

$$M^z_{ang} = P_3; \tag{3,46}$$

$$M^{z}_{lat} = 1/P_3 . \qquad (3,47)$$

The image broadening with a monoenergetic ion beam, at the image distance l''_e, due to the second order angular aberration equals:

$$A_{11}\alpha_e^2 = r_e\{K_{11} - (K_1/L_1)L_{11}\}\alpha_e^2; \qquad (3,48)$$

due to the sagittal second order angular aberration:

$$A_{33}\alpha_{ze}^2 = r_e\{K_{33} - (K_1/L_1)L_{33}\}\alpha_{ze}^2; \qquad (3,49)$$

due to the agammatism:

$$A_{34}\alpha_{ze}(\delta/r_e) = r_e\{K_{34} - (K_1/L_1)L_{34}\}\alpha_{ze}(\delta/r_e); \qquad (3,50)$$

and due to the image curvature:

$$A_{44}(\delta/r_e)^2 = r_e\{K_{44} - (K_1/L_1)L_{44}\}(\delta/r_e)^2. \qquad (3,51)$$

For an ion beam, travelling in the object space parallel to the median plane ($\alpha_{ze} = 0$), the radius of curvature of the image R_{im} is found by elimination of (δ/r_e) from (3,19) and (3,51):

$$R_{im} = r_e \cdot \tfrac{1}{2}\,\frac{\{\Pi_4 - (K_1/L_1)P_4\}^2}{K_{44} - (K_1/L_1)L_{44}}. \qquad (3,52)$$

Whereas curvature of the boundaries of a magnetic sector field affects the second order aberrations in the median plane (i.e. those proportional to α_m^2, to $\alpha_m\beta$, and to β^2), with an electrostatic sector field it affects the remaining second order aberrations outside the median plane (i.e. those proportional to α_{ze}^2, to $\alpha_{ze}(\delta/r_e)$, and to $(\delta/r_e)^2$). It will be shown in chapter 6, that this statement remains valid for a tandem arrangement of an electrostatic sector field plus a magnetic sector field with a common median plane. At least in principle, four of the six relevant second order aberrations may be eliminated by a suitable choice for the radii of curvature of the boundaries.

The general case of the toroidal condensor comprises two important specifications. One of these is the *spherical condensor*, with $c = R'_e = +1$. It provides stigmatic focusing, as the radial and the axial image coincide.

The second, more widely used, specification, is the *cylindrical condensor*. ($c = 0$; $R'_e = +1$). Expressions for the coefficients

κ_i, λ_i, for the median plane of a cylindrical electrostatic sector field were published by Hintenberger and König [35]; their results are identical to (3, 25)-(3, 26) with the appropriate specifications.

3f: *Symmetric arrangement.*

In an arrangement where the object and image distances are equal, and where the plane $w = \phi_e/2$ is an additional plane of symmetry, we have:

$$l' = l''_e = r_e \frac{\cot(\phi_e^*/2)}{\kappa}; \qquad (3,53)$$

$$M_{ang} = M_{lat} = M_{ax} = -1; \qquad (2,109)$$

$$D_v = 4\, r_e/\kappa^2. \qquad (3,54)$$

If the condensor is also cylindrical, $c=0$ and $\kappa=\sqrt{2}$, and thus:

$$l'_e = l''_e = r_e \frac{\cot(\phi_e/\sqrt{2})}{\sqrt{2}}; \qquad (3,55)$$

$$D_v = 2\, r_e. \qquad (3,56)$$

CHAPTER 4

SHAPE OF THE POLE SHOES AND DEFLECTING ELECTRODES

4a: *The scalar magnetic potential.*

The scalar magnetic potential φ_m is related to the magnetic field strength $\vec{B}$ through its definition:

$$\vec{B} = - \text{grad}\, \varphi_m , \qquad (4,1)$$

which determines φ_m except for an additional constant. We will choose this constant such as to make $\varphi_m = 0$ at the main path. Then $\varphi_m = 0$ in the median plane, and φ_m is anti-symmetric with respect to the median plane.

Retaining terms up to the fourth order in $\vec{B}$, we find from (4,1) and (2,27)-(2,32) with (2,34)-(2,35):

$$\begin{aligned}\varphi_m/B = &- v + nuv + \tfrac{1}{2}\{X(1-n)-2n\}u^2v - \tfrac{1}{6}\{X(1-n)-n\}v^3 + \\ &- C_3u^3v + \left\{\tfrac{1}{2}n - \tfrac{1}{6}X(1-n)+C_3\right\}uv^3 + \\ &- C_4u^4v + \left\{-\tfrac{1}{2}n+\tfrac{1}{6}X(1-n)+\tfrac{1}{2}C_3+2C_4\right\}u^2v^3 + \\ &+\left\{\tfrac{1}{40}n - \tfrac{1}{120}X(1-n) - \tfrac{1}{10}C_3 - \tfrac{1}{5}C_4\right\}v^5 + \ldots \qquad (4,2)\end{aligned}$$

The so far undetermined coefficients C_3 and C_4 define the fourth and fifth order contributions to the scalar magnetic potential, and appear in the third and fourth order approximation of the ion trajectories.

If the permeability of the pole shoe material is very high, their surfaces are very nearly equipotential surfaces for the scalar magnetic potential. We will start with this approximation, and estimate the effect of the finite pole shoe permeability in sect. 4d. At first we will assume infinite radial extension of the pole faces. The deviations caused by the finite extension are small at a few gap widths away from the edges. A means for extending the usuable region is given in sect. 4e.

In the following section we will deduce the required shape of the pole faces for creating a specified field shape, whereas in sect. 4c we will deduce the field shape from a given pole face profile.

4b: *Shape of the pole faces required for the elimination of the second order angular aberration in a symmetrical arrangement with normal incidence and exit at plane boundaries.*

Inserting $\rho = 0$ in (2, 114), we find that A_{11} vanishes in this case if:

$$X = \frac{3\,(1-\cos\phi_m^*)}{\cos\phi_m^* + 5}. \qquad (4, 3)$$

The second order approximation of the ion trajectories does not justify a preference for any of the infinite number of field shapes differing only in the contributions of the third and higher order terms C_3, C_4, .. etc. The pole face profile for any of these field shapes is best found by an iterative process. Writing (4, 2) in the form:

$$\varphi_m/B = f_1(u).v + f_3(u).v^3 + f_5(u).v^5 + \ldots \qquad (4, 2a)$$

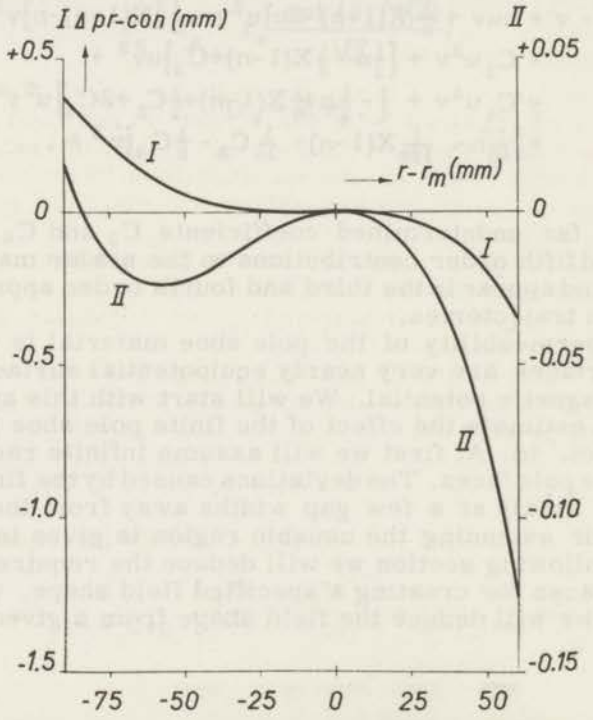

Fig. 9. Pole face profiles for n = 0.91; X = +0.22131; r_m = 200 mm; 2b = 20 mm. I: C_3 = C_4 = 0. II: C_3 = -0.75348; C_4 = +0.68563. The ordinates represent the differences in the distances from the median plane between the profile and the conical shape for n = 0.91.

and specifying the circle u_o, v_o which should be included in the pole face in question, the iteration proceeds along:

$$\varphi_m(u_o, v_o) = \varphi_{mo}; \tag{4,4}$$

$$v_{n+1}(u) = \frac{\varphi_{mo}/B - f_3(u).v_n^3 - f_5(u).v_n^5 - \ldots}{f_1(u)}. \tag{4,5}$$

Fig. 9 gives the deviations from the conical shape of two such profiles. With the sector angle $\phi_m = \pi$, and n = 0.91, A_{11} vanishes in this case if X = +0.22131. The calculations were made assuming r_m = 200 mm; and a gap width 2b = 20 mm. The abscis is the radial coordinate $r-r_m$; the ordinate is the difference in the distances from the median plane of the profile in question and the conical profile resulting in n=0.91. Both curves I and II refer to n=0.91; X=0.22131. In I, $C_3 = C_4 = 0$. In II, C_3 = -0.75348; C_4 = +0.68563; these values occur in the field shape between conical pole faces with n = 0.91. With conical pole faces, we have X = 2n = 1.82, as will be shown in the following section, resulting in A_{11} = +7.2238.

4c: *Field shape with conical pole faces.*

It was demonstrated in the preceding section, that although in principle any desired field shape may be realised by appropriate shaping of the pole faces, very small deviations in the pole face profile result in serious deviations in the field shape. These complex surfaces are difficult to machine with the required precision.

A conical profile, however, can be machined and measured with a much higher precision. A curved entrance and/or exit boundary in such an arrangement can eliminate the second order angular aberration.

For the calculation of the field shape between conical pole faces, we use again the scalar magnetic potential φ_m. Defining the conical profile by:

$$v = au + b, \tag{4,6}$$

we must find the parameters which satisfy the equations:

$$\left(\frac{dv}{du}\right)_{u=0,\,v=b} = -\left(\frac{\partial\varphi_m}{\partial u} \Big/ \frac{\partial\varphi_m}{\partial v}\right)_{u=0,\,v=b} = a; \tag{4,7}$$

$$\left(\frac{d^2v}{du^2}\right)_{u=0,\,v=b} = \left(\frac{-(\partial^2\varphi_m/\partial u^2)(\partial\varphi_m/\partial v)^2-(\partial^2\varphi_m/\partial v^2)(\partial\varphi_m/\partial u)^2+2(\partial^2\varphi_m/\partial u\partial v)(\partial\varphi_m/\partial u)(\partial\varphi_m/\partial v)}{(\partial\varphi_m/\partial v)^3}\right)_{u=0,\,v=b} = 0. \qquad (4,8)$$

If we expand both a and X in a power series in b, and equate terms with equal powers of b at both sides, we find from (4, 7):

$$a = nb + \text{terms proportional to } b^3; \qquad (4,9)$$

and from (4, 8):

$$X = 2n + \text{terms proportional to } b^2. \qquad (4,10)$$

The accuracy of (4, 9)-(4, 10) is amply sufficient for nearly all practical cases. More accurate expressions are (Boerboom, Tasman and Wachsmuth [39]):

$$a = nb + \tfrac{1}{6}n(1-n)b^3 + \ldots \qquad (4,11)$$

$$X = 2n + \tfrac{1}{3}n(1-n)b^2 + \ldots \qquad (4,12)$$

$$C_3 = -n^3 + \tfrac{1}{6}n(1-n)^2(1+2n)b^2 + \ldots \qquad (4,13)$$

$$C_4 = n^4 - \tfrac{1}{6}n(1-n)^2(1+2n+3n^2)b^2 + \ldots \qquad (4,14)$$

4d: *Influence of the finite permeability of the pole shoe material.*

Due to the finite permeability of the pole shoes, their surfaces need not be equipotential surfaces for the scalar magnetic potential. Remanent magnetism may contribute to the field, but it is unlikely to have appreciable influence on the field shape at inductions above 1000 Gauss, which are of main interest in mass spectrometry.

If the flux density at the transitions between the yoke and the pole shoes may be assumed to be homogeneously distributed, the situation is equivalent to that with slightly thinner pole shoes with infinite relative permeability μ, their thickness being multiplied by $(\mu-1)/\mu$. If the excitation current is increased such as to restore the desired field strength at the main path, the finite permeability results in a decrease in the effective value of n:

$$n_{eff} = \frac{\mu-1}{\mu}n \quad (\mu=\infty). \qquad (4,15)$$

The relations (4, 11)-(4, 20) remain valid if n_{eff} is substituted for n.

Complications arise due to the dependence of the permeability on the induction. To get an idea of the order of magnitude of this effect, let us suppose that the pole shoe thickness is about equal to the gap width, and that in a layer of about half the pole shoe thickness adjacent to the gap the induction corresponds to that in the gap whereas in the rest of the pole shoe it is homogeneously distributed. The field strength in the median plane is roughly inversely proportional to the distance of the "virtual" pole faces, which has increased due to the finite permeability of the "inhomogeneous layer" by the factor $\mu/(\mu-1)$. Considering only the first order term in the field shape expansion, we find from (2, 33):

$$n = -\frac{\partial(\ln B)}{\partial(\ln r)} \approx n_{(\mu=\text{const.})} \left\{1 - d(1/\mu)/d(\ln B)\right\} \qquad (4, 16)$$

Figs. 10 and 11 represent $1/\mu$ and $d(1/\mu)/d(\ln B)$ respectively for some soft magnetic materials according to the manufacturers' specifications. For these materials the effects expressed by (4, 15)-(4, 16) are negligible as compared with the inavoidable machining inaccuracies in the region between 100 Gauss and the induction at maximum permeability.

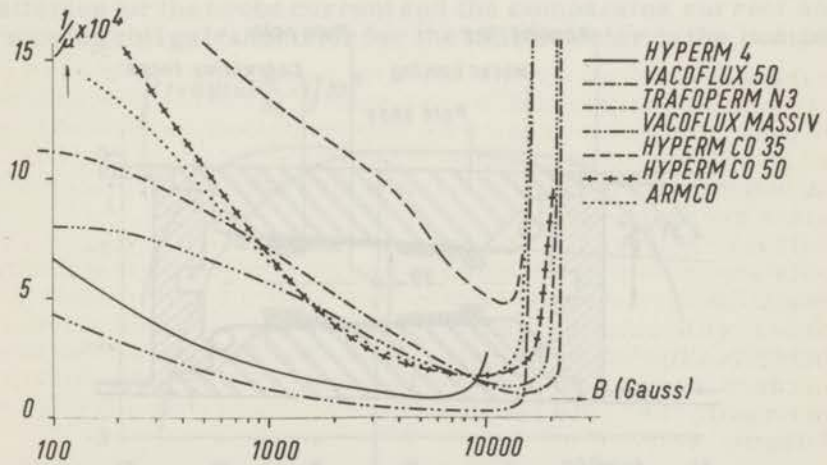

Fig. 10. $1/\mu$ as a function of the induction of some soft magnetic materials, according to the manufacturers' specifications for the properly heat-treated condition. (Trafoperm and Vacoflux: Vakuumschmelze A. G., Hanau, Germany; Hyperm: Fried. Krupp Widia Fabrik, Essen, Germany; Armco: Armco Corp., Middletown, Ohio, USA.)

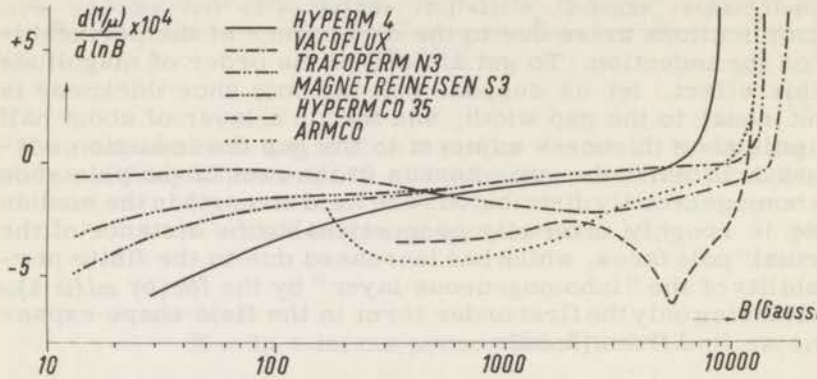

Fig. 11. $d(1/\mu)/d(\ln B)$ as a function of the induction for the same materials as in Fig. 10, according to the manufacturers' specifications.

These predictions were tested with an actual set of conical pole faces. These pole faces were mounted with a gap width 2b=22 mm at the radius of the main path r_m = 200 mm, and extended radially to -28 mm and +32 mm from the main path. (Fig. 12.) The cone angle was calculated to obtain n = 0.91. The pole faces were very carefully machined, heat treated, and ground from Trafoperm N-3, which is a 2.9% Si-Fe alloy, made by the Vakuumschmelze, Hanau, Germany.

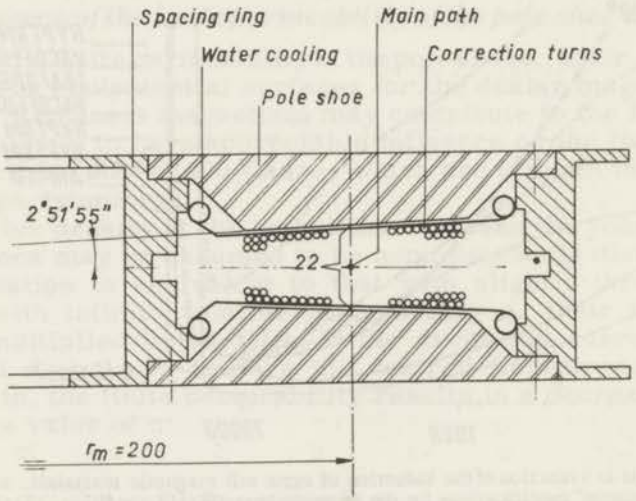

Fig. 12. Radial cross section of the pole shoe mounting. On the pole faces water cooled, copper disks are shown, carrying the correction tums discussed in sect. 4e.

The field shape was measured with a Hall generator (Siemens, Type FA 21), with a specified sensitive area of approximately $1.5 \times 3\ mm^2$. In the mounting in the probe, the larger of these two dimensions was in radial direction. The position of the sensitive area was established by moving the probe between two opposed magnetised sewing needles. By comparison of the resulting signal as a function of probe position, with the calculated field between two opposed magnetic charges at a distance of the needle tip-to-tip distance plus twice the tip radius, the effective extension of this sensitive area in radial direction was found to be smaller than 0.3 mm. The readings were taken as point readings.

The particular Hall generator was calibrated against proton resonance. Attempts were made to minimise temperature fluctuations by thermal insulation of the probe, which was not thermostated, however. No temperature correction was applied. To reduce the internal heating of the probe and the thermal lag through the change in resistance in varying fields, the Hall generator was supplied with only 20 mA, controlled by measuring the voltage developed across a 100 Ohm resistor with a precision comparator. The Hall signal was compared with a voltage derived from a mercury cell with an appropriate series resistance through a "Dekapot" decade potentiometer with 10 p.p.m. resolution. A Hewlett-Packard Model 425A micro-volt-ammeter with a sensitivity of $\pm 10\ \mu V$ f.s.d. served as a null detector. By very careful shielding, using shielded batteries for the probe current and the comparator current and a moving coil galvanometer for the null detector in the compa-

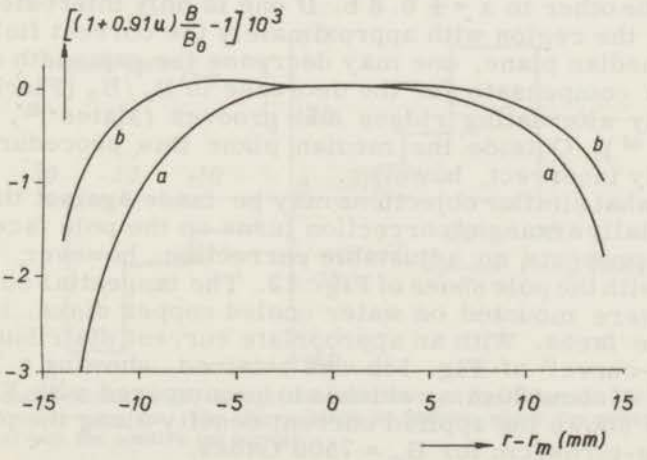

Fig. 13. The "error-curve" of the field shape, $(1 + 0.91\ u)B/B_o - 1$, as a function of $r - r_m$; a: without correction turns; b: with the current distribution through the correction turns as shown in Fig. 15.

rator, the total noise and short term instability could be reduced to about $\pm 0.5\,\mu V$, corresponding to an accuracy of $1 : 2 \times 10^4$ at 10 kiloGauss, or $1 : 2 \times 10^3$ at 1000 Gauss. The voltage of the mercury cell was found to be constant to about $1 : 10^5$ over the time needed for the measurement of about 30 points of the field shape. The magnet current was also checked on the comparator, and found to be constant to about $1 : 2 \times 10^4$ over the same period.

From (4, 9)-(4, 14) it follows that the field shape between ideal conical pole faces is given by $B_z/B_0 = 1/(1 + nu)$, where $u = (r-r_m)/r_m$.

The "error-curve", $(1 + 0.91\,u)B/B_0 - 1$, as a function of $r - r_m$, was found to be independent of the induction at the main path B_0, within the accuracy of the measurements, for inductions B_0 from 1000 Gauss to 12 kiloGauss. Without any correcting device for the finite radial pole face extension, a region of about 7 mm in radial direction corresponded to the theoretical prediction within the accuracy of the measurements.

4e: *Influence of the finite radial extension of the pole faces.*

Calculations and measurements [40-43] have shown, that the influence of the edges is negligible at a few gap widths away from the edges. See also Fig. 13. With a gap width 2b much smaller than the radius of deflection r_m, one may discuss the effect of one edge independent of the other.

In Fig. 14, two curves B_z/B_0 as a function of the radius, are shown, taken from the measurements of Septier [44] on plane parallel pole faces. One of these applies to the median plane $z = 0$, the other to $z = \pm 0.8$ b. If one is only interested in extending the region with approximately the correct field shape in the median plane, one may decrease the gap width near the edge to compensate for the decrease in B_z/B_0 (Fischer [20]), or apply alternating ridges and grooves (Mates [45], Zilverschoon [46]). Outside the median plane this procedure is essentially incorrect, however.

Somewhat similar objections may be made against the use of tangentially arranged correction turns on the pole faces. This device presents an adjustable correction, however, and was tested with the pole shoes of Fig. 12. The tangential correction turns were mounted on water cooled copper disks, laying on the pole faces. With an appropriate current distribution, the "error-curve" of Fig. 13b was obtained, showing a "correct region" of about 20 mm, which is to be compared with Fig. 13a. Fig. 15 shows the applied current density along the profile in Ampère-turns/cm for $B_0 = 7500$ Gauss.

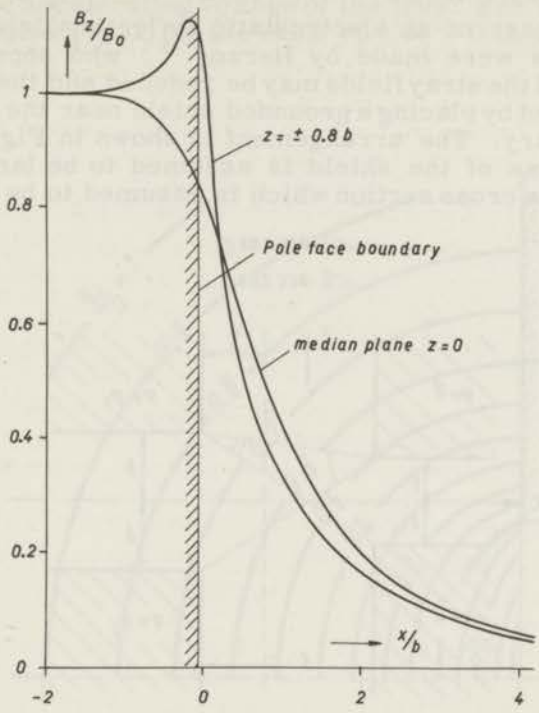

Fig. 14. B_z/B_o as a function of the radius, from the measurements of Septier [44]. The curves apply to the median plane z = 0, and to z = ± 0.8b.

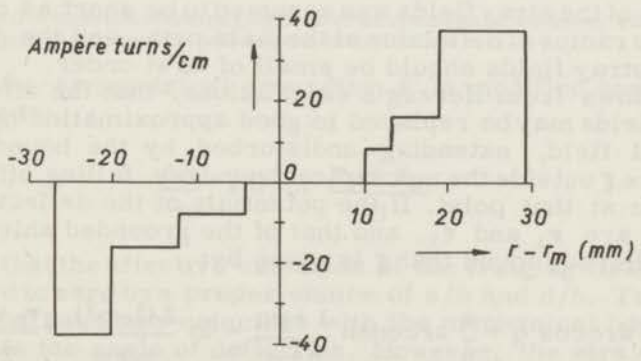

Fig. 15. Required current density through the correction turns for correction with B_o = 7500 Gauss, in Ampère-turns/cm. The sign is taken as positive where the positive current flows parallel with the positive ion current.

4f: *Effect of fringing fields.*

For the case of an electrostatic deflecting field, extensive calculations were made by Herzog [48], who showed that the extension of the stray fields may be reduced and their influence compensated by placing a grounded shield near the entrance or exit boundary. The arrangement is shown in Fig. 16, where the thickness of the shield is assumed to be large. Fig. 16 represents a cross section which is assumed to be independent

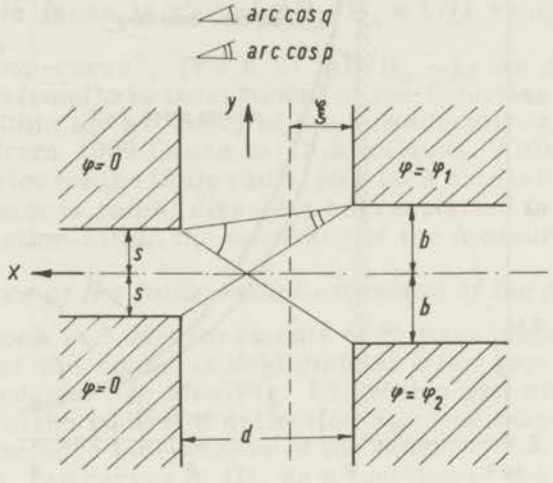

Fig. 16. Thick fringing field shield for an electrostatic condensor.

of the z-coordinate (normal to the plane of paper). The extension of the stray fields was assumed to be short as compared with the radius of deflection of the main path, and the deflection in the stray fields should be small of first order.

It follows from Herzog's calculations, that the effect of the stray fields may be replaced in good approximation by a hypothetical field, extending undisturbed by the boundary to a distance ξ outside the mechanical boundary, falling off abruptly to zero at that point. If the potentials of the deflecting electrodes are φ_1 and φ_2, and that of the grounded shield equals zero, Herzog found that ξ is given by:

$$\frac{\xi}{b} = \frac{1}{\pi}\left\{\frac{d}{b}\arccos q + \frac{s}{b}\operatorname{arccosh}\frac{1+pq}{p+q} - \ln\frac{2(1-q^2)}{p+q} + \frac{\varphi_1+\varphi_2}{2U}\ln 2\right\}, \tag{4,17}$$

where U is the accelerating voltage of the ions. For reference, Herzog's graph of (4, 17) for the case $\varphi_1 + \varphi_2 = 0$ is reproduced here in Fig. 17.

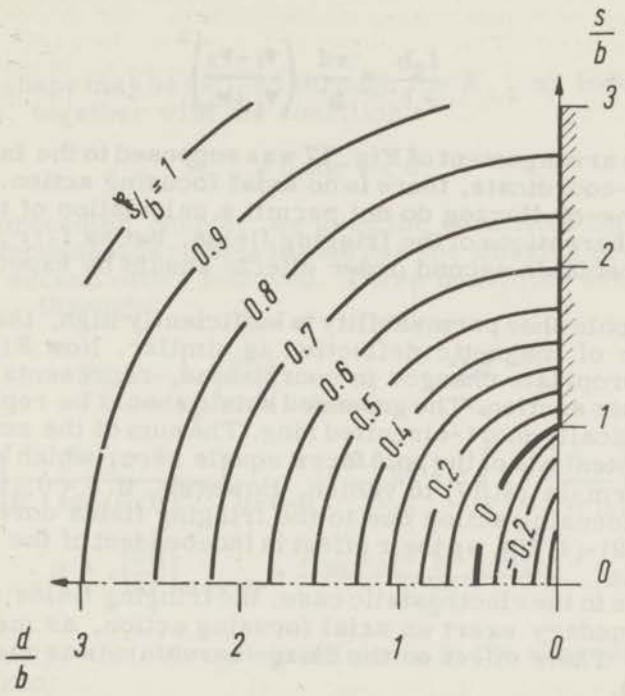

Fig. 17. Effective extension of the fringing fields of an electrostatic condensor with a thick shield. The graph is symmetrical with respect to the line s/b = 0.

In case of a-symmetrical grounding, ξ is modified somewhat according to:

$$\frac{\Delta \xi}{b} = 0.11 \frac{\varphi_1 + \varphi_2}{U}. \qquad (4,18)$$

It follows that the effective extension of the fringing fields may be reduced to zero by a proper choice of s/b and d/b. Then the hypothetical boundary coincides with the mechanical boundary as regards the angle of deflection. However, the stray fields exert also a focusing action, consisting of two terms. One of these, with radial focal length f_1, is independent of $\varphi_1 + \varphi_2$, whereas the other term, with radial focal length f_2 vanishes for $\varphi_1 + \varphi_2 = 0$. In fact, Herzog found that:

$$\frac{f_1 b}{r_e^2} = \frac{\pi}{\frac{b}{d}(\arccos p - \arccos(-q)) - \operatorname{arccosh}\frac{1+pq}{p+q} + \ln\frac{2(1-q^2)}{p+q}}; \tag{4,19}$$

$$\frac{f_2 b}{r_e^2} = \frac{\pi d}{b}\left(\frac{\varphi_1-\varphi_2}{\varphi_1+\varphi_2}\right)^2. \tag{4,20}$$

As the arrangement of Fig. 17 was supposed to the independent of the z-coordinate, there is no axial focusing action. The calculations of Herzog do not permit a calculation of the second order aberrations of the fringing fields, but as f_1/r_e is large, no appreciable second order effects should be expected.

If the pole shoe permeability is sufficiently high, the situation in case of magnetic deflection is similar. Now Fig. 17, with the appropriate changes in coordinates, represents a tangential cross section. The grounded shield should be replaced by a magnetically short-circuited ring. The sum of the scalar magnetic potentials of the pole faces equals zero, which causes the last term in (4, 17) to vanish. However, if $\xi = 0$, there is no radial focusing action due to the fringing fields corresponding to (4, 19)-(4, 20), as their effect is independent of the radial coordinate.

Unlike in the electrostatic case, the fringing fields at an oblique boundary exert an axial focusing action, as mentioned in (2, 57). Their effect on the image curvature was mentioned in (2, 104).

In the absence of fringing field shields, ξ as given by (4, 17) becomes infinite, which is a consequence of the assumed infinite pole shoe thickness. Actual measurements with finite pole shoe thickness resulted in values for ξ/b ranging from 2.0 to 2.2 . (König and Hintenberger [42] ; Nier [49]).

4g: *Field shape of the toroidally curved electrostatic field.*

The electrostatic potential φ obeys the Laplacian equation:

$$\nabla^2\varphi = 0. \tag{3,2}$$

Expanding φ in a power series in u and v around the main path:

$$\varphi = \sum_{i,k=0}^{\infty} A_{i,k}\, u^i v^k, \tag{3,1}$$

(where the symmetry causes the $A_{i,k}$ with k = odd vanish), we have the relation from (3, 1)-(3, 2):

$$(k+2)(k+1)(A_{i,k+2} + A_{i+1,k+2}) = -(i+3)(i+2)A_{i+3,k} - (i+2)^2 A_{i+2,k} \qquad (4, 21)$$

The field shape may be defined through the $A_{i,0}$ as independent variables, together with the condition:

$$A_{i,k} = 0 \text{ for } i < 0. \qquad (4, 22)$$

In the preceding chapter we used the quantities E_o, c, and R_e' as independent variables to express the imaging properties up to the second order included. These quantities are related to the $A_{i,k}$ through:

$$E_o = -\frac{1}{r_e}\left(\frac{\partial \varphi}{\partial u}\right)_{u=v=0} = -\frac{A_{10}}{r_e}. \qquad (4, 23)$$

$$c = \frac{r_e}{R_e} = \left(\frac{-d^2u/dv^2}{\{1+(du/dv)^2\}^{3/2}}\right)_{u=v=0} = \frac{2A_{02}}{A_{10}} = -\left(1 + 2\frac{A_{20}}{A_{10}}\right). \qquad (4, 24)$$

$$R_e' = \left(\frac{\partial R}{\partial r}\right)_{u=v=0} = \frac{A_{20}A_{02} - \frac{1}{2}A_{10}A_{12}}{A_{02}^2}. \qquad (4, 25)$$

Conversely, the relevant coefficients in the expansion (3, 1) are equal to:

$$A_{00} = U; \qquad A_{10} = -r_e E_o; \qquad A_{20} = r_e E_o \left(\frac{1+c}{2}\right);$$

$$A_{02} = -r_e E_o c; \qquad A_{30} = -r_e E_o \left\{\frac{1+c}{3} + \frac{c^2}{6}(1+R_e')\right\}; \qquad (4, 26)$$

$$A_{12} = r_e E_o \left\{\frac{c}{2} + \frac{c^2}{2}\right\}(1+R_e').$$

4h: *Shape of the deflecting electrodes.*

The toroidal radii of curvature follow directly from the toroidal radius of curvature of the equipotential surface comprising the main path, $R_e = r_e/c$, and its first radial derivative

R_e'. Designating the radii of curvature of the electrodes by R_a, $r_e + a$, and R_b, $r_e - b$, respectively, we thus have:

$$R_a \approx (r_e/c) + aR_e'; \qquad R_b \approx (r_e/c) - bR_e'; \tag{4,27}$$

The electrodes should be at potentials V_a and V_b:

$$V_a = U + r_e E_o(-a + \tfrac{1}{2}(1+c)a^2); \qquad V_b = U + r_e E_o(b + \tfrac{1}{2}(1+c)b^2). \tag{4,28}$$

The condition that the intersections of the electrode surfaces with a plane w = const. should be parts of circles, defines the higher order terms omitted in (4, 28). Liebl and Ewald [24] quote the following expressions for $R_e' < 0.5$, which should be exact to the third order:

$$R_a = \tfrac{1}{2}\left\{a + k + \frac{k^2(1-2R_e')}{a+k}\right\}; \qquad R_b = \tfrac{1}{2}\left\{-b + k + \frac{k^2(1-2R_e')}{-b+k}\right\}; \tag{4,29}$$

$$k = R_e/(1 - R_e').$$

CHAPTER 5

ADJUSTABLE DEVICES FOR THE ELIMINATION OF ABERRATIONS

5a: *Scope of the adjustments.*

For systems comprising either an inhomogeneous magnetic or a toroidal electrostatic sector field, the calculations presented in chapters 2 and 3 determined the magnitude of the aberrations up to the second order. Likewise, systems consisting of a tandem arrangement of an electrostatic field, followed by a magnetic field, will be discussed in chapter 6. In all cases, the zeroth order aberration, as well as at least some of the first and second order aberrations, can be eliminated by a proper choice of the instrument parameters.

However, it seems desirable to incorporate some adjustable devices to compensate the effect of slight deviations from the prescribed parameters. In sect. 5f, an auxiliary device is presented for the elimination of the image curvature, which is not readily achieved by a careful choice of the instrument parameters alone.

The discussion of the elimination of the first order velocity aberration will be presented in the next chapter. The present chapter deals with the zeroth order, and one second order aberration and two first order aberrations:

1. The zeroth order approximation corresponds to the requirement, that the trajectory of the main path should fit into the instrument design for ions of the appropriate mass-to-charge ratio and energy.

2. The image should be formed at the collector slit. Deviation from the correct image distance l''_m results in a first order aberration.

3. The object and image slits should be correctly aligned, i.e. they should be parallel to each other and normal to the median plane of the deflecting field. Moreover, in a tandem arrangement, the median planes of the deflecting field should coincide. Misalignment results in a first order aberration.

4. The image curvature (δ^2-aberration) is best eliminated by an auxiliary device.

5b: *The trajectory of the main path.*

The accelerating voltage of the ions and the field strengths in the deflecting fields should be adjusted to satisfy (2, 6)-(2, 7), (2, 39). Moreover, some additional adjustement may be incorporated, either mechanically by bellow devices, or electro-

statically by using variable deflecting fields. (Fig. 18). The position of entrance and exit are affected by deflections near

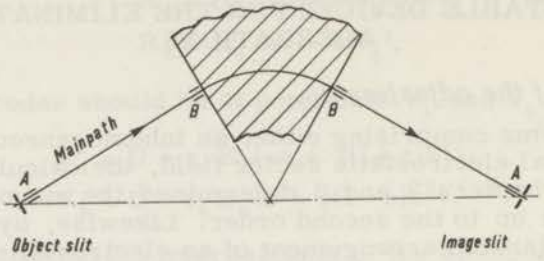

Fig. 18. Adjustment of the trajectory of the main path by variable electrostatic deflecting fields.

the slits (A), whereas deflections near the field boundaries (B) affect the angles of entrance and exit into the deflecting field.

5c: *Adjustment of object and image distances.*

In the usual symmetrical design of single focusing homogeneous field sector type mass spectrometers, this adjustment may be effected by moving the analyser tube relative to the deflecting field parallel to the plane $w = \phi_m/2$. This results in a simultaneous change of the object and image distances and of the radius of the main path. Only the ratios l'_m/r_m and l''_m/r_m are ion-optically relevant, and as an increase in l'_m and l''_m is accompanied by a decrease in r_m, both variations act in the same sense.

Complications arise, however, when the deflecting field is inhomogeneous and /or the boundaries are curved, and for $\phi_m = \pi$. Now the adjustment may be achieved mechanically, or ion-optically by placing an ion lens of variable strength between slit and field boundary. Magnetic lenses are apt to introduce complications with magnetic scanning, and rotate the image (see sect. 5d).

Care should be taken in the choice of the type of lenses in view of their aberrations. Systems with two planes of symmetry exhibit no second order aberrations, but their third order aberrations may become objectionable. For a rotationally symmetric lens system, consisting of coaxial tubes of equal diameter D, the order of magnitude of the aberration may be derived from data of Zworykin [50] and Klemperer [51]. Ions entering the lens as a parallel beam at a distance r from the axis are focused at a shorter distance than the paraxial ions; for weak lenses this difference in focal length is of the order of:

$$\frac{\Delta f}{f} \approx 1.5 \left(\frac{r}{D}\right)^2. \qquad (5,1)$$

These lenses are essentially positive. The object and image distances should thus be made shorter than the prescribed value to make them applicable. Except for very small adjustment ranges the aberration (5, 1) is so serious, that the advantage of the facility is largely lost. These lenses compare unfavourably with the deflecting fields in view of their aberrations, because the distance from the axis is measured in units D instead of in usually much larger units r_m or r_e.

However, electrostatic quadrupole lenses with hyperbolic equipotentials do not exhibit serious aberrations except for the influence of the end effects, which is proportional to the opening-to-length ratio.

5d: *Alignment of the object and image slits.*

Rotation out of its correct position over the angle ϑ of an image slit of height h, corresponds to an image broadening $h\vartheta$. Misalignment of the object slit may be taken into account similarly as a virtual object broadening.

The obvious way of correcting misalignment is rotating the slits mechanically into their correct position. It is also possible to incorporate a device for the continuous rotational adjustment by means of electrostatic or magnetic fields.

A quadrupole field with the potential distribution

$$\varphi = U + Vyz, \qquad (5,2)$$

and with the field components

$$E_y = - Vz, \qquad (5,3)$$

$$E_z = - Vy, \qquad (5,4)$$

placed near the corresponding slit, exerts a rotating action. The equipotential surfaces are hyperbolic cylinders. Fig. 19 represents a cross section with a plane x = const. The field may be generated by hyperbolic cylindrical electrodes or approximated with circular cylindrical electrodes.

At first, we assume the quadrupole field (5, 2) to be present over an effective length L, starting at a distance D from e. g. the object slit. (Shaded area in Fig. 20). Considering a trajectory emerging from the slit with $\alpha_m = \alpha_{zm} = 0$; $\delta \neq 0$; we find from (5, 3) for the point where it leaves the quadrupole field:

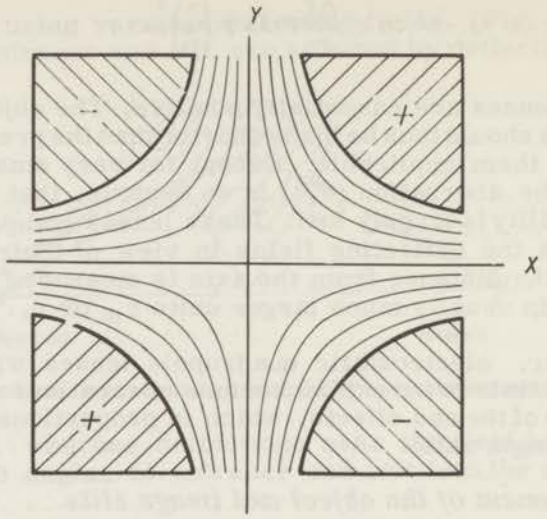

Fig. 19. Intersection with a plane x = const. of the quadrupole field (5, 2) for virtual slit rotation.

$$\frac{dy_1}{dx_1} = \frac{1}{2}\frac{V}{U} L\delta; \qquad (5, 5)$$

$$y_1 = -\frac{1}{4}\frac{V}{U} L^2\delta. \qquad (5, 6)$$

Hence the path seems to come from a virtual object point, displaced over the distance Δ:

$$\Delta = \left(\frac{L}{2} + D\right)\frac{LV}{2U}\delta; \qquad (5, 7)$$

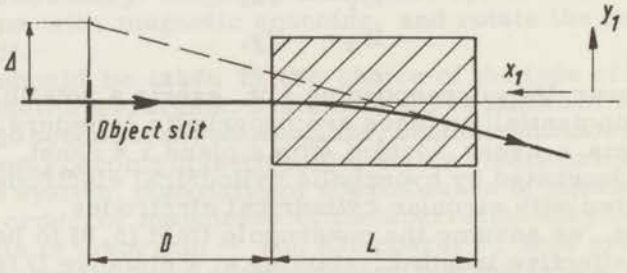

Fig. 20.

which is equivalent to a virtual rotation of the object slit over the angle:

$$\vartheta = \frac{\Delta}{\delta} = (\frac{L}{2} + D)\frac{LV}{2U} . \qquad (5,8)$$

For trajectories with $\alpha_{zm} \neq 0$, the above reasoning remains valid, provided that:

$$\alpha_{zm} \ll \frac{\delta}{\frac{1}{2}L + D} . \qquad (5,9)$$

Trajectories with $\alpha_m \neq 0$ undergo an irrelevant deflection in the z-direction due to (5, 4).

In the arrangement of Fig. 20, the virtual slit rotation is accompanied by a deflection of the trajectories outside the median plane. Rotation without resulting deflection is possible by an arrangement as in Fig. 21, where the available length L is divided in two parts of length L/2, in the second of which the parameter V is made the reverse of that in the first part. At the exit of the second part we now have:

$$dy_1/dx_1 = 0; \qquad (5,10)$$

$$y_1 = \Delta = -\frac{L^2V}{8\ U}\delta; \qquad (5,11)$$

and thus:

$$\vartheta = -\frac{L^2V}{8\ U} . \qquad (5,12)$$

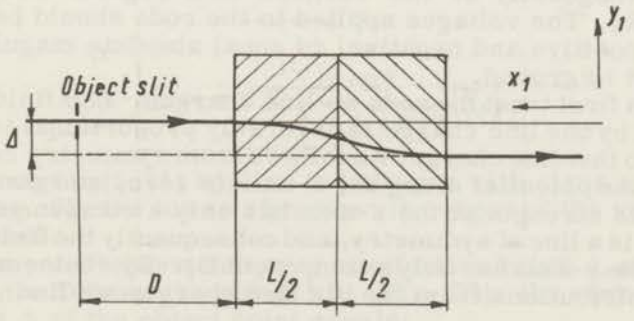

Fig. 21.

The restriction (5, 9) remains unchanged. The resulting rotation is smaller than (5, 8), and in the opposite sense.

It is also possible to rotate a slit virtually by means of a longitudinal magnetic field. As may be derived from Busch' theorem (Pierce [52]), a magnetic field component B_x in the direction of the main path causes rotation of the beam over the angle:

$$\vartheta = \tfrac{1}{2}\sqrt{\frac{e}{2mU_a}}\int_a^b B_x\,dx = \frac{1}{2r_m}\int_a^b \frac{B_x}{B_o}\,dx. \qquad (5,13)$$

The integral is to be evaluated along the main path, where the longitudinal field is supposed to extend from x=a to x=b. B_o is the magnetic field strength at the main path in the deflecting field.

Besides a rotating action, a longitudinal magnetic field exerts also a focusing action, acting as a (weak) lens with focal length f given by:

$$\frac{r_m}{f} = \frac{1}{4r_m}\int_a^b \left(\frac{B_x}{B_o}\right)^2 dx. \qquad (5,14)$$

If the distance a - b is not small as compared with r_m, the focusing action accompanying small rotations is neglegible.

5e: *Correction of the image curvature.*

An electrostatic hexapole field may be used to create a virtual object or image curvature, which may be made the reverse of that produced by the rest of the system, such as to result in an image free from the δ^2-aberration.

The arrangement, illustrated in Fig. 22, consists of six thin cylindrical rods with radius r_h, intersecting the plane of drawing orthogonally at the corners of a regular hexagon with sides R_h. The voltages applied to the rods should be alternatively positive and negative, of equal absolute magnitude with respect to ground.

Let us first treat the rods as line charges. The field strength caused by one line charge is inversely proportional to the distance to that line charge. As follows from symmetry considerations, the potential along the z-axis is zero, and consequently the field strength at the z-axis has only a component E_y. The y-axis is a line of symmetry, and consequently the field strength along the y-axis has only a component E_y. By vector addition of the contributions from the six line charges we find:

Field strength along the z-axis:

$$E_y(\text{z-axis}) = \frac{K}{R_h} \frac{6(z/R_h)^2}{1 + (z/R_h)^6}; \qquad (5,15)$$

Field strength along the y-axis:

$$E_y(\text{y-axis}) = \frac{K}{R_h} \frac{6(y/R_h)^2}{1 - (y/R_h)^6}. \qquad (5,16)$$

Taking the origin at zero potential, we find the potential along the y-axis by integration of (5, 16):

$$V(\text{y-axis}) = K \ln \frac{1 + (y/R_h)^3}{1 - (y/R_h)^3}. \qquad (5,17)$$

The factor K is proportional to the charge per unit length. Now assuming thin rods with radius r_h instead of the line charges, the relation between K and the voltages on the rods V_r reads:

$$V_r \approx \pm K \ln \frac{1 + (1-q)^3}{1 - (1-q)^3} \approx \pm K \ln \frac{2}{3q}. \qquad (5,18)$$

where:

$$q = r_h/R_h \ll 1. \qquad (5,19)$$

Writing:

$$Q = 6/\ln \frac{2}{3q}, \qquad (5,20)$$

we have:

$$E_y(\text{z-axis}) \approx \pm Q \frac{z^2/R_h^3}{1 + (z/R_h)^6} |V_r|. \qquad (5,21)$$

The upper sign in (5, 21) applies to voltages with signs as indicated in Fig. 22; the lower sign when the signs of the voltages are reversed.

If the hexapole field extends over an effective length L starting at a distance D from the object slit (Fig. 20), the virtual displacement Δ of the object point equals:

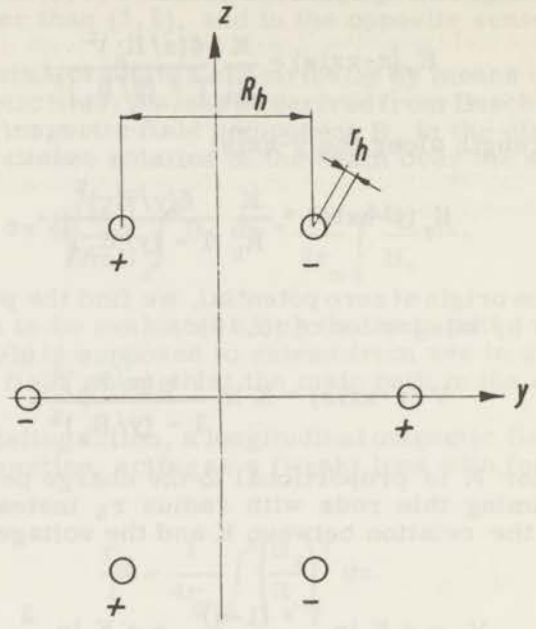

Fig. 22. Electrostatic hexapole field for correcting the image curvature.

$$\Delta \approx \mp \frac{L^2 + 2LD}{4U} \frac{\delta^2 Q}{R_h^3} |V_r| , \qquad (5, 22)$$

provided that the condition (5, 9) holds. The object is thus curved virtually with a radius of curvature R_{obj} equal to:

$$R_{obj} \approx \mp \frac{2U\, R_h}{(L^2 + 2LD)\, Q |V_r|} . \qquad (5, 23)$$

However, this effect is accompanied by a radial deflection of the trajectories outside the median plane. Continuously variable virtual object curvature is possible without remaining radial deflection by an arrangement as in Fig. 21, where the signs of the voltages in the second part of length L/2 should be the reverse of those in the first part. Then we have:

$$R_{obj} \approx \pm \frac{4\, U\, R_h^3}{L^2\, Q\, |V_r|}, \qquad (5, 24)$$

the sign of the curvature being related to the voltages in the first part.

A hexapole field near the image slit influences the image curvature in the same way, and thus a straight image is obtainable. Strictly, one hexapole system placed somewhere between object and image slit suffices to eliminate the δ^2-aberration; however, if the condition (5, 9) does not apply, the relation between the resulting object or image curvature and the applied voltages is not of the simple form of (5, 23) or (5, 24).

CHAPTER 6

ION OPTICS OF THE DOUBLE FOCUSING MASS SPECTROMETER

6a: *Radial imaging properties of the tandem arrangement; first order double focusing.*

In a tandem arrangement as considered in this chapter, the ion beam passes at first through an electrostatic deflecting field, and subsequently through a magnetic deflecting field, not overlapping the electrostatic field. It will be shown, that by a suitable choice of the parameters at least the first order velocity aberration at the position of the mass spectrum may be eliminated, producing an image which is in first order independent of the velocity spread or energy spread of the ion beam. Thus one of the limiting factors in the resolving power of single focusing mass spectrometers is eliminated.

The discussion will be restricted to a combination of two sector fields in the sense as defined in chapters 2 and 3. The influence of the stray fields as expressed by (2, 57) is accounted for. The influence of the stray fields on the image curvature (2, 104) will be mentioned lateron.

At first we will assume the ions to be of mass m_o and charge e_o, and use β to denote the relative velocity deviation:

$$v = v_o(1+\beta). \tag{2, 37}$$

From now on we will use α to denote the radial aperture angle in the object space:

$$\alpha = -\, dy_1/dx_1, \tag{6, 1}$$

and α_z to indicate the axial aperture angle in the object space:

$$\alpha_z = -\, dz_1/dx_1. \tag{6, 2}$$

We will express the trajectories in the general coefficients (3, 20)-(3, 27), (3, 32)-(3, 37), (2, 49)-(2, 56), (2, 75)-(2, 78). With the abbreviations:

$$[K] = K_1\alpha + K_2\beta + K_{11}\alpha^2 + K_{12}\alpha\beta + K_{22}\beta^2 + \\ + K_{33}\alpha_z^2 + K_{34}\alpha_z(\delta/r_e) + K_{44}(\delta/r_e)^2; \tag{6, 3}$$

$$[L] = L_1\alpha + L_2\beta + L_{11}\alpha^2 + L_{12}\alpha\beta + L_{22}\beta^2 + \\ + L_{33}\alpha_z{}^2 + L_{34}\alpha_z(\delta/r_e) + L_{44}(\delta/r_e)^2; \qquad (6,4)$$

$$[\Pi] = \Pi_3\alpha_z + \Pi_4(\delta/r_e); \qquad (6,5)$$

$$[P] = P_3\alpha_z + P_4(\delta/r_e); \qquad (6,6)$$

we may write the expressions (3, 18)-(3, 19) in the form:

$$y_2 = r_e[K] + x_2[L]; \qquad (6,7)$$

$$z_2 = r_e[\Pi] + x_2[P]. \qquad (6,8)$$

The deflection in the magnetic field may be either in the same sense as in the electrostatic field (Fig. 23), or in the opposite sense (Fig. 24). The magnetic field sees the ion trajectory as if it originates from an object at the object distance:

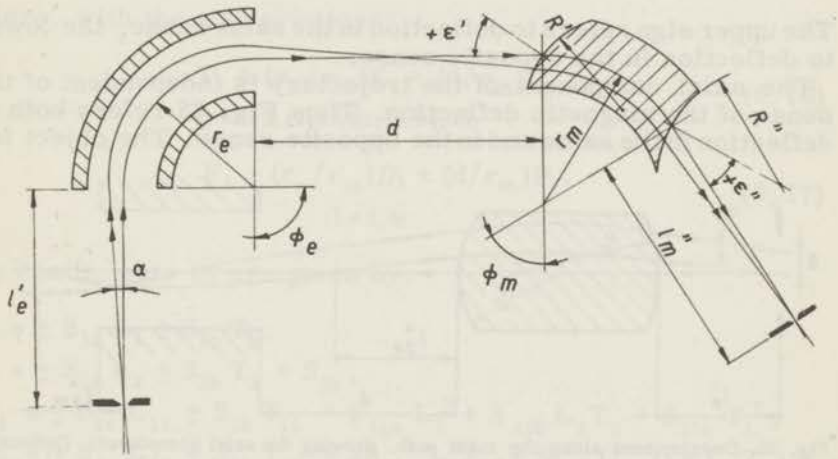

Fig. 23. Deflection in the same sense. Projection on the median plane.

$$l'_m = d + r_e[K]/[L], \qquad (6,9)$$

whereas the aperture angle equals:

$$\alpha_m = \pm[L]. \qquad (6,10)$$

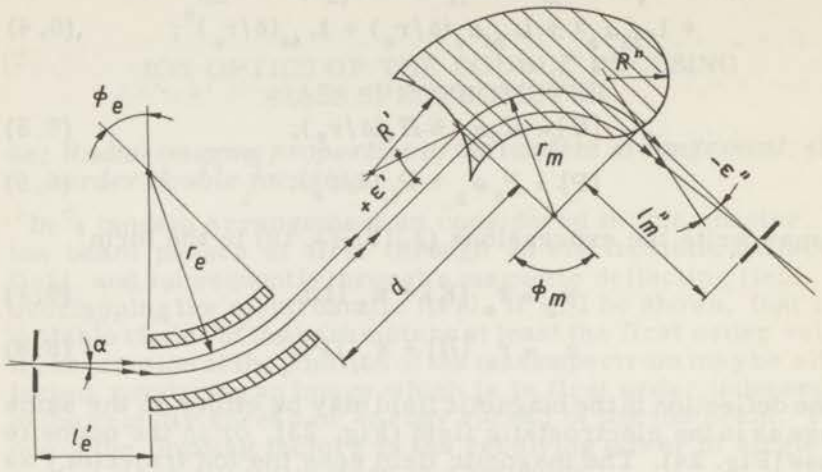

Fig. 24. Deflection in the opposite sense. Projection on the median plane.

The upper sign refers to deflection in the same sense, the lower to deflection in the opposite sense.

The axial component of the trajectory is independent of the sense of the magnetic deflection. Thus Fig. 25 refers both to deflection in the same and in the opposite sense. The object for

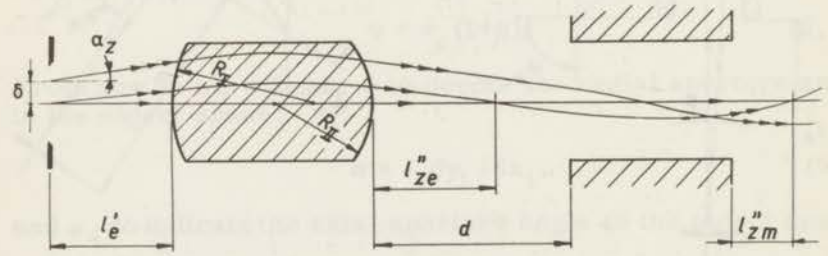

Fig. 25. Development along the main path, showing the axial components. Deflection either in the same or in the opposite sense.

the magnetic field is located at the distance from the median plane:

$$\delta^* = r_e\{[\Pi] - [P][K]/[L]\}, \qquad (6,11)$$

whilst the axial aperture angle is:

$$\alpha_{zm} = [P]. \qquad (6,12)$$

Writing the abbreviations:

$$S_j = \mu_j + \nu_j (l''_m / r_m), \qquad (j = 1a, 1b, 2a, 11a, 11b, 11c, 12a, 12b, 22a, 33a, 33b, 33c, 34a, 34b, 44a.) \tag{6,13}$$

and using the relations:

$$S_{34a} = S_{33b}; \qquad S_{34b} = 2\, S_{44a} = 2\, S_{33c}; \tag{6,14}$$

the radial component of the ion trajectory y_B at the image distance l''_m is found from (2, 47) with (6, 3)-(6, 6), (6, 9)-(6, 14) to be given by:

$$y_B / r_m = B_1\alpha + B_2\beta + B_{11}\alpha^2 + B_{12}\alpha\beta + B_{22}\beta^2 + B_{33}\alpha_z^2 + B_{34}\alpha_z(\delta/r_e) + B_{44}(\delta/r_e)^2, \tag{6,15}$$

where, with the abbreviations:

$$T_i = (r_e / r_m)K_i + (d/r_m)L_i; \qquad (i = 1, 2, 11, 12, 22, 33, 34, 44) \tag{6,16}$$

$$F_i = (r_e / r_m)\Pi_i + (d/r_m)P_i; \qquad (i = 3, 4) \tag{6,17}$$

the coefficients B_i are given by:

$$\begin{aligned}
B_1 &= \pm S_{1a} L_1 \pm S_{1b} T_1; \\
B_2 &= \pm S_{1a} L_2 \pm S_{1b} T_2 + S_{2a}; \\
B_{11} &= \pm S_{1a} L_{11} \pm S_{1b} T_{11} + S_{11a} L_1^2 + S_{11b} L_1 T_1 + S_{11c} T_1^2; \\
B_{12} &= \pm S_{1a} L_{12} \pm S_{1b} T_{12} + 2S_{11a} L_1 L_2 + S_{11b} (L_1 T_2 + L_2 T_1) + \\
&\quad + 2S_{11c} T_1 T_2 \pm S_{12a} L_1 \pm S_{12b} T_1; \\
B_{22} &= \pm S_{1a} L_{22} \pm S_{1b} T_{22} + S_{11a} L_2^2 + S_{11b} L_2 T_2 + S_{11c} T_2^2 + \\
&\quad \pm S_{12a} L_2 \pm S_{12b} T_2 + S_{22a}; \\
B_{33} &= \pm S_{1a} L_{33} \pm S_{1b} T_{33} + S_{33a} P_3^2 + S_{33b} P_3 F_3 + S_{33c} F_3^2; \\
B_{34} &= \pm S_{1a} L_{34} \pm S_{1b} T_{34} + 2S_{33a} P_3 P_4 + S_{33b} (P_3 F_4 + P_4 F_3) + \\
&\quad + 2S_{33c} F_3 F_4; \\
B_{44} &= \pm S_{1a} L_{44} \pm S_{1b} T_{44} + S_{33a} P_4^2 + S_{33b} P_4 F_4 + S_{33c} F_4^2 .
\end{aligned} \tag{6,18}$$

The expressions for B_1-B_{22} are identical to those published by Hintenberger and König [53]; the expression for B_{33} is equivalent to that published by Wachsmuth, Liebl, and Ewald [54].

First order direction focusing occurs if:

$$B_1 = 0; \tag{6,19}$$

and first order velocity focusing if:

$$B_2 = 0. \tag{6,20}$$

To achieve first order double focusing, both (6,19) and (6,20) should be satisfied. This determines the image and object distances as [53]:

$$\frac{l''_m}{r_m} = -\frac{a_z + b_z(r_e/r_m) + c_z(d/r_m)}{a_n + b_n(r_e/r_m) + c_n(d/r_m)}; \tag{6,21}$$

$$\frac{l'_e}{r_e} = -\frac{A_z + B_z(r_e/r_m) + C_z(d/r_m)}{A_n + B_n(r_e/r_m) + C_n(d/r_m)}; \tag{6,22}$$

where the abbreviations read with the sector fields treated in Chapters 2 and 3:

$$\begin{aligned} a_z &= \pm\lambda_{2a}\mu_{1a} + \mu_{2a}; & a_n &= \pm\lambda_{2a}\nu_{1a} + \nu_{2a}; \\ b_z &= \pm\kappa_{2a}\mu_{1b}; & b_n &= \pm\kappa_{2a}\nu_{1b}; \\ c_z &= \pm\lambda_{2a}\mu_{1b}; & c_n &= \pm\lambda_{2a}\nu_{1b}; \end{aligned} \tag{6,23}$$

$$\begin{aligned} A_z &= \pm\lambda_{1a}\mu_{2a}; & A_n &= \pm\lambda_{1b}\mu_{2a}; \\ B_z &= \pm\kappa_{1a}(\bar{\nu}_{2a} + \bar{\mu}_{2a}t') + \kappa_{2a}; & B_n &= \pm\kappa_{1b}(\bar{\nu}_{2a} + \bar{\mu}_{2a}t') + \lambda_{2a}; \\ C_z &= \pm\lambda_{1a}(\bar{\nu}_{2a} + \bar{\mu}_{2a}t'); & C_n &= \pm\lambda_{1b}(\bar{\nu}_{2a} + \bar{\mu}_{2a}t'). \end{aligned} \tag{6,24}$$

For a trajectory with $\alpha_z = 0$, the axial coordinate z_B at the image distance l''_m is given by:

$$z_B/r_m = \left\{\langle\sigma_{3a} + (l''_m/r_m)\tau_{3a}\rangle P_4 + \langle\sigma_{3b} + (l''_m/r_m)\tau_{3b}\rangle F_4\right\}(\delta/r_e) = G(\delta/r_e). \tag{6,25}$$

The image broadening due to the $(\delta/r_e)^2$ aberration with coefficient B_{44} corresponds to an image curvature with radius R_{im}:

$$r_m / R_{im} = \tfrac{1}{2} B_{44} / G^2. \qquad (6,26)$$

This curvature should be added to that resulting from the fringing fields of the magnetic sector field:

$$r_m / R_{fr} = S_{1b} - 1. \qquad (2,104)$$

The mass dispersion in the y-direction per unit $\delta m / m_o$ equals:

$$D_m = \tfrac{1}{2} r_m S_{2a}. \qquad (6,27)$$

The angular magnification in radial direction is found as the product of the angular magnifications of the electrostatic and magnetic field:

$$M_{ang} = \pm L_1 / S_{1b}. \qquad (6,28)$$

As object and image are at the same electrostatic potential, the radial lateral magnification is the inverse of M_{ang}:

$$M_{lat} = \pm S_{1b} / L_1. \qquad (6,29)$$

The mass resolving power is given by:

$$R = D_m / (s' M_{lat} + s'' + \Sigma A_i). \qquad (2,106)$$

In a double focusing arrangement, the image planes where $B_1 = 0$ and where $B_2 = 0$ intersect at the main path at the image distance l''_m. The inclinations were calculated by Liebl [55], who found for the direction focusing plane:

$$\tan \chi_R = - \frac{S_{2a} (\pm \nu_{1a} L_1 \pm \nu_{1b} T_1)}{\pm S_{12a} L_1 \pm S_{12b} T_1}; \qquad (6,30)$$

and for the energy focusing plane:

$$\tan \chi_E = - \frac{S_{2a} (\pm \nu_{1a} L_2 \pm \nu_{1b} T_2 + \nu_{2a})}{\pm S_{12a} L_2 \pm S_{12b} T_2 + 2 S_{22a} + S_{2a}}. \qquad (6,31)$$

6b: *Axial imaging properties of the tandem arrangement; first order stigmatic focusing.*

After passing through the electrostatic field, the axial component of the ion trajectory (3, 8) corresponds to first order axial focusing at the axial image distance l''_{ze}:

$$l''_{ze}/r_e = -\Pi_3/P_3; \qquad (6,32)$$

and after passing through the magnetic field at the axial image distance l''_{zm}:

$$\frac{l''_{zm}}{r_m} = -\frac{\sigma_{3a}+\sigma_{3b}(d-l''_{ze})/r_m}{\tau_{3a}+\tau_{3b}(d-l''_{ze})/r_m}. \qquad (6,33)$$

Equating (6, 33) to (6, 21), we find the condition for stigmatic focusing as a cubic relation between (r_e/r_m) and (d/r_m):

$$A_1 + A_2(r_e/r_m) + A_3(d/r_m) + A_4(r_e/r_m)^2 + A_5(r_e/r_m)(d/r_m) + A_6(d/r_m)^2 + A_7(r_e/r_m)^3 + A_8(r_e/r_m)^2(d/r_m) + A_9(r_e/r_m)(d/r_m)^2 + A_{10}(d/r_m)^3 = 0. \qquad (6,34)$$

With the abbreviations:

$$P_z = \pi_{3a}A_n - \pi_{3b}A_z; \quad P_n = \rho_{3a}A_n - \rho_{3b}A_z;$$
$$Q_z = \pi_{3a}B_n - \pi_{3b}B_z; \quad Q_n = \rho_{3a}B_n - \rho_{3b}B_z; \qquad (6,35)$$
$$R_z = \pi_{3a}C_n - \pi_{3b}C_z; \quad R_n = \rho_{3a}C_n - \rho_{3b}C_z;$$

$$a_1 = \sigma_{3a}a_n - \tau_{3a}a_z; \quad a_2 = \sigma_{3b}a_n - \tau_{3b}a_z;$$
$$b_1 = \sigma_{3a}b_n - \tau_{3a}b_z; \quad b_2 = \sigma_{3b}b_n - \tau_{3b}b_z; \qquad (6,36)$$
$$c_1 = \sigma_{3a}c_n - \tau_{3a}c_z; \quad c_2 = \sigma_{3b}c_n - \tau_{3b}c_z;$$

the coefficients in (6, 34) are given by:

$$A_1 = a_1P_n; \quad A_2 = a_1Q_n + a_2P_z + b_1P_n; \quad A_3 = a_1R_n + (a_2+c_1)P_n;$$
$$A_4 = a_2Q_z + b_1Q_n + b_2P_z; \quad A_5 = a_2(Q_n+R_z) + b_1R_n + b_2P_n + c_1Q_n + c_2P_z;$$
$$A_6 = (a_2+c_1)R_n + c_2P_n; \quad A_7 = b_2Q_z; \quad A_8 = b_2(Q_n+R_z) + c_2Q_z;$$
$$A_9 = b_2R_n + c_2(Q_n+R_z); \quad A_{10} = c_2R_n. \qquad (6,37)$$

A system which satisfies (6, 21)-(6, 22) and (6, 34) provides first order stigmatic double focusing, with axial angular magnification:

$$M^z_{ang} = \frac{\rho_{3a} + \rho_{3b}(l'_e/r_e)}{\sigma_{3b} + \tau_{3b}(l''_m/r_m)}, \qquad (6,38)$$

and axial lateral magnification (see 6, 25):

$$M^{z}_{lat} = \frac{\sigma_{3b} + \tau_{3b}\,(l''_m/r_m)}{\rho_{3a} + \rho_{3b}\,(l'_e/r_e)} = G\,\frac{r_m}{r_e}. \qquad (6,39)$$

6c: *The Mattauch arrangement.*

If ions of equal energy travel parallel between the electrostatic and the magnetic field, and the deflection in these fields occurs in opposite direction, the previous expressions take a particularly simple form. This case is commonly realised in mass spectrographs. We now have:

$$L_1 = 0; \qquad (6,40)$$

and because of (6, 19):

$$S_{1b} = 0; \qquad (6,41)$$

as the solution $T_1 = 0$ is devoid of physical meaning. (6, 41) is equivalent to:

$$l''_m/r_m = -\mu_{1b}/\nu_{1b}; \qquad (6,41a)$$

and (6, 40) to:

$$l'_e/r_e = -\lambda_{1a}/\lambda_{1b}. \qquad (6,40a)$$

On equating either (6, 41a) to (6, 21) or (6, 40a) to (6, 22), we find the condition for first order double focusing as:

$$\lambda_{2a} = \mu_{1b}\,\nu_{2a} - \mu_{2a}\,\nu_{1b}. \qquad (6,42)$$

The condition for stigmatic focusing takes a particularly simple form as only one root of (6, 34) remains. On equating (6, 41a) to (6, 33), we find the condition:

$$\frac{d}{r_m} + \frac{\pi_{3a}\lambda_{1b} - \pi_{3b}\lambda_{1a}}{\rho_{3a}\lambda_{1b} - \rho_{3b}\lambda_{1a}} \cdot \frac{r_e}{r_m} + \frac{\sigma_{3a}\nu_{1b} - \tau_{3a}\mu_{1b}}{\sigma_{3b}\nu_{1b} - \tau_{3b}\mu_{1b}} = 0. \qquad (6,43)$$

In view of (6, 42), the mass dispersion in the y-direction, per unit $\delta m/m_o$, equals:

$$D_m = -\tfrac{1}{2} r_m\,\lambda_{2a}/\nu_{1b} = \qquad (6,44)$$

$$= \tfrac{1}{2} r_m\,(1-n)^{-1}\,\frac{1-(1-n)^{-\frac{1}{2}}\tan(\phi^{*}_m/2)\,t'}{1-(1-n)^{-\frac{1}{2}}\cot\phi^{*}_m\,(t'+t'')-(1-n)^{-1}\,t't''}.$$

The radial magnifications take the form:

$$M_{ang} = (r_e / r_m)(\nu_{1b} / \lambda_{1b}) = 1/M_{lat} . \qquad (6,45)$$

With a very narrow image slit and in the absence of aberrations, the essential quantity which determines the mass resolving power is D_m/M_{lat}, which equals in this case:

$$D_m/M_{lat} = -\tfrac{1}{2} r_e \lambda_{2a} / \lambda_{1b} = r_e/\kappa^2 . \qquad (6,46)$$

As compared with the traditional arrangement with a cylindrical condensor ($\kappa^2 = 2-c = 2$), the quotient D_m/M_{lat} has increased by the factor $2/\kappa^2$. For normal entry and exit in the magnetic field, the mass dispersion has increased by the factor $1/(1-n)$ as compared with the traditional arrangement with a homogeneous magnetic field (n=0).

CHAPTER 7

NUMERICAL EVALUATION OF THE CONDITIONS FOR FIRST ORDER STIGMATIC DOUBLE FOCUSING, AND FOR THE ELIMINATION OF THE RADIAL SECOND ORDER ABERRATIONS

7a: *Computation procedure.*

The first order equations to be satisfied are:

$$B_1 = 0; \tag{6,19}$$

$$B_2 = 0; \tag{6,20}$$

(which are equivalent to (6,21)-(6,22)), and:

$$l''_{zm} = l''_m; \tag{7,1}$$

which is equivalent to (6,34). Of the second order aberrations, those proportional to α^2, $\alpha\beta$ and β^2, seem to be the most important; thus we put the conditions, in the symbols of (6,15):

$$B_{11} = 0; \tag{7,2}$$

$$B_{12} = 0; \tag{7,3}$$

$$B_{22} = 0. \tag{7,4}$$

We chose as independent variables:

$$\phi_m;\ \phi_e;\ n;\ c;\ t';\ t'';\ r_e/r_m.$$

Then d/r_m is fixed through (6,34), and l''_m/r_m and l'_e/r_e through (6,21)-(6,22). In this work we assumed the pole faces to be conical and the gap width to be very small as compared with r_m, and thus from (4,12): $X = 2n$. Now R'_e, r_m/R', and r_m/R'', are fixed through (7,2)-(7,4). Through the boundary curvatures of the electrostatic field we are in a position to eliminate two more aberrations, for which we chose:

$$B_{33} = 0; \tag{7,5}$$

$$B_{34} = 0. \tag{7,6}$$

(7,5)-(7,6) then determine r_e/R_I and r_e/R_{II}. The resulting value of the remaining radial second order aberration, proportional to δ^2, was computed.

The choice of (7, 5)-(7, 6) is somewhat arbitrary. However, the fringing fields contribute to the image curvature (2, 104) in a way which can not be minimalised by shields, whereas it can be eliminated separately through a simple device such as an electrostatic hexapole field (5, 31) or (5, 32).

To represent a physically acceptable combination, several additional conditions are required. All distances should be real and positive. The maximum acceptable distances are a matter of personal taste; for reasons of simplicity, related to the binary representation of the numbers in the computing machine used, we chose:

$$0 \leqslant d/r_m \leqslant +16; \tag{7, 7}$$

$$0 \leqslant l'_e/r_e \leqslant +16; \tag{7, 8}$$

$$0 \leqslant l''_m/r_m \leqslant +16. \tag{7, 9}$$

Likewise, the acceptable boundary curvature was subjected to the restrictions:

$$-8 \leqslant r_m/R' \leqslant +8; \tag{7, 10}$$

$$-8 \leqslant r_m/R'' \leqslant +8. \tag{7, 11}$$

On applying similar restrictions to the boundary curvatures of the electrostatic field, it was found that acceptable solutions were rare. As in particular the aberrations proportional to α^2, $\alpha\beta$, and β^2 tend to increase sharply with virtual increase of the radius, their elimination was thought to be more important than of those proportional to α_z^2 and $\alpha_z\delta$. Thus the conditions (7, 5)-(7, 6) were replaced by:

$$|B_{33}| + |B_{34}| = \text{minimum}, \tag{7, 12}$$

together with:

$$-6 \leqslant r_e/R_I \leqslant +6; \tag{7, 13}$$

$$-6 \leqslant r_e/R_{II} \leqslant +6. \tag{7, 14}$$

(7, 12) is clearly equivalent to (7, 5)-(7, 6) if the curvatures fall within the acceptable range.

A computer programma was made along these lines for the ARMAC automatic magnetic drum computer of the Mathematisch Centrum in Amsterdam.

At any given set of the independent variables ϕ_m, ϕ_e, n, c, t', t'', the value of r_e/r_m was varied stepwise by a constant factor from 0.5 to 2, the procedure being repeated after each change in the other independent variables. The first root of (6, 34) was extracted by iteration according to Newton; the rest of the calculation is then straightforward. (7, 2)-(7, 4) are three simultaneous linear equations with three unknowns, (7, 5)-(7, 6) are two linear equations with two unknowns. If in the r_e/R_I - r_e/R_{II} - plane the intersection of the lines (7, 5) - (7, 6) does not fall within the square around the origin permitted through (7, 13)-(7, 14), it follows from the linearity that (7, 12) is satisfied either at the intersection of either (7, 5) of (7, 6) and a side of the square, or at a corner.

First order stigmatic focusing could be achieved by choosing $c = +1$; $n = +\frac{1}{2}$, which causes all radial and axial images to coincide. This special case was not treated here. Then (6, 34) becomes trivial, and the solutions produced by the machine depend on the rounding off errors, and are devoid of physical meaning.

7b: *Combinations with deflection in the same sense. The "pretzel"-configuration.*

With $n = 0.91$, $t' = t'' = 0$, no acceptable solutions with deflection in the same sense were found with $\phi_m = 90^\circ$ or 120°, $60^\circ \leqslant \phi_e \leqslant 180^\circ$, and $1.720 \leqslant c \leqslant 1.885$. Neither did tests with $n = 0.765$; $t' = t'' = 0$, $1.525 \leqslant c \leqslant 1.740$, and the same ranges for ϕ_m and ϕ_e produce any acceptable results.

However, the weak radial converging action of deflecting fields with virtually enlarged radius makes a new class of arrangements possible with angles of deflection exceeding 270°, for which the name "pretzel"-configuration might be proposed. Acceptable solutions were found for $\phi_m = \phi_e = 300^\circ$. This geometry requires the additional conditions:

$$d > r_e + r_m; \tag{7, 15}$$

$$l'_e/r_e > \tfrac{1}{2}; \tag{7, 16}$$

$$l''_m/r_m > \tfrac{1}{2}. \tag{7, 17}$$

Acceptable solutions were found with $n = 0.91$ and $n = 0.765$. c was given the values 1.885; 1.875; 1.850; 1.815; 1.765; 1.720. t' was varied from -1.00 to +1.00 in +0.25 steps, keeping $t'' + t' = 0$.

Varying r_e/r_m, all other parameters being kept constant, mainly affects d/r_m (which increases with increasing r_e/r_m), and the boundary curvatures. R'_e was found to be nearly constant

and equal to +0.5 over the whole range investigated here. A decrease in c results in a decrease in l'_e/r_e, a decrease in n corresponds to a decrease in l''_m/r_m. In many cases, the inclinations of the focusing planes as computed from (6, 30)-(6, 31) differed by less than 1°. As could be expected these inclinations depend strongly on t' and t''. Solutions with normal incidence and exit are unfavourable because of the large M^z_{lat}. Even though stigmatic focusing is achieved in these arrangements, this large axial magnification prohibites all ions emerging from a short object slit to be collected through an image slit of comparable length. Keeping $t' + t'' = 0$, it was found that M^z_{lat} could be reduced by increasing t', and by decreasing c.

Some of the solutions are presented in Table 1. As an example, case No. 3 is illustrated in Fig. 26.

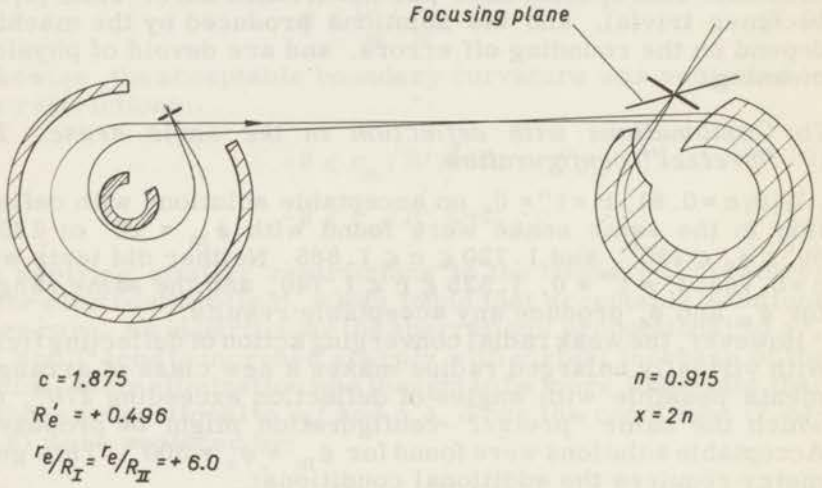

Fig. 26. Case No. 3.

7c: *Combinations with deflection in the opposite sense.*

One example of this class has been presented by Wachsmuth, Liebl, and Ewald [54]. These authors looked for a Mattauch arrangement satisfying (7, 2)-(7, 5) and the additional condition:

$$X_R = X_E , \qquad (7, 18)$$

leaving $r_e/R_I = r_e/R_{II}$. For reference, their solution is reproduced here as case No. 10 in Table 2.

The same independent variables as in case No. 10 were now fed into the computer programme used here. The results are

represented as case No. 11 in Table 2. Now the conditions (6, 40)-(6, 42) of the Mattauch arrangement are no longer stringently imposed, and small deviations from No. 10 are caused by rounding off errors. The condition (7, 18) was dropped, and (7, 5) was replaced by (7, 12)-(7, 14), resulting in different boundary curvatures for the electrostatic field.

The values for χ_R and χ_E in case No. 10, quoted by Wachsmuth et al.[54], were found to be incorrect. It seems that these authors might have overlooked the dependence of χ_R and χ_E on r_m/R'', as a combination with the same parameters but $r_m/R'' = 0$, would produce their values of χ_R and χ_E.

Some more examples of this class as represented in Table 3, show similar trends as found in those of Table 1. In many respects these combinations possess more desirable properties than those with deflection in the same sense, as in Table 1, and the combination chosen by Wachsmuth et al. appears to be a favourable one. As an example, case No. 14 is illustrated in Fig. 27.

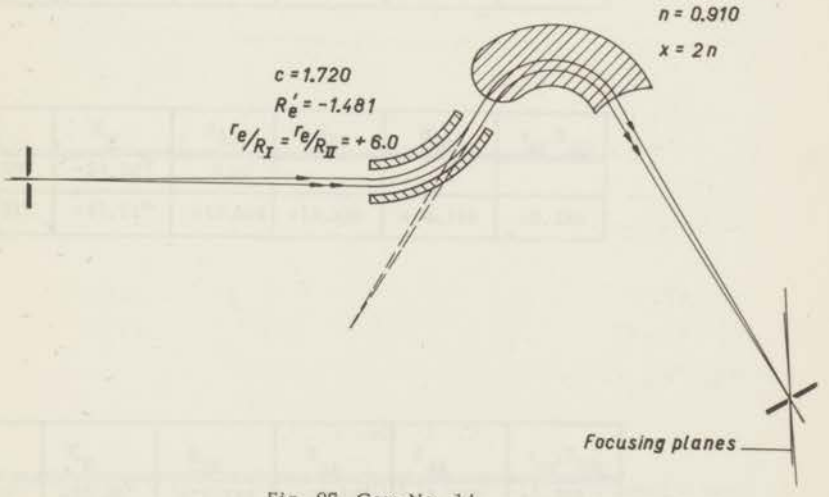

Fig. 27. Case No. 14.

TABLE 1

"Pretzel"-arrangements with deflection in the same sense.

No.	ϕ_e	c	ϕ_m	n	t'	t"	r_e/r_m	l'_e/r_e	d/r_m	l''_m/r_m	R'_e	r_m/R'	r_m/R''	r_e/R_I	r_e/R_{II}	M_{lat}	M^z_{lat}	D/r_m	X_R	X_E	B_{33}	B_{34}	B_{44}	r_m/R_{im}
1	300°	1.850	300°	0.915	0.0	0.0	1.000	0.783	8.826	2.146	+0.538	+0.200	-4.277	+6.000	+6.000	+0.814	-18.248	+9.30	- 6.64°	- 6.86°	-2.226	+2.237	-41.701	-1.643
2	300°	1.850	300°	0.915	+0.5	-0.5	1.000	0.888	4.763	1.739	+0.515	+0.893	-1.119	+6.000	+6.000	+0.314	- 7.923	+3.71	-43.69°	-46.06°	-0.857	+1.385	-12.715	-1.340
3	300°	1.850	300°	0.915	+1.0	-1.0	1.000	0.955	3,769	0.966	+0.504	+0.382	-1.460	+6.000	+6.000	+0.156	- 3.840	+1.85	-44.79°	-45.93°	-0.423	+0.771	- 5.467	-1.306
4	300°	1.875	300°	0.915	+1.0	-1.0	1.000	0.726	7.218	0.955	+0.496	+0.524	-1.480	+6.000	+6.000	+0.155	- 8.126	+1.89	-45.03°	-45.74°	-0.290	+1.403	-33.014	-1.331
5	300°	1.885	300°	0.915	+1.0	-1.0	1.000	0.663	9.716	0.915	+0.492	+0.571	-1.488	+6.000	+6.000	+0.154	-11.243	+1.90	-45.10°	-45.65°	-0.279	+1.607	-68.685	-1.337
6	300°	1.850	300°	0.875	+1.0	-1.0	1.000	0.952	4.032	0.840	+0.507	+0.475	-1.731	+6.000	+6.000	+0.166	- 2.677	+1.96	-45.31°	-46.51°	-0.456	+0.722	- 7.620	-1.660
7	300°	1.850	300°	0.875	+1.0	-1.0	0.707	0.990	2.560	0.856	+0.505	+1.548	-1.705	+6.000	+6.000	+0.225	- 2.467	+1.90	-42.48°	-44.05°	-0.454	+0.493	- 2.094	-1.521
8	300°	1.850	300°	0.875	+1.0	-1.0	1.414	0.930	6.101	0.828	+0.508	+0.017	-1.747	+6.000	+6.000	+0.120	- 2.810	+2.00	-48.01°	-48.92°	-0.461	+1.023	-20.913	-1.724
9	300°	1.850	300°	0.875	+1.0	-1.0	2.000	0.917	9.019	0.820	+0.509	-0.217	-1.757	+6.000	+6.000	+0.087	- 2.896	+2.03	-50.37°	-51.05°	-0.464	+1.432	-50.700	-1.824

TABLE 2

Arrangements with deflection in the opposite sense.

No.	ϕ_e	c	ϕ_m	n	t'	t"	r_e/r_m	l'_e/r_e	d/r_m	l''_m/r_m	R'_e	r_m/R'	r_m/R''	r_e/R_I	r_e/R_{II}	M_{lat}	M^z_{lat}	D/r_m	X_R	X_E	B_{33}	B_{34}	B_{44}	r_m/R_{im}
10	61.35°	1.75	128.60°	0.889	0.0	0.0	1.800	3.371	0.292	3.232	-1.419	+1.855	-1.124	+2.94	+2.94				-24.33°	-24.33°	0.00			
11	61.35°	1.75	128.60°	0.889	0.0	0.0	1.800	3.371	0.289	3,231	-1.432	+1.870	-1.130	+6.000	+6.000	+0.625	+0.734	+4.50	-47.51°	-47.51°	+13.509	+19.320	+ 4.149	+0.189

TABLE 3

Arrangements with deflection in the opposite sense.

No.	ϕ_e	c	ϕ_m	n	t'	t"	r_e/r_m	l'_e/r_e	d/r_m	l''_m/r_m	R'_e	r_m/R'	r_m/R''	r_e/R_I	r_e/R_{II}	M_{lat}	M^z_{lat}	D/r_m	X_R	X_E	B_{33}	B_{34}	B_{44}	r_m/R_{im}
12	60°	1.720	120°	0.910	0.0	0.0	1.000	2.947	0.140	4.873	-1.618	+5.732	-1.008	+6.000	+6.000	+1.684	+1.293	+5.83	-25.89°	-29.04°	+12.134	+20.565	+5.118	+0.481
13	60°	1.720	120°	0.910	0.0	0.0	1.260	2.935	0.238	4.838	-1.525	+3.586	-1.042	+6.000	+6.000	+1.333	+1.289	+5.80	-24.72°	-27.21°	+ 6.800	+18.764	+5.083	-0.081
14	60°	1.720	120°	0.910	0.0	0.0	1.587	2.924	0.362	4.804	-1.481	+2.326	-1.030	+6.000	+6.000	+1.055	+1.286	+5.77	-25.61°	-27.88°	+ 4.346	+18.918	+5.370	-0.394
15	60°	1.720	120°	0.910	0.0	0.0	2.000	2.914	0.518	4.772	-1.466	+1.551	-0.987	+6.000	+6.000	+0.836	+1.283	+5.74	-28.09°	-30.38°	+ 3.503	+20.395	+5.888	-0.586
16	60°	1.765	120°	0.910	0.0	0.0	2.000	3.399	0.402	4.894	-1.433	+1.571	-0.886	+6.000	+6.000	+0.742	+1.093	+5.86	-32.84°	-36.09°	+14.291	+25.847	+5.858	-0.442
17	60°	1.815	120°	0.910	0.0	0.0	2.000	4.129	0.285	5,047	-1.401	+1.595	-0.777	+6.000	+6.000	+0.636	+0.899	+6.01	-40.21°	-45.19°	+35.635	+34.178	+5.843	-0.178
18	60°	1.850	120°	0.910	0.0	0.0	2.000	4.825	0.209	5,165	-1.380	+1.614	-0.703	+6.000	+6.000	+0.561	+0.772	+6.12	-47.35°	-54.15°	+61.962	+42.283	+5.850	+0.125
19	60°	1.875	120°	0.910	0.0	0.0	2.000	5.466	0.158	5.257	-1.367	+1.629	-0.650	+6.000	+6.000	+0.506	+0.684	+6.21	-53.87°	-62.30°	+91.438	+49.857	+5.864	+0.449
20	60°	1.885	120°	0.910	0.0	0.0	2.000	5.767	0.138	5.295	-1.362	+1.635	-0.629	+6.000	+6.000	+0.484	+0.650	+6.25	-56.87°	-66.02°	> 100	+53.456	+5.873	+0.615

INDEX OF SYMBOLS

$\vec{A}$	Magnetic vector potential.
$A_{11}, A_{33}, A_{34}, A_{44}$	Coefficients of second order aberrations, (2, 99)-(2, 102).
a_n, A_n, a_z, A_z	see (6, 22)-(6, 23).
A_w	w-component of $\vec{A}$.
α	u'(0); in Ch. 6-7 also: $-dy_1/dx_1$.
α_e	$-dy_1/dx_1$, electrostatic case, see Fig. 7.
α_m	$-dy_1/dx_1$, magnetic case, see Fig. 2.
α_z	v'(0); in Ch. 6-7 also: $-dz_1/dx_1$.
α_{ze}, α_{zm}	$-dz_1/dx_1$, see Figs. 2 and 7.
b	half gap width at the main path; in (4, 6)-(4, 14) expressed in units r_m.
$\vec{B}$	Magnetic field strength.
B, B_o	Absolute value of the magnetic field strength at the main path.
B_1, B_2	see (2, 30)-(2, 32), (2, 34)-(2, 35).
$B_1, B_2, B_{11}, B_{12}, B_{22}, B_{33}, B_{34}, B_{44}$	see (6, 14)-(6, 17).
b_n, B_n, b_z, B_z	see (6, 22)-(6, 23).
B_u, B_v, B_x, B_z	component of the magnetic field strength in the u-, v-, x-, and z-direction.
β	$\delta v/v_o$, relative velocity spread, see (2, 37).
c	r_e/R_e, see Fig. 6.
C_3, C_4	see (4, 2); coefficients in field shape expansion.
c_n, C_n, c_z, C_z	see (6, 22)-(6, 23).
d	distance between electrostatic and magnetic field in tandem arrangement.
D_m	mass dispersion in the y_2-direction per unit $\delta m/m_o$.

D_v	velocity dispersion in the y_2-direction per unit β.
δ	distance of the object point to the median plane, see Figs. 2 and 7.
e	charge of the proton.
E	electrostatic field strength.
E, E_1, E_2	see (3, 9).
E_o	electrostatic field strength at the main path.
$\epsilon, \epsilon', \epsilon''$	inclinations of the field boundaries, see Fig. 3.
η	$(e/2mU)^{\frac{1}{2}}$.
η_o	see (2, 38).
F	ion-optical "index of refraction", see (2, 3).
$F_{00}, F_{10}, F_{20}, F_{02}, F_{30}, F_{12}$	coefficients in the expansion of F, see (2, 5).
F_3, F_4	see (6, 16).
f, f_z	radial and axial focal lengths, see (2, 80), (2, 85), (3, 36), (3, 40).
f'_{str}, f''_{str}	see (2, 57).
g	see (2, 5).
G	see (6, 24)-(6, 25).
g', g'', g'_z, g''_z	see (2, 80), (2, 85), (3, 36), (3, 40).
k_1, k_2	see (2, 10)-(2, 11).
$K_1, K_2, K_{11}, K_{12}, K_{22}, K_{33}, K_{34}, K_{44}$	see (3, 20).
κ	$(2-c)^{\frac{1}{2}}$.
$\kappa_{1a}, \kappa_{1b}, \kappa_{2a}, \kappa_{11a}, \kappa_{11b}, \kappa_{11c}, \kappa_{12a}, \kappa_{12b}, \kappa_{22a}, \kappa_{33a}, \kappa_{33b}, \kappa_{33c}, \kappa_{34a}, \kappa_{34b}, \kappa_{44a}$	see (3, 25), (3, 32).

l'_m, l'_e	object distances in the magnetic and electrostatic case.
l''_m, l''_e	image distances in the magnetic and electrostatic case.
$L_1, L_2, L_{11}, L_{12}, L_{22}, L_{33}, L_{34}, L_{44}$	see (3, 21).
$\lambda_{1a}, \lambda_{1b}, \lambda_{2a}, \lambda_{11a}, \lambda_{11b}, \lambda_{11c}, \lambda_{12a}, \lambda_{12b}, \lambda_{22a}, \lambda_{33a}, \lambda_{33b}, \lambda_{33c}, \lambda_{34a}, \lambda_{34b}, \lambda_{44a}$	see (3, 26), (3, 33).
m	mass of the ion.
M_{lat}, M_{ang}, M_{ax}	lateral, angular, and axial magnification in radial direction.
M^z_{lat}, M^z_{ang}	lateral and angular magnification in axial direction.
$M_1, M_2, M_{11}, M_{12}, M_{22}, M_{33}, M_{34}, M_{44}$	see (2, 49).
$\mu_{1a}, \mu_{1b}, \mu_{2a}, \mu_{11a}, \mu_{11b}, \mu_{11c}, \mu_{12a}, \mu_{12b}, \mu_{22a}, \mu_{33a}, \mu_{33b}, \mu_{33c}, \mu_{34a}, \mu_{34b}, \mu_{44a}$	see (2, 54)-(2. 76).
n	$-(r/B)(\partial B/\partial r)$, see (2, 33).
$N_1, N_2, N_{11}, N_{12}, N_{22}, N_{33}, N_{34}, N_{44}$	see (2, 50).
$\nu_{1a}, \nu_{1b}, \nu_{2a}, \nu_{11a}, \nu_{11b}, \nu_{11c}, \nu_{12a}, \nu_{12b}, \nu_{22a}, \nu_{33a}, \nu_{33b}, \nu_{33c}, \nu_{34a}, \nu_{34b}, \nu_{44a}$	see (2, 55), (2, 77).
P_3, P_4, Π_3, Π_4	see (3, 22)-(3, 23).
$\pi_{3a}, \pi_{3b}, \pi_{4a}$	see (3, 27), (3, 34).
r	radius
R	mass resolving power, see (1, 1).
r_e, r_m	radius of deflection of the main path in the electrostatic and magnetic field.

R_e	see Fig. 6; radius of toroidal curvature.
R_e'	see (3, 8).
R'	radius of the magnetic entrance boundary, (Fig. 3).
R''	radius of the magnetic exit boundary, (Fig. 3).
R_I, R_{II}	electrostatic entrance and exit boundary radius, Fig. 8.
R_{im}	radius of a curved image.
ρ', ρ''	see (2, 75).
$\rho_{3a}, \rho_{3b}, \rho_{4a}$	see (3, 27), (3, 34).
S_i	$\mu_i + \nu_i(l_m''/r_m)$, see (6, 12).
s', s''	object and image slit widths.
$\sigma_{3a}, \sigma_{3b}, \sigma_{4a}$	see (2, 56), (2, 78).
Σ_3, Σ_4	see (2, 51).
t	$\tan \epsilon$
$t'; t''$	$\tan \epsilon'$; $\tan \epsilon''$; see (2, 75).
T	$\tan (\phi_m^*/2)$.
T_3, T_4	see (2, 52).
T_i	$(r_e/r_m)K_i + (d/r_m)L_i$, see (6, 15).
$\tau_{3a}, \tau_{3b}, \tau_{4a}$	see (2, 56), (2, 78).
u	$(r-r_m)/r_m$.
U	accelerating voltage of the ions.
$u'; u''$	du/dw; d^2u/dw^2.
v	z/r_m.
$v'; v''$	dv/dw; d^2v/dw^2.
w	path coordinate, see Figs. 1 and 5.
w^*	$(1-n)^{\frac{1}{2}} w$, (Chapter 2); κw, (Chapter 3).

$w^{\dagger}$	$n^{\frac{1}{2}}w$, (Chapter 2); $c^{\frac{1}{2}}w$, (Chapter 3).
X	second order magnetic field shape parameter, see (2, 35); (4.10).
x_1, y_1, z_1	cartesian coordinates in the object space, see Figs. 1 and 5.
x_2, y_2, z_2	cartesian coordinates in the image space, see Figs. 1 and 5.
ξ	distance between the hypothetical sector field boundary and the mechanical pole face or electrode boundary.
φ	eletrostatic potential.
φ_m	scalar magnetic potential.
ϕ_e	electrostatic sector angle.
ϕ_m	magnetic sector angle.
ϕ_e^*	$\kappa\phi_e$.
$\phi_e^{\dagger}$	$c^{\frac{1}{2}}\phi_e$.
ϕ_m^*	$(1-n)^{\frac{1}{2}}\phi_m$.
$\phi_m^{\dagger}$	$n^{\frac{1}{2}}\phi_m$.
ψ	angular coordinate.
χ_R	inclination of the plane of direction focusing.
χ_E	inclination of the plane of energy focusing.

REFERENCES

1. A. V. Duvrovin et al.: Dokl. Akad. Nauk SSSR 102, 719 (1955).
2. J. D. Morrison and H. E. Stanton: J. Chem. Phys. 28, 9 (1958).
3. J. T. Kerr, G. R. Bainbridge, J. W. Dewdney, and H. E. Duckworth: "Advances in Mass Spectrometry" (London 1959), p. 1.
   T. L. Collins and K. T. Bainbridge: "Nuclear Masses and their Determination" (Ed. H. Hintenberger, London 1957), p. 213.
4. K. Ogata and H. Matsuda: "Nuclear Masses and their Determination" (Ed. H. Hintenberger, London 1957), p. 202; Z. Naturforschg. 10a, 843 (1955).
5. F. Everling et al.: "Nuclear Masses and their Determination", (Ed. H. Hintenberger, London 1957), p. 221.
6. C. M. Stevens, Argonne National Laboratory, Argonne, Ill., private communication.
7. N. E. Alekseevski et al.: Dokl. Akad. Nauk SSSR 100, 229 (1953).
8. R. F. K. Herzog: Acta Phys. Austr. 4, 431 (1950-1951).
9. H. Ewald and H. Liebl: Z. Naturforschg. 10a, 872 (1955).
10. H. Ewald and H. Liebl: Z. Naturforschg. 12a, 28 (1957).
11. O. Hachenberg: Ann. Phys. Lpz. 2, 225 (1948).
12. R. Albrecht: "Berechnung des Potentiales in doppelt gekrümmten Kondensatoren", Diplomarbeit T. H. München, 1955.
13. R. Albrecht: Z. Naturforschg. 11a, 156 (1956).
14. H. A. Enge: Rev. Sci. Instr. 30, 248 (1959).
15. N. Svartholm and K. Siegbahn: Rev. Sci. Instr. 19, 594 (1948).
16. N. Svartholm: Ark. Fys. 2, 20 (1950).
17. H. W. Franke: Oest. Ing. Arch. 5, 371 (1951); ibid. 6, 105 (1952).
18. H. Grümm: Acta Phys. Austr. 8. 119 (1953).
19. A. Hedgran, K. Siegbahn, and N. Svartholm: Proc. Phys. Soc. London, Ser. A 63, 960 (1950).
20. D. Fischer: Z. Phys. 133, 455, 471 (1952).
21. C. Mileikowsky: Ark. Fys. 4, 337 (1952); ibid. 7, 33 (1953).
22. F. Viehböck, private communication.
23. H. Liebl and H. Ewald: Z. Naturforschg. 14a, 199 (1959).
24. H. Liebl and H. Ewald: Z. Naturforschg. 14a, 842 (1959).
25. H. Ewald, H. Liebl, and G. Sauerman: Z. Naturforschg. 14a, 129 (1959).
26. G. Sauerman and H. Ewald: Z. Naturforschg. 14a, 137 (1957).
27. H. Wachsmuth, H. Liebl, and H. Ewald: Z. Naturforschg. 14a, 844 (1959).

28. W. Glaser: "Handbuch der Physik", (Ed. S. Flügge, Berlin 1956), 33, pp. 306 ff.
29. W. Glaser: Z. Phys. 89, 451 (1933).
30. H. A. Tasman and A. J. H. Boerboom: Z. Naturforschg. 14a, 121 (1959).
31. H. Wachsmuth, A. J. H. Boerboom, and H. A. Tasman: Z. Naturforschg. 14a, 818 (1959).
32. R. F. K. Herzog: Z. Naturforschg. 8a, 191 (1953).
33. L. A. König and H. Hintenberger: Z. Naturforschg. 12a, 377 (1957).
34. H. A. Tasman, A. J. H. Boerboom, and H. Wachsmuth: Z. Naturforschg. 14a, 822 (1959).
35. H. Hintenberger and L. A. König: Z. Naturforschg. 12a, 773 (1957).
36. A. J. H. Boerboom: "De Ionenoptiek van de Massaspectrometer", (Thesis, Leyden, 1957); Appl. sci. Res. B 7, 52 (1958).
37. C. E. Berry: Rev. Sci. Instr. 27, 849 (1956).
38. H. Liebl and H. Ewald: Z. Naturforschg. 12a, 541 (1957).
39. A. J. H. Boerboom, H. A. Tasman, and H. Wachsmuth: Z. Naturforschg. 14a, 816 (1959).
40. N. D. Coggeshall: J. Appl. Phys. 18, 855 (1947),
41. G. P. Barnard: "Modern Mass Spectrometry", (London, 1953), p. 35.
42. L. A. König and H. Hintenberger: Z. Naturforschg. 10a, 877 (1955).
43. W. Ploch and W. Walcher: Z. Phys. 127, 274 (1950).
44. A. Septier: "Sur le champ de fuite des déflecteurs magnétiques, etc." CERN 59-1, Division du Synchrotron à Protons, Décembre 1958.
45. J. Mates: "Magnet Report", TID-5118, April 1953.
46. C. J. Zilverschoon: "An Electromagnetic Isotope Separator", (Thesis, Amsterdam, 1954).
47. H. Wild and O. Huber: Helv. Phys. Acta 30, 3 (1957).
48. R. Herzog: Z. Phys. 97, 596 (1935).
49. A. O. Nier: Rev. Sci. Instr. 11, 212 (1940).
50. V. K. Zworykin et al.: "Electron Optics and the Electron Microscope", (New York, 1948), Chapter 16.
51. O. Klemperer: "Electron Optics", (Cambridge, 1953), Chapter VI.
52. J. H. Pierce: "Theory and Design of Electron Beams", (New York, 1954), p. 76.
53. H. Hintenberger and L. A. König: Z. Naturforschg. 12a, 140; 773 (1957).
54. H. Wachsmuth, H. Liebl, H. Ewald: Z. Naturforschg. 14a, 844 (1959).
55. H. Liebl: Optik 16, 19 (1959).

SUMMARY

It is found that the mass dispersion of magnetic analysing fields for mass spectrometers may be increased without increase in radius of deflection by employing inhomogeneous magnetic fields. If at the main path $-(r/B)\partial B/\partial r = n$ $(0 \leqslant n < 1)$, the mass dispersion and resolution are increased essentially by the factor $1/(1-n)$.

The imaging properties of this type of sector fields are derived up to the second order. The shape of the pole faces and the influence of boundary inclination and curvature are discussed. Several adjustable devices are discussed for the elimination of first and second order aberrations.

Actual measurements with a pair of very carefully made conical pole faces show agreement with the calculated field shape. It is shown that the influence of the finite radial extension may be reduced by appropriate correction turns.

Similar considerations apply to toroidally curved electrostatic sector fields, where the energy dispersion can be increased as compared with that in the cylindrical electrostatic field. The imaging properties are derived up to the second order along the same lines as for the inhomogeneous magnetic sector fields. The required shape of the deflecting electrodes is mentioned.

For a so-called tandem arrangement of a toroidally curved electrostatic sector field followed by an inhomogeneous magnetic sector field, the imaging properties are derived up to the second order, including the trajectories outside the median plane. The conditions are presented for double focusing and for stigmatic focusing.

For deflection in the same sense in these subsequent fields, numerical evaluation revealed the possibility of a new type of "pretzel"-arrangement, consisting of 300° electrostatic deflection followed by 300° magnetic deflection. In these arrangements stigmatic double focusing may be achieved in first order, together with elimination of the second order aberrations in the median plane and minimalisation of those outside the median plane. Stigmatic double focusing with subsequent deflection in the opposite sense is also possible; some numerical examples are given. In all these examples the resolution, depending on the ratio of the mass dispersion to the lateral magnification, is considerably increased as compared with similar combinations of homogeneous magnetic fields with cylindrical electrostatic fields, whereas the stigmatic focusing obtained may improve the transmission and sensitivity of the instrument.

SAMENVATTING

De massa dispersie van magnetische analysator velden voor massaspectrometers kan zonder vergroting van afbuigstraal vergroot worden door gebruik te maken van inhomogene magneetvelden. Indien ter plaatse van de hoofdbaan $-(r/B)\partial B/\partial r = n$ $(0 \leqslant n < 1)$, worden massadispersie en oplossend vermogen ruwweg vergroot met de factor $1/(1-n)$.

Van dit type velden werden de afbeeldingseigenschappen tot in tweede orde doorgerekend. De invloed van scheve en/of gekromde veldbegrenzingen wordt behandeld, zowel als de vorm van het poolschoenprofiel. Verschillende instelmogelijkheden worden besproken voor de opheffing van eerste en tweede orde afbeeldingsfouten.

De veldvorm, gemeten tussen een stel zeer zorgvuldig vervaardigde conische poolschoenen, komt overeen met de theoretisch berekende. Er wordt aangetoond, dat de afval naar de randen door de eindige radiele uitgebreidheid van de poolschoenen, verminderd kan worden door het aanbrengen van correctiewindingen.

Ook in toroidaal gekromde electrostatische sectorvelden treedt een soortgelijk effect op, waar n.l. de energiedispersie vergroot kan worden vergeleken met het cylindrische electrostatische veld. Tot in tweede orde werden de afbeeldingseigenschappen afgeleid, op dezelfde wijze als voor de inhomogene magneetvelden. De vereiste electrodenvorm wordt aangeduid.

Van een z.g. tandem-opstelling van een toroidaal gekromd electrostatisch afbuigveld, gevolgd door een inhomogeen magneetveld, werden de afbeeldingseigenschappen tot in tweede orde afgeleid, met inbegrip van de banen buiten het mediaanvlak. De voorwaarden voor dubbelfocussering en voor puntvormige afbeelding worden gegeven.

Numerieke uitwerking toonde aan, dat bij gelijkgerichte afbuiging in deze twee opeenvolgende velden een nieuw soort "krakeling"-opstelling mogelijk is, bestaande uit 300° electrostatische afbuiging, gevolgd door 300° magnetische afbuiging. Hierin kan puntvormige dubbelfocussering verkregen worden in eerste orde, met opheffing van de tweede orde afbeeldingsfouten in het mediaanvlak en minimalisering van die daarbuiten. Het is ook mogelijk puntvormige dubbelfocussering te verkrijgen met opeenvolgende afbuiging in tegengestelde richting: er worden enige numerieke voorbeelden gegeven. Het oplossend vermogen, bepaald door de verhouding van dispersie en dwarsvergroting, is in al deze gevallen aanzienlijk groter dan in soortgelijke combinaties van homogene magneetvelden met cylindrische electrostatische velden. De puntvormige afbeelding kan de lichtsterkte en gevoeligheid van het instrument ten goede komen.

ACKNOWLEDGEMENTS

I wish to thank Dr Ir A. J. H. Boerboom for his suggestions, helpful criticism, and effective cooperation.

The assistance of Drs B. L. Schram in the magnetic field measurements is kindly acknowledged.

The discussions with Prof. Dr H. Hintenberger and Dr L. A. König of the Max Planck Institut für Chemie in Mainz, and with Prof. Dr H. Ewald and Dr H. Liebl of the Technische Hochschule, München, contributed considerably to this work.

At this point I also wish to thank the staff of the Laboratorium voor Massaspectrografie for their pleasant cooperation and discussions in the past five years; in particular Drs J. Los, Drs T. J. P. H. Babeliowsky, and Mr. J. Schutten for the many discussions, Mr. A. P. de Jongh and our workshop for their devotion to the constuctional design and realisation of the inhomogeneous field mass spectrometer, Mr. F. L. Monterie for his manual skill, Mr. P. J. van Deenen and Mr. Tj. van der Hauw for their practical skill in electronics, and Mr. J. P. J. Janssen and Mr. J. A. van Wel for their skill in glass blowing.

My much too short stay at the Argonne Natoinal Laboratory, Physics Division, was of considerable importance for my physical education. I greatly appreciated experiencing the kind hospitality and sharing the rich experiences of Dr William A. Chupka, Dr Joseph Berkowitz, Dr Manfred Kaminsky, and Dr Norman A. Frigerio.

The numerical evaluation in Chapter 7 was accomplished with the help of the ARMAC automatic magnetic drum computer of the Mathematisch Centrum in Amsterdam, to which I am greatly indebted for putting the machine to my use. I wish to acknowledge the assistance of Dr J. A. Zonneveld and Mr. J. van Loenen.

I wish to express my appreciation for the kind and effective assistance of Dr N. F. Verster, of Philips Gloeilampenfabriek N. V., Eindhoven, who allowed the calibration of the Hall generator for the field measurements to be done in his proton resonance calibrating instrument.

STELLINGEN

1. Bij de metingen van Miller en Kusch aan de damp van alkalihalogeniden uit een koper vervaardigde oven, geeft reactie met het ovenmateriaal te hoge waarden voor het gehalte aan dimeer en trimeer.

   R. C. Miller en P. Kush: J. Chem. Phys. 25, 860 (1956); 27, 981 (1958).

2. De gevolgtrekkingen van Datz en Taylor uit hun oppervlakteïonisatie metingen, leiden tot onwaarschijnlijke resultaten betreffende de reflectie van Li op Pt.

   S. Datz en E. H. Taylor: J. Chem. Phys. 25, 389 (1956).

3. De door Akishin et al gepubliceerde waarden over de massaspectra van NaCl, Na_2Cl_2, LiF en Li_2F_2, zijn onjuist. Met name is hun hoge waarde voor de verhouding $Na^+/NaCl^+$ uit monomeer NaCl waarschijnlijk een gevolg van onzuiverheden in hun monster.

   P. Akishin, L. N. Gorokhov, en L. N. Sidorov: Zhur. fiz. Khim. 33, 2822 (1959).

4. De metingen van thermische accomodatiecoëfficiënten door Schäfer zijn bij zo hoge druk uitgevoerd, dat zijn interpretatie, waarbij hieruit gemiddelde verblijftijden aan de wand worden afgeleid, ongeoorloofd is.

   Kl. Schäfer: Fortschr. chem. Forschg. 1, 61 (1949-1950).
   Kl. Schäfer en H. Gerstacher: Z. Elektrochem. 59, 1023 (1955); 60, 874 (1956).

5. De bewering van Septier, dat de radiale en axiale krommingen van de effectieve veldgrens van een magnetisch sectorveld om principiële redenen elkaars tegengestelde zouden zijn, is onjuist.

   A. Septier: "Sur le champ de fuite des déflecteurs magnétiques, etc.", CERN 59-1, Décembre 1958.

6. De effectieve uitgebreidheid van het gevoelige gebied van de Siemens Hall sonde type FA 21, is zeer veel kleiner dan de door de fabrikant gespecificëerde effectieve afmetingen

   Dit proefschrift, Ch. 4, sect. 4d.

7. De voornaamste oorzaak, waarom de pompsnelheid van glazen kwikdiffusiepompen zo veel geringer is dan die van metalen pompen van gelijke geometrie en vermogen, ligt in de slechte warmtegeleiding door de glazen wand tussen condensaat en koelmiddel.

8. Bij de gevoeligheid van de Knudsen manometer is niet alleen een afhankelijkheid van de gassoort, doch evenzeer van de voorgeschiedenis van het instrument te verwachten.
   W. Stechelmacher: J. Sci. Instr., suppl. 1, (1950), p. 60.
   S. Weber: Kgl. Danske Vidensk. Selskab, Math. Phys. Medd. 24 (1947), No. 4.
   E. Fredlund: Ann. Phys. Lpz. (1932) No. 5, 617.

9. Bij de metingen door Romanov en Starodubtsev van de veldsterkte-afhankelijkheid van de oppervlakteïonisatieopbrengst van Na op polykristallijn W, is de gevonden lineaire afhankelijkheid van de logarithme van de Na^+-ionenstroom met de veldsterkte E, in plaats van de te verwachten afhankelijkheid met $E^{\frac{1}{2}}$, te verklaren uit te lage veldsterkten bij de metingen.
   A. M. Romanov en S. V. Starodubtsev: Soviet Phys. Techn. Phys. 2, 652 (1957).
   E. Ya. Zandberg: Zhur. tekn. Fiz. 28, 2434 (1958).

10. Voor het meten van kleine ladingen kan men met voordeel gebruik maken van de sterke verandering in absorptiespectrum bij oxydatie of reductie van vele organische stoffen.

11. De vraag, of in het Ag - Phtalocyanine complex éénwaardig dan wel tweewaardig Ag is ingebouwd, kan beantwoord worden door dit met D_2SO_4 te laten uitwisselen, en massaspectrometrisch te bepalen of hierbij één dan wel geen atoom D per molecuul complex wordt opgenomen.

12. Het is gewenst de verplichte winkelsluitingen over verschillende middagen etc. te spreiden tussen verschillende gelijksoortige zaken in dezelfde buurt.